University of Alberta

Characterization of late-diagenetic calcites of the Devonian Southesk-Cairn Carbonate Complex (Alberta Basin): constraints from petrography, stable and radiogenic isotopes, fluid inclusion and organic matter maturity data.

by

Natalie Aubet

A thesis submitted to the Faculty of Graduate Studies and Research
in partial fulfillment of the requirements for the degree of

Master of Science

Department of Earth and Atmospheric Sciences

Spring 2010
Edmonton, Alberta

Examining Committee

Dr. Hans G. Machel, Department of Earth and Atmospheric Sciences

Dr. Jeremy Richards, Department of Earth and Atmospheric Sciences

Dr. Douglas Schmitt, Department of Physics

ABSTRACT

The Alberta Basin has been the subject of various diagenetic studies but the precise understanding of the processes behind deep burial cementation remains unclear. This study investigates late-diagenetic calcites from the Devonian Southesk-Cairn Carbonate Complex with the purpose of constraining temperature, relative timing and chemistry of the paleo-fluids involved during calcite precipitation. Two types of late-diagenetic calcites were petrographically and geochemically characterized. Whereas calcite-I resulted from thermochemical sulfate reduction, calcite-II precipitated with no or little oxidized organic carbon present. As shown by the Sr isotopic signatures, some reservoirs were exposed to radiogenic Sr-bearing fluids. A slight trend of increasing fluid inclusion homogenization temperatures with depth is only seen in calcite-I, and bitumen reflectance also increases with depth following a normal burial gradient. These results, however, are not conclusive to interpret the influence of tectonically-driven fluids during deep burial.

ACKNOWLEDGMENTS

This study was funded in part by a National Sciences and Engineering Research Council grant awarded to Dr. Hans G. Machel and Dr. Jeremy Richards, and by the AAPG Grants-in-Aid program.

The author would like to thank Dr. H.G. Machel and Dr. Jeremy Richards for their critical reviews, guidance, and support. Thanks to Dr. Karlis Muehlenbachs, Dr. Sarah Gleeson, Dr. Iain Samson, Olga Levner, and Julito Reyes for laboratory support and useful comments, and to Dr. Kurt Konhauser for his encouragement along the way. I owe my thanks to Dr. Tom Chacko for his valuable help, and to Vivianne Robertson for her editing assistance in the early version of this thesis. I am grateful to Ernesto Pecoits for priceless discussion and editorial suggestions throughout many stages of the completion of this thesis. Thanks to all my friends for their constant love and support.

This thesis is entirely dedicated to my parents.

TABLE OF CONTENTS

LIST OF TABLES

LIST OF FIGURES

CHAPTER 1

CHAPTER 2

CHAPTER 3

CHAPTER 4

CHAPTER 1

GENERAL INTRODUCTION

1.1. RATIONALE

The Southesk-Cairn Carbonate Complex (SCCC), located in the Foreland Fold and Thrust Belt of the Western Canada Sedimentary Basin, constitutes one of the largest geological features of the Alberta Basin (**Figure 1.1**). Deposited throughout much of the Devonian period, the complex is particularly important as an exploration target for natural gas and oil.

A number of previous studies have suggested that the SCCC experienced an intricate diagenetic history in which several diagenetic processes have overlapped in time and space (Kaufman et al., 1990; Amthor et al., 1993; Patey, 1995; Buschkuehle, 2003). However, relatively little information exists regarding deep burial. In this context, a more precise understanding of the paragenetic sequence will provide the necessary framework to interpret the geochemical signatures and, thus, to unravel the processes involved during the precipitation of diagenetic mineral phases. Particularly, late- diagenetic carbonate cements commonly preserve the geochemical signatures of the deep burial fluid-regime at the time of the mineral formation; thus, such cements can be effectively used as "time capsules" for the study of burial diagenesis.

Previous studies of fluid-flow dynamics in Devonian aquifers of the western Alberta Basin have shown no connection between the shallow groundwater flow systems near the disturbed belt and deep systems located in

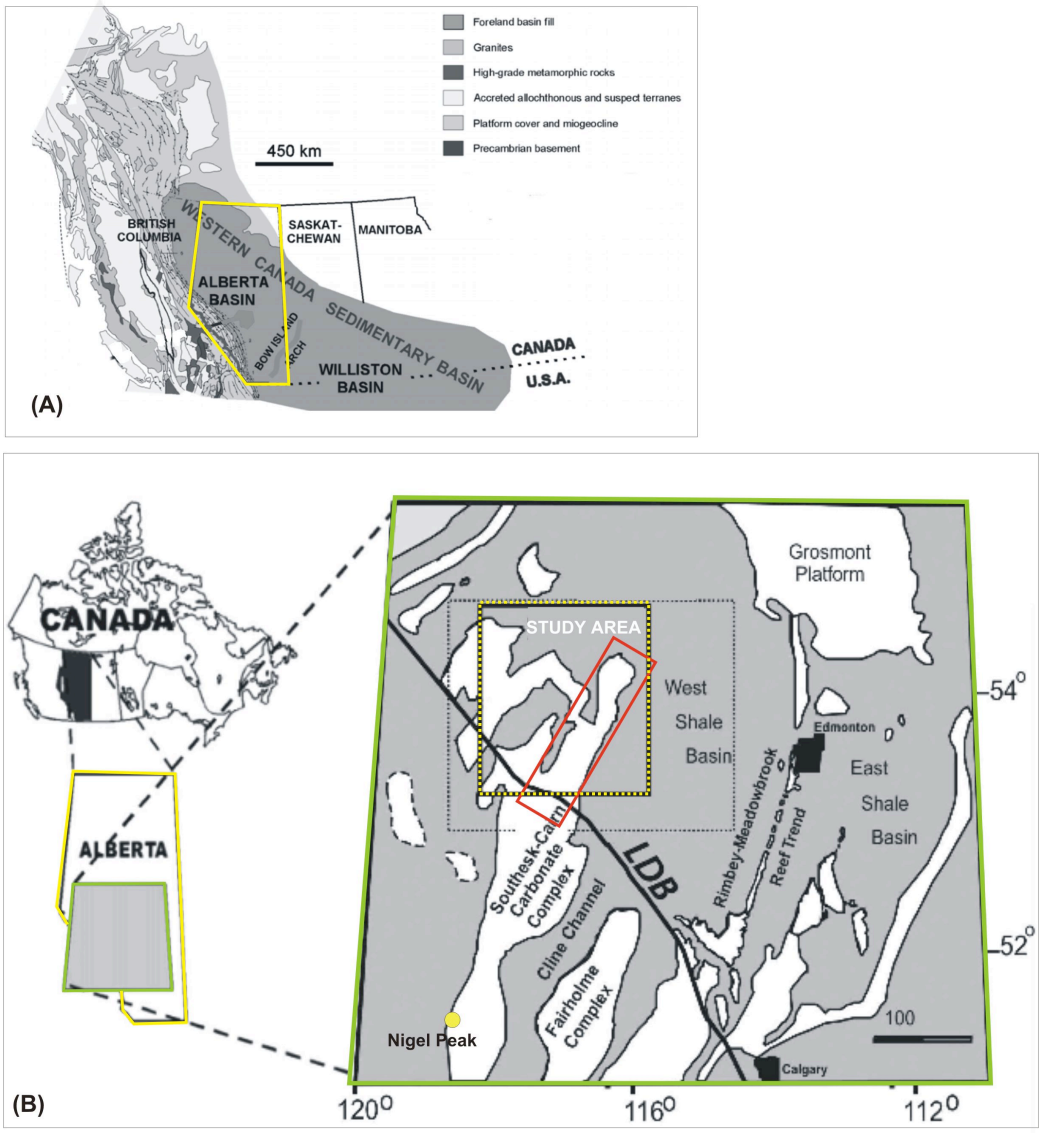

Figure 1.1. (A) Location of the Western Canada Sedimentary Basin (WCSB) relative to the Canadian Cordillera (Modified after Price, 1994). (B) Restored map illustrating part of the Alberta Basin and indicating the location of Devonian platforms (Southesk Cairn Carbonate Complex; Fairholme Complex; and Grosmont Platform). Red rectangle indicates the Marlboro-Windfall section (Modified after Buschkuehle, 2003).

the non-deformed part of the basin (Bachu, 1995; Wilkinson, 1995). Accordingly, various flow-driving mechanisms have been suggested as being responsible for the geochemical signatures of various diagenetic products and formation fluids (Ge and Garven, 1989; Bachu, 1995; Bachu, 1999; Machel et al., 1996; Machel and Cavell, 1999; Buschkuehle and Machel, 2002). Particularly, the “squeegee” model proposed by Oliver (1986), thought to have caused basin-wide migration of ore-forming brines and hydrocarbons in compressional tectonic settings, has been applied to the western Alberta Basin by Machel and Cavell (1999). Assuming that the diagenetic products generated by squeegee-type flow may be recording migration by such tectonically expelled fluids, several studies have focused on the geochemistry of late-diagenetic phases. Indeed, strontium isotope values recorded in calcite and dolomite cements from the SCCC suggest an extra-basinal fluid source from what is now the Foreland Fold and Thrust Belt system (Machel and Cavell, 1999) during the Laramide Orogeny. Anomalously high 87Sr/86Sr ratios have been identified in the petrographically similar late-diagenetic phases at several Devonian stratigraphic levels (Leduc and Nisku Formations) in areas such as Obed, which is part of the SCCC (Patey, 1995; Machel et al., 1996), and nearby locations such as Simonette (Duggan, 1997; Rock, 1999), the Peace River Arch (McKenzie, 1999), and Kaybob (Green, 1999; Smith, 2001; Green and Mountjoy, 2003).

Despite this advances, several aspects of the fluids expelled during tectonic compression and sedimentary loading of thrusts sheets in the SCCC are not clear (Green, 1999; Vandeginste et al., 2008). For example, limited information exists regarding the ultimate origin of the Sr isotopic signatures of late-diagenetic phases, which may have been formed by tectonically expelled fluids due to either horizontal or vertical fluid-flow (see Oliver, 1986). More

information on the regional distribution of O, C, and Sr isotopic compositions of cements and their temperatures of precipitation is needed to determine whether these radiogenic isotope signals resulted from basement
denudation and vertical fluid flow along fractures, or from up-dip migration of radiogenic brines form Proterozoic levels.

In either case, it has been suggested that the variable isotopic ratios (O, C, and Sr) recorded in deep burial calcite and dolomite cements resulted from overlapping of thermochemical sulfate reduction (TSR) and squeegee-type fluid flow in space and time (Buschkuehle, 2003; Machel and Buschkuehle, 2008). Furthermore, these authors found radiogenic Sr isotope signals only up to about 100 km into the foreland basin, concluding that squeegee-type fluid flow was spatially restricted to a narrow region near the fold- and-thrust belt, and probably short lived. This conclusion is supported by hydrogeologic modeling studies (Machel and Cavell, 1999).

1.2. OBJECTIVES

This research focuses on the petrological, geochemical, isotopic, and fluid inclusion characterization of late-diagenetic calcite cements from the SCCC. The central objectives of this research are to constrain:

(1) The temperature and relative timing of the mineral cement growth (*e.g.*, does temperature indicate maximum burial or fluid injection?); (2) The chemistry of paleo-fluids (*e.g.*, what was the composition of fluids during the event(s) responsible for the generation of the late-stage cements in the area?).

Pyrobitumen (solid bitumen, “dead oil”) is commonly associated with late-diagenetic cements, and was investigated to facilitate comparison of organic

thermal maturation data relative to the formation temperatures of the calcitic phases from fluid inclusion measurements.

Although TSR and squeegee-type fluid flow have been suggested to overlap during burial (Machel and Buschkuehle, 2008), these two processes have not been clearly characterized in the SCCC. Specifically, petrographic similarity of late-digenetic calcite cements is insufficient evidence to prove cogenesis. Thus, further objectives of this study are to:

(1) Provide criteria to recognize and discriminate TSR calcites and "squeegee"- and/or fault–influenced calcites; (2) Indicate spatial and temporal relationships relative to other late-diagenetic phases (*e.g.* saddle dolomite, anhydrite, elemental sulfur, and solid bitumen);

(3) Define the extent of influence of the TSR in Upper Devonian units from the SCCC.

1.3. STUDY AREA, SAMPLING TECHNIQUES, AND METHODS

The study area lies approximately 50 - 100 km east of the fold-and-thrust belt of the Western Canada Sedimentary Basin in the western part of the Alberta Basin. It is located between townships 49 and 61, and ranges 16 through 25 west of the fifth meridian (Figure 1.2) and includes the Hinton, Dalehurst, Obed, Marlboro, Pine Creek, and Windfall oil and gas fields from the Middle Devonian Swan Hills, as well as the Upper Devonian Leduc and Wabamun stratigraphic levels (**Figure 1.3**). A sample suite collected by Buschkuehle (2003) has been re-examined (540 core samples from 52 localities) in order to obtain late-diagenetic calcites (i.e., vug and vein fillings). Diagenetic phases analyzed here also include late-diagenetic dolomite cements, secondary anhydrite, and solid bitumen.

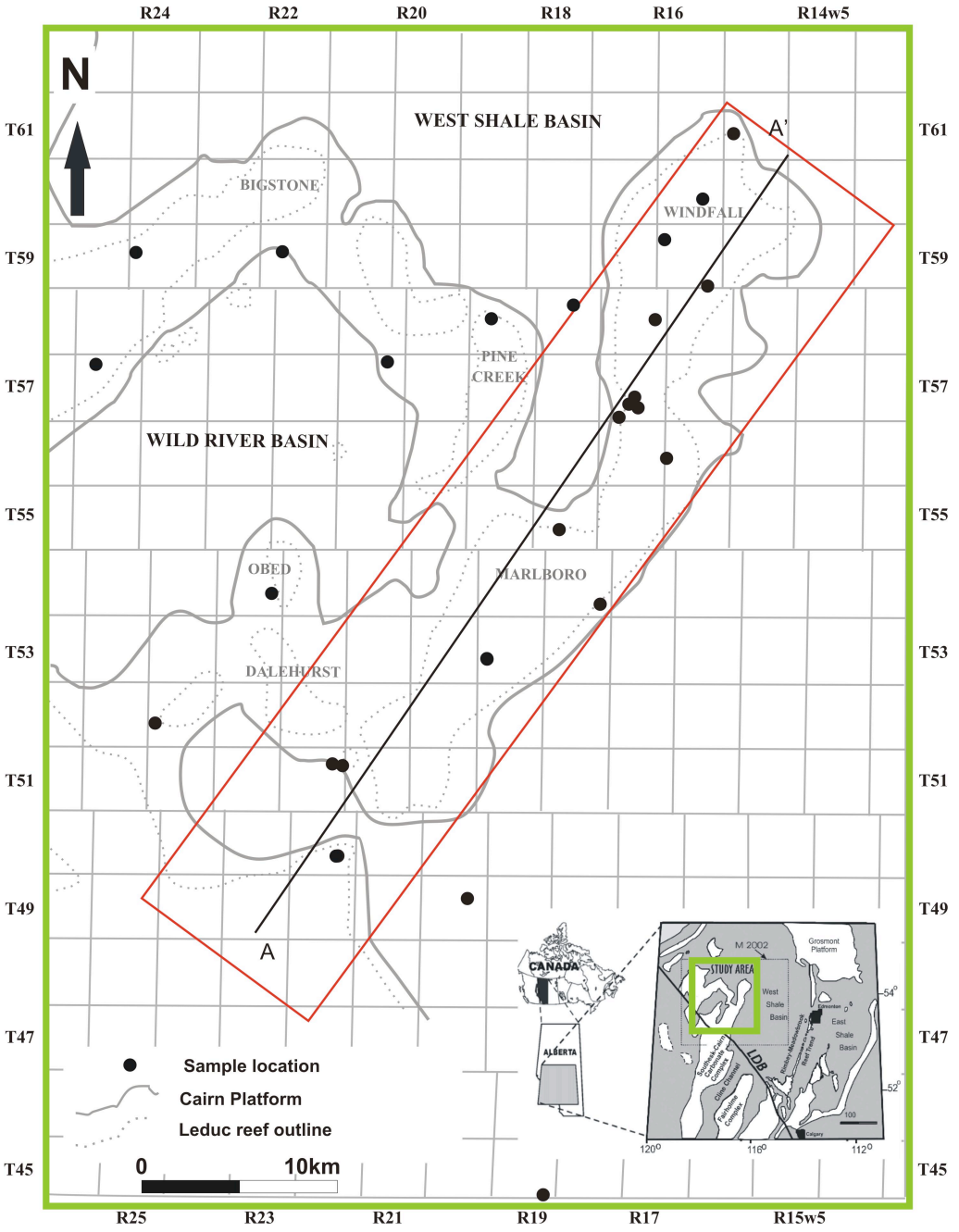

Figure 1.2. Location map of the study area showing sample location (modified from Buschkuehle, 2003). A-A': line of cross-section.

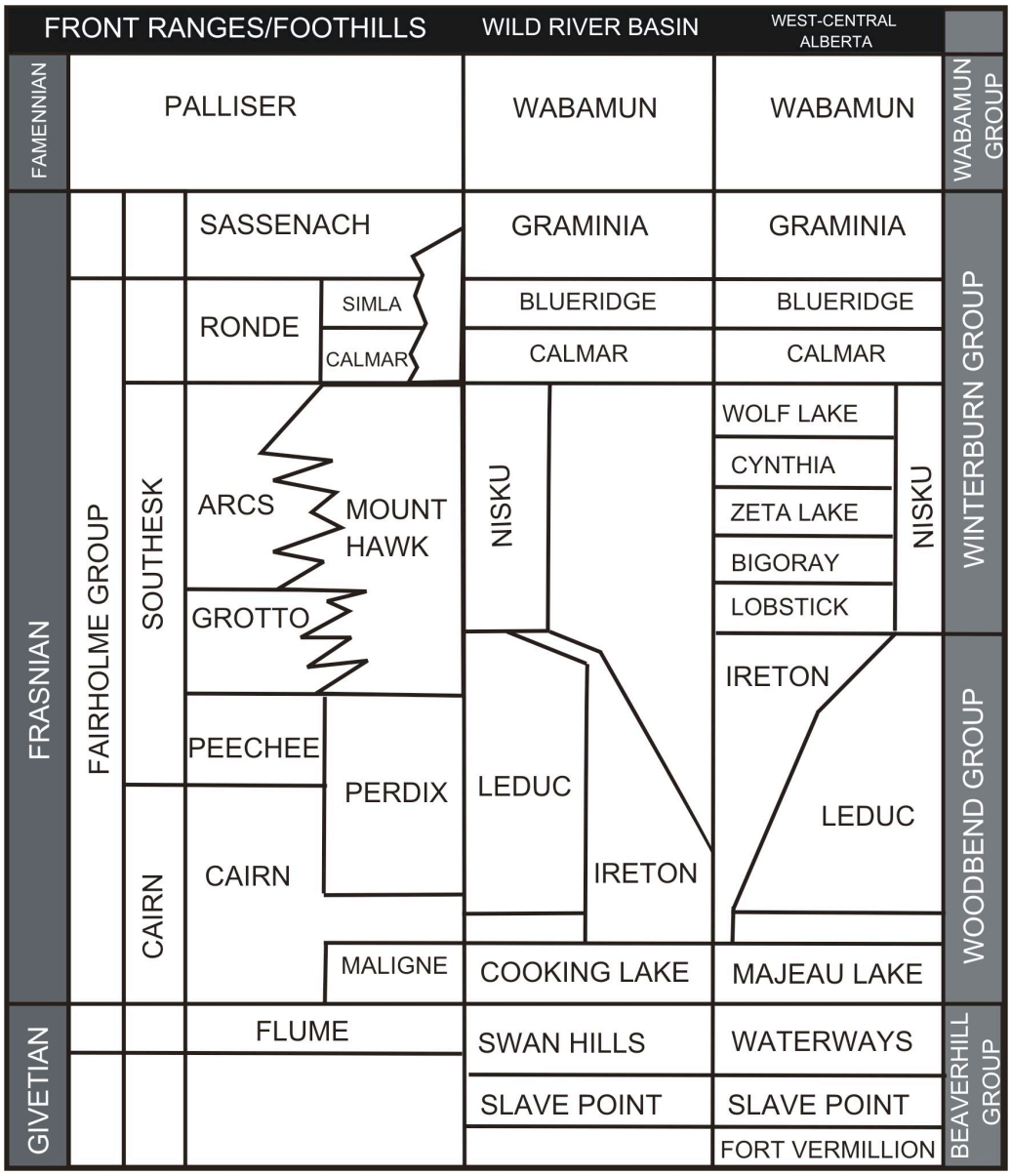

Figure 1.3. Stratigraphic correlation of the Upper Devonian sequence between subsurface and outcrop in the Foothills and Front Ranges of the Rocky Mountains (modified from Buschkuehle, 2003).

In addition, a total of 21 wells were examined and sampled at the Core Research Centre of the EUB (Energy and Utilities Board) in Calgary, Alberta (**Table 1.1**). In order to test the initial hypothesis that deep formation fluids were expelled from the Rockies into the foreland basin in an up-dip direction, a dip cross section has been constructed (**Figure 1.2**).

Table 1.1. Sample summary. Abbreviation: $\%B_0$ = bitumen reflectance; Mt = microthermometry; Raman = Raman microspectroscopy.

Location	Sample	Stratigraphic level	Depth (m)	O-and C-isotopes	Mt.	$\%B_0$	Raman	$^{87}Sr/^{86}Sr$
2/15-9-57-17W5	NA 200	Leduc	3162.75	✓	✓			✓
7-18-52-24W5	NA 254	Leduc	4824.5	✓	✓		✓	
10-32-44-19W5	NA 10	Leduc	5363.9	✓	✓	✓		
10-32-44-19W5	NA 303	Leduc	5326.3	✓				
10-23-58-17W5	NA 323	Nisku	3033	✓	✓			✓
16-18-61-15W5	NA 320	Leduc/Nisku	2768.5		✓			✓
15-9-57-17W5	NA 330	Leduc	3149.5	✓	✓			✓
5-25-51-22W5	NA 271	Leduc	4473	✓	✓			✓
2-14-50-22W5	NA 297	Leduc	3918.5	✓	✓	✓	✓	✓
9-5-57-17W5	NA 270	Leduc	3188	✓	✓			✓
6-16-55-18W5	NA 290	Leduc	3319.3	✓	✓	✓		✓
15-9-57-17W5	NA 123	Leduc	3162	✓	✓			
10-12-54-18W5	NA 333	Swan Hills	3557.9	✓	✓		✓	✓
9-17-53-19W5	NA 311	Leduc	3695.4	✓	✓	✓		✓
3-26-49-20W5	NA IV	Swan Hills	4577		✓		✓	
1-18-56-16W5	NA 273	Leduc	2951.2	✓	✓			✓
11-29-59-16W5	NA 116	Nisku	2734.4	✓	✓	✓		✓
16-22-58-19W5	NA 208	Leduc	3375.4	✓	✓			✓
13-15-60-16w5	NA 160	Nisku	2563			✓		
6-34-57-21w5	NA 3434	Leduc	3434.3			✓		
9-20-59-22w5	NA 2563	Leduc	3805.6	✓		✓		✓

Diagenetic phases were identified on the basis of paragenetic association. Geochemical techniques used in this study include stable ($\delta^{13}C$ and $\delta^{18}0$) and radiogenic ($^{87}Sr/^{86}Sr$) isotope analyses, fluid inclusion microthermometry, Raman spectroscopy, and bitumen reflectance. Details of these procedures are summarized in the methodology section of Chapter 2.

1.4. GEOLOGICAL SETTING, STRATIGRAPHY, AND PREVIOUS WORK

Located in the west-central part of Alberta, the Middle to Upper Devonian Southesk-Cairn Carbonate Complex (SCCC) is a major northeast- to southwest-trending platform sequence with a thickness of up to 550m and an extension of about 145 km from the limit of the disturbed belt to its northeastern edge in the foreland basin (Dolphin and Klovan, 1970; **Figure 1.2**). The Complex is comprised of strata from the Middle to Upper Devonian and includes four stratigraphic units: Beaverhill Lake, Woodbend, Winterburn, and Wabamun groups (**Figure 1.3**; Switzer et al., 1994 in Mossop and Shetsen, 1994). The study area encompasses the Windfall, Marlboro, Pine Creek, Obed, and Dalehurst fields. Samples were taken mainly from the Leduc Formation (Woodbend Group), but a few late-diagenetic cements from the Nisku and Swan Hills Formations have also been included in this study.

Overall, the SCCC consists of stacked cyclical ramps, shelf carbonates, and associated anhydrite deposits (Mossop and Shetsen, 1994). Its stratigraphic architecture was controlled by sea-level fluctuations and constitutes a major (2nd and 3rd order) transgressive-regressive couplet (Switzer et al., 1994). Lateral variations of facies are recorded as a consequence of these transgressive and regressive sea level fluctuations. Depositional environments of the SCCC carbonates are separated into: (1) platform; (2) reef; and (3) basinal settings

(Buschkuehle, 2003). Carbonates of the Beaverhill Lake Group represent part of the “platform stage” and the transgressive onlap of dominantly marine sediments along a passive continental margin. The overlying Woodbend Group represents a transgression, whereas the Winterburn and Wabamun Groups record a regression in the basin (Dolphin and Klovan, 1970).

Based on an extensive sedimentological study, Buschkuehle (2003) summarized the most conspicuous lithofacies of the SCCC as: (a) evaporitic mudstones facies; (b) Amphipora-bearing wackestone facies; (c) Amphipora-rich facies; (d) stromatoporoid frame and boundstone facies; (e) fossiliferous rudstones facies; (d) floatstone facies; and (g) basinal facies.

The SCCC has undergone a complex diagenetic history (Kaufman et al., 1990; Amthor, et al., 1993; Patey, 1995; Buschkuehle, 2003) with as many as twenty-four diagenetic products (**Figure 1.4**; Machel and Buschkuehle, 2008). Machel and Buschkuehle (2008) integrated all diagenetic phases into five diagenetic stages to characterize the major changes in fluid regimes in the basin during burial. These stages were defined on the basis of physical and chemical changes, and can be linked with the following diagenetic settings: (I) synsedimentary and shallow burial; (II) intermediate burial; (III) deep burial; (IV) maximum burial; and (V) present depth. Two out of the seven types of calcite detailed in the paragenetic sequence (types VI and VII of Figure 3 in Machel and Buschkuehle, 2008) were generated during deep to maximum burial (Stage IV, Phase 22; see **Figure 1.4**). These calcites are the main focus of the present study. The origin of these late-stage cements is relatively well understood and has been constrained by means of petrography, geochemistry, and fluid inclusion analysis (*e.g.*, Patey, 1995; Green, 1999;

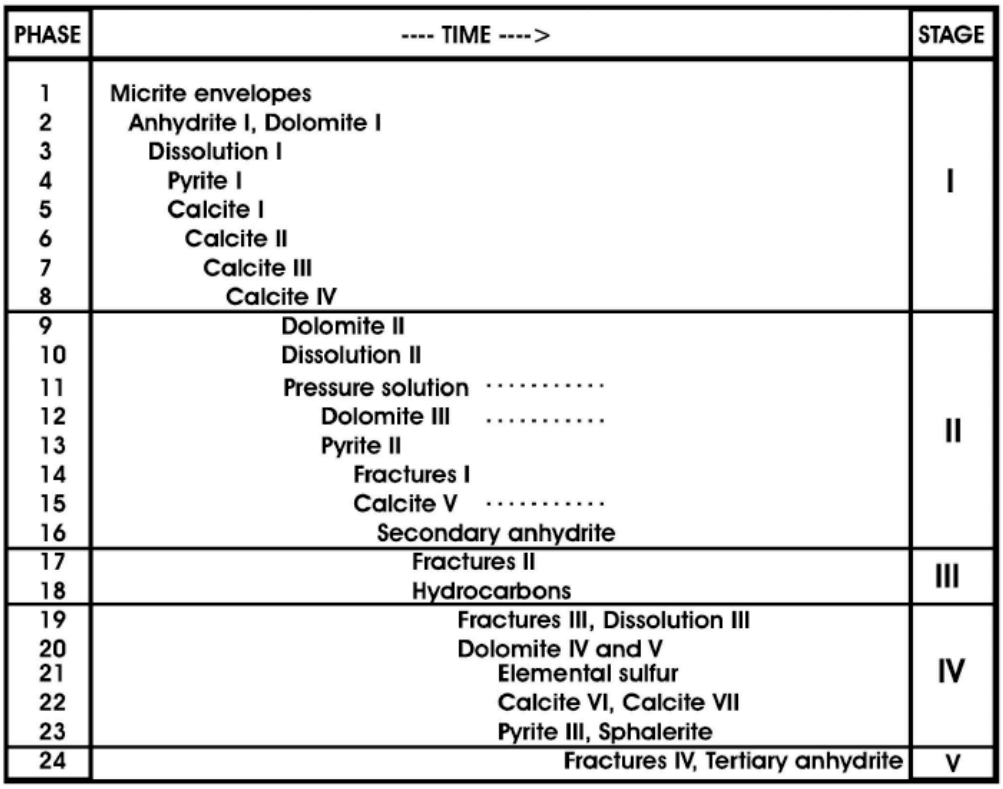

Figure 1.4. Diagenetic paragenetic sequence of the SCCC (Modified from Machel and Buschkuehle, 2008).

Machel and Cavell, 1999; Smith, 2001; Buschkuehle, 2003). Their precipitation corresponds in time with deepest burial of the Complex during the Laramide Orogeny, and records the probable overlapping effects of TSR and tectonically-expelled fluids (Machel and Buschkuehle, 2008). Minor saddle dolomite cements, secondary anhydrite, elemental sulfur, and solid bitumen that also influence the reservoir quality are genetically linked with these late-diagenetic carbonates (Patey, 1995; Machel and Buschkuehle, 2008).

1.5. TSR AND SQUEEGEE FLUID FLOW DURING DEEP BURIAL

The abiological reduction of inorganic sulfate to sulfide coupled with the oxidation of hydrocarbons to CO_2 is commonly referred to as thermochemical sulfate reduction (TSR; Orr, 1974, Orr, 1977; Goldstein and Aizenshtat, 1994; Machel, et al., 1995; Nöth, 1997). From a reservoir point of view, the most important TSR product is H_2S, the amount (% in gas reservoir) of which is controlled by: (1) availability of sulfate; (2) lack of metals to inhibit hydrogen sulfide stabilization, (3) availability of reactive gas condensate; and (4) a closed system to prevent H_2S "migration" (see Machel, 2001). The generic reaction can be expressed as follows:

Hydrocarbon + SO_4^{2-} ⇒ altered hydrocarbons + solid bitumen + HCO_3^- (CO_2) + H_2S (HS^-) + heat

(Machel et al., 1995) Reaction (1)

or:

Hydrocarbon + $CaSO_4$ ⇒ $CaCO_3$ + H_2S + H_2O ± S ± CO_2

(Worden and Smalley, 1996) Reaction (2)

As shown by these equations, TSR leads to sour gas (H_2S) production and calcite precipitation (or dolomite, if significant Mg is available), as well as CO_2, elemental sulfur, and water formation (Machel, 1987; Worden et al., 1996). Because TSR is a self- catalyzing process, any increase in temperature will cause the reaction to proceed faster (Orr, 1974; Machel et al., 1995; Noth, 1997).

Criteria for recognizing TSR in ancient rocks are based on the analysis of: (1) mineral associations; (2) mineral precipitation temperatures, commonly through fluid inclusion microthermometry; (3) O and C isotope geochemistry of the carbonate by- products; and (4) S isotope geochemistry of elemental sulfur, sulfates, and sulfur in solid bitumen. Accordingly, for the calcite + solid bitumen + elemental sulfur + saddle dolomite association, temperatures above 100˚C, depletion in $\delta^{13}C$, and overlapping isotope values of sulfur in bitumen, elemental sulfur, and sulfates, are evidence of TSR in the geological record (Krouse et al., 1988; Machel et al., 1995).

The TSR process has been well documented in several deeply buried carbonate reservoirs in Alberta, the US Gulf coast, and the Middle East (Krouse et al., 1988; Sassen, 1988; Claypool and Mancini, 1989; Heydari and Moore, 1989; Worden and Smalley, 1996; Zhang et al., 2005; Worden and Cai, 2006). Furthermore, TSR has been involved in the generation of metal sulfide ores in several sedimentary settings around the world (*e.g.*, Powell and Macqueen, 1984; Leventhal, 1990; Bechtel et al., 2001). Many of the best-known sour gas fields are located in Middle and Upper Devonian carbonates of the Western Canada Sedimentary Basin (*e.g.*, Leduc and Nisku formations). For example, TSR has been identified in oil and gas reservoirs such as Obed (Patey, 1995; Manzano et al., 1997; Smith, 2001; Buschkuehle, 2003), Simonette (Duggan, 1997), Kaybob South (Green, 1999), Rosevear (Kaufman et al., 1990), Burnt

Timber and Crossfield East (Yang et al., 2001), as well as in outcrops of correlative units in the Front Ranges of the Rocky Mountains (Smith, 2001; Vandeginste et al., 2008). In the present area of study, the Southesk Cairn Carbonate Complex, late-diagenetic cements (sparry calcite and saddle dolomite) were interpreted to have formed in a deep burial diagenetic setting (Patey, 1995; Green, 1999; Buschkuehle, 2003), and TSR was invoked as being responsible for the geochemical signatures of the majority of these diagenetic phases (Machel and Buschkuehle, 2008). The paragenetic sequence, geochemistry and formation temperatures of these deep burial phases are relatively well constrained. However, limited information exists regarding calcite generated by TSR and calcite generated by other deep burial processes (*e.g.*, fault-related calcite precipitation).

The linkage between basinal fluid migration and tectonics has been the subject of various studies. Specifically, several authors have discussed the importance of deformation-induced fluid flow, also called “squeegee” fluid flow, (*e.g.*, Etheridge et al., 1983; Oliver, 1986; Cox, 1999) and its influence on mineralization. “Squeegee” fluid flow, could play a key role during diagenesis, hydrocarbon formation, and ore accumulation in sedimentary basins (Oliver, 1986) because it could mobilize heat and redistribute materials from the foreland system. Consequently, injection of hot fluids into the basin may disturb the normal geothermal regime.

The influence of tectonically-driven fluids on late-diagenetic calcites from the SCCC was first proposed by Machel et al. (1996). Evidence supporting this contention came from Sr-isotopic compositions and anomalous homogenization temperatures in late-diagenetic calcite cements showing higher values than those estimated to have occurred during maximum burial. In subsequent studies, a

general northeastward flow direction through the complex had been interpreted from variable 87Sr/86Sr-ratios in these calcite cements (Machel and Cavell, 1999; Machel and Buschkuehle, 2008). However, fluid injection via subvertical faults during late burial had also been proposed to play an important role in the spatial distribution and isotopic composition of cements in these Devonian carbonates (*e.g.*, Green, 1999; Duggan et al., 2001; Smith, 2001; Buschkuehle, 2003; Machel and Buschkuehle, 2008).

The thermal history of a sedimentary basin can be investigated by using either (1) thermal maturation indicators, such as vitrinite or bitumen reflectance, or (2) paleothermometers such as fluid inclusion homogenization temperatures, to determine maximum or minimum temperatures of crystallization, respectively. Vitrinite reflectance (VRr) is the most commonly used method for assessing thermal maturity (*e.g.*, Tissot and Welte, 1984; Allen and Allen, 1990). However, when vitrinite is not present, alternative reflectance methods may be used. Bitumen reflectance has been demonstrated to be a reliable indicator of organic maturation in sedimentary successions (*e.g.*, Jacob, 1989).

Bitumen occurring in sedimentary rocks has three common definitions. One is chemical, and characterizes bitumen as the portion of the organic matter that is soluble in organic solvents (Tissot and Welte, 1984). The other is petrographic, and characterizes bitumen as the organic matter filling voids and fractures in rocks, further classified based on reflectance, fluorescence intensity, and solubility (see Curiale, 1986; Jacob, 1989). Low maturity distinguishes pre-oil bitumen from post-oil bitumen, which is also known as pyrobitumen that often forms from the thermal maturation of crude oil. The third classification is genetic and subdivides bitumen in primary and secondary. Primary bitumens result from the transformation of kerogen whereas secondary bitumens derived from the

thermal, microbial or oxidative alteration of liquid hydrocarbons or pre-existing bitumen (Curiale, 1993).

Maturation of organic matter is an irreversible process and commonly records the maximum temperature to which a rock sequence has been exposed (Teichmuller, 1973; Ammosov and Sharkova, 1975; Mckenzie and Mckenzie, 1983). However, bitumen reflectance might not necessarily indicate the maturity of the host strata in cases where short “flashes” of heat did not last long enough for thermal equilibration of the entire sequence (Wilson, 2000). The irreversible character of this process is useful for interpreting the fluid inclusion data from co-existing minerals. Given that more than one population of fluid inclusions can be present in the same mineral, possible thermal re- equilibration (Gratier and Jenatton, 1984; Prezbindowski and Larese, 1987; Barker and Goldstein, 1990) during successive thermal regimes can be identified by integrating fluid inclusion microthermometric data with reflectance data of co-existing organic matter (Thomson et al., 1992). Furthermore, the relative timing of the late-diagenetic calcites can be constrained by combining detailed fluid inclusion data with thermal maturation analyses. Temperatures higher than expected from burial at normal geothermal gradients commonly indicate the influence of hot fluids from outside the geothermal system or locally elevated regional heat flow. Thus, the paleotemperatures obtained from bitumen reflectance are useful for estimating burial depth and the relative timing of cementation.

1.6. THESIS ORGANIZATION

This thesis is organized into four chapters, as follows. Chapter 1 introduces the topic, location, and objectives of this study, and also describes the geological framework and previous studies carried out in the region. Carbon, O

and Sr isotopic compositions, fluid inclusion microthermometry, Raman microspectroscopy, and bitumen reflectance methodologies and results are presented in Chapter 2. Chapter 3 discusses the geochemical, fluid inclusion, and bitumen reflectance dataset, and provides an interpretation for formation of the late-diagenetic calcites in the SCCC. Finally, Chapter 4 presents the conclusions drawn from the results obtained.

CHAPTER 2

METHODS AND RESULTS

2.1. ANALYTICAL METHODS

The complete sample suite used by Buschkuehle (2003) was reviewed for this study (520 samples, 52 cores). In addition, 21 cores from the SCCC were logged and sampled: 7 wells in Windfall, 3 in Marlboro, 4 in Dalehurst, 3 in Obed, and 4 in Pine Creek field were examined. Petrographic analyses were performed on 132 thin sections, which were stained with Alizarin Red S and potassium ferricyanide to determine calcite, dolomite, and iron content in both mineral phases. Twenty-three sections were analyzed by cathodoluminiscence (CL) at the Department of Earth and Atmospheric Sciences (University of Alberta) using a cold cathodo Premier Zeiss Jenapol ELM-3R Luminoscope with a beam voltage of 15 kV and a beam current of 0.5 mA.

Carbonate powders for carbon and oxygen isotopic analysis were obtained by using a dental drill, and were analyzed in the Stable Isotope Laboratory of the University of Alberta. Late-diagenetic phases were extracted separately, and a total of 7 dolomites and 48 calcites (42 from the subsurface and 6 from outcrop) were analyzed. Carbon and oxygen isotope analyses were obtained by the phosphoric acid method at room temperature (McCrea, 1950). All results are reported in per mil relative to Vienna Pee Dee Belemnite (VPDB), and no phosphoric acid fractionation was applied to the dolomite samples. Reproducibility was checked providing an analytical precision of better than

±0.1‰ for $\delta^{13}C$ (1σ) and $\delta^{18}O$ (1σ). From analysis of reference standards, analytical accuracy is estimated to be ± 0.2‰.

Microthermometric determinations on fluid inclusions were carried out on 17 calcite samples. Samples were classified petrographically, and fluid inclusions suitable for microthermometric analysis and Raman spectroscopy were selected. Fluorescence microscopy was used to indentify oil-bearing inclusions. Measurements focused on primary and pseudosecondary inclusions as defined by Roedder (1984). A Linkam_TMHMSG 600 heating/freezing stage (University of Alberta) mounted on a binocular Olympus BX50 microscope fitted with a 40x long-working-distance objective lens was used. Calibration was carried out with synthetic fluid inclusions at -56.6˚C and 0.0˚C (*e.g.*, the melting points of pure carbon dioxide and pure water, respectively). Accuracy of these measurements is ± 0.2˚C below 0˚C and ± 1˚C at higher temperature. Homogenization temperatures were measured first and in increasing order, before measurement of freezing temperatures to avoid the effect of stretching. To avoid decrepitation, most of the samples were not heated to above 200 ˚C.

Strontium isotope ratios of 11 calcites were measured using 20 mg aliquots of sample powder. Following acid digestion, the extraction was conducted using conventional cation exchange procedures (Baadsgard, 1987). $^{87}Sr/^{86}Sr$ ratios were determined at the University of Alberta using a VG 354 thermal ionization mass spectrometer. All Sr isotope ratios are presented relative to a value of 0.710245 for the NIST SRM987 standard. The mean standard error was ± 0.000025, and in-run precision was better than ± 0.000020 (2σ).

For in-situ Sr isotope analysis, 4 calcites, 3 saddle dolomites, 1 anhydrites, and 3 matrix dolomites were analyzed using a 213 nm laser ablation unit (New Wave Research) coupled to a NuPlasma HR MC-ICP-MS instrument at

the University of Alberta. Petrographic sections were ablated using a spot size of 320μm with a 20 Hz repetition rate, and laser output at approximately 3 mJ. Precision and reproducibility were verified using an internal standard consisting of a coral with an average value of 0.70910 ± 0.00005 (2σ; n>50, Schmidberger et al., 2003). Analysis of this standard during this study yielded values of $^{87}Sr/^{86}Sr$ of 0.709170, and 2σ was better than ± 0.000550.

Laser Raman spectroscopic analyses were performed at the Department of Earth and Environmental Sciences (University of Windsor) on a Dilor SuperLabram spectrometer. The laser source was an argon ion laser with wavelength of 514.5 nm and a source power of 700 nW. Raman spectra were assessed over a time span of 10 s at selected temperatures. An Olympus BX 40x microscope objective was used to focus the laser beam on separate inclusion phases and to collect the scattered light. The acquired spectra were compared with a compiled dataset for the most common substances (Dubessy et al., 1992).

Samples for bitumen reflectance were selected from eight localities along the Marlboro-Windfall section. The occurrence of solid bitumen is localized and unpredictable, thus the distribution of samples reflects the relative abundance of solid bitumen in the area. Polished probe mounts were prepared for all the core samples for petrographic analysis and bitumen reflectance measurements. Reflectance observation and measurements were made under oil immersion (50x magnification lens) using a LEICA microscope combined with a LEITZ-MPVGEOR high-resolution photometer for spectral measurements in the Organic Petrology Laboratory at the Geological Survey of Canada (Calgary). Several glass standards (0.49%, 1.025% and 1.817% Ro) were used for calibrating the microphotometric system, and images were taken and processed using the software AxioVision 4.6.3 (04-2007). Optical microtextures of the anisotropic

pyrobitumens were classified using the coke terminology of Grint and Marsh (1981) and White (1976).

2.2. RESULTS

2.2.1. Mineralogy and Petrography

Detailed petrographic descriptions of the SCCC rocks given by Green (1999), Smith (2001), and Buschkuehle (2003) were confirmed in this study and are not repeated here. However, further analysis of the late-diagenetic calcite cements has led to the recognition of two types of calcite (**Figure 2.1**) and their paragenetically associated phases (saddle dolomite, elemental sulfur, anhydrite, and solid bitumen). Calcite-I and II can be correlated with the calcite VII and VI of Machel and Buschkuehle's paragenetic sequence.

2.2.1.1. Calcite-I

Calcite-I forms subhedral to euhedral crystals with variable sizes, typically from coarse to very coarse (0.5 to 2 cm). Calcite-I characteristically fills vugs, but it also appears filling moldic pores. Crystals are limpid to semi-translucent, rarely twinned, and non-luminescent under CL (**Figure 2.2**). Another distinctive feature of calcite-I is its paragenetic association with subhedral saddle dolomite that occurs as the first pore-filling phase lining the vugs, as well as anhydrite, solid bitumen, and elemental sulfur (**Figure 2.3**). The bulk of secondary anhydrite is older than calcite-I and was precipitated after saddle dolomite. Specifically, in the uppermost parts of the Marlboro-Windfall section, remnants of secondary anhydrite occur as inclusions in calcite (**Figure 2.4**). Furthermore, solid bitumen is present coating saddle dolomite, anhydrite, and locally calcite-I in large vugs.

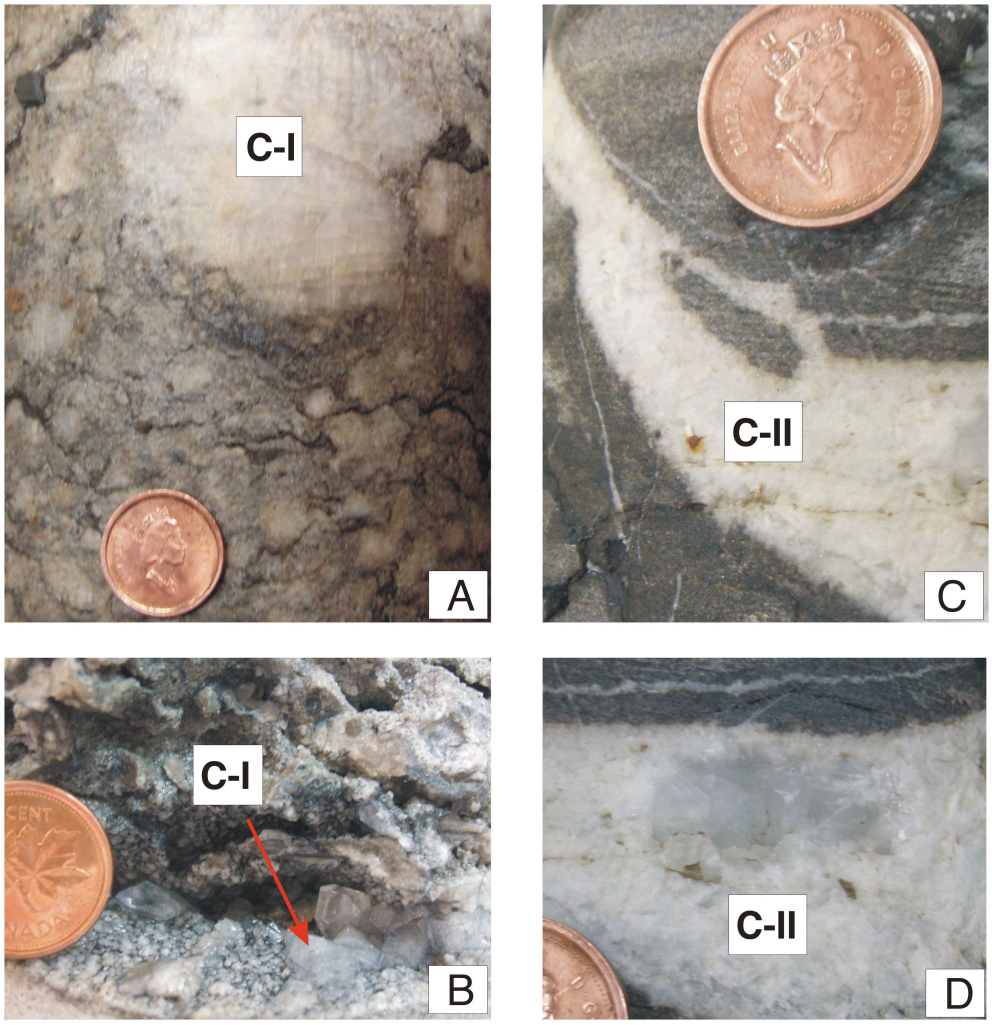

Figure 2.1. Late-diagenetic calcite cements I and II. Calcite-I lines and/or fills vugs and molds **(A)**, **(B)** whereas limpid to white calcite-II occurs filling fractures **(C)**, **(D)**.
Abbreviations: C-I = calcite-I; C-II = calcite-II. **(A-B)** NA IIIb. Location: 16-22-58-19W5. Depth: 3354m. **(C-D)** NA 333. Location: 15-09-57-18W5. Depth: 3162m.

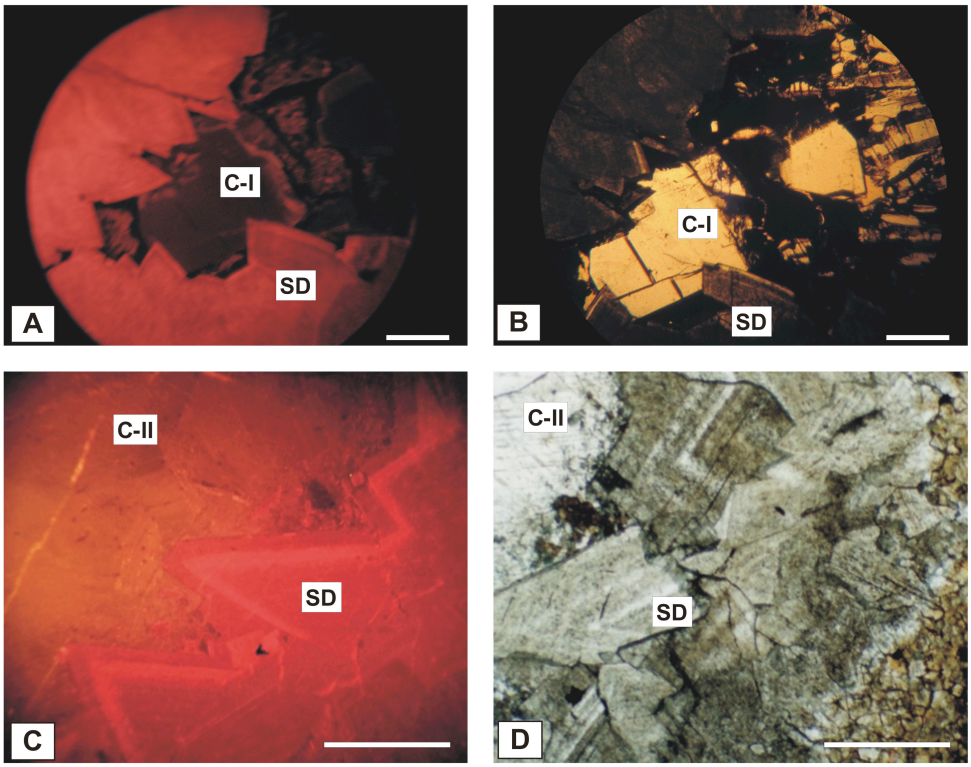

Figure 2.2. Thin section photomicrographs of calcite-I and II. Calcite-I and related saddle dolomite under cathodoluminescence **(A)**, and in cross-polarized light **(B)**. Calcite-II postdating saddle dolomite under cathodoluminescence **(C)**, and in cross-polarized light **(D)**. Note the thin bright orange zones in the saddle dolomites, the non-luminescent character or calcite-I (**A**), and the orange-red CL of calcite-II **(C)**.
Scale bar = 1mm. Abbreviations: C-I = calcite-I; C-II = calcite-II.
(A-B) Sample NA 311. Location: 9-17-53-19W5. Depth: 3695.4m. **(C-D)** Sample NA 290. Location: 6-16-55-18W5. Depth: 3319.3m.

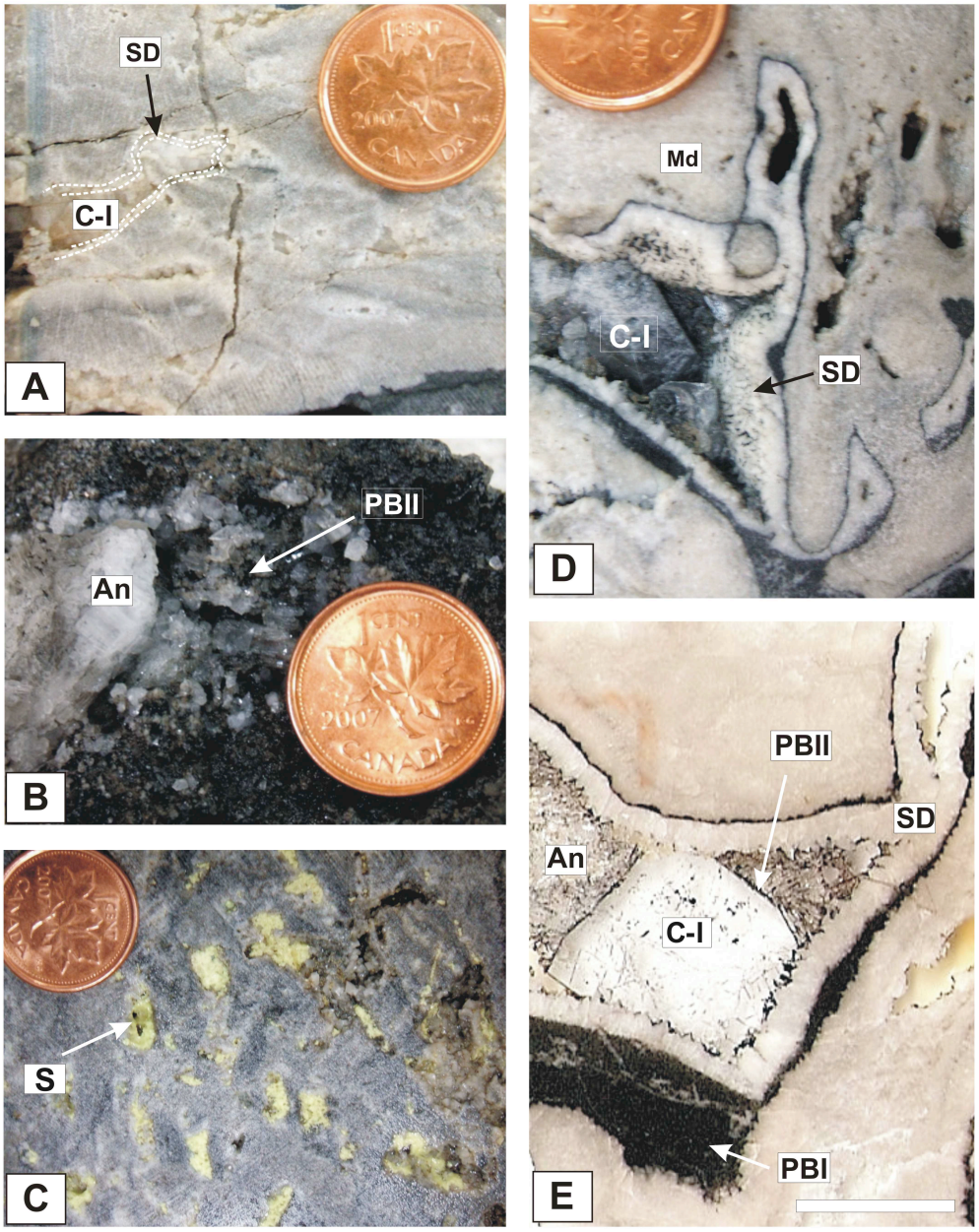

Figure 2.3. Core samples of calcite-I. **(A)** Calcite-I postdating saddle dolomite. Sample NA III. Location: 16-22-58-19W5. Depth: 3375m. **(B)** Solid bitumen (PB II) coating anhydrite in large vugs. Sample NA 2563. Location: 9-20-59-22W5. Depth: 3805.6m. **(C)** Elemental sulfur in small vugs. Sample NA XI. Location: 10-27-52-24W5. Depth: 4691.3m. **(D-E)** TSR mineral assemblage infilling large vugs. Sample: NA 311. Location: 9-17-53-19W5. Depth: 3695.4m. The paragenesis can be summarized as follows: (1) solid bitumen I, (2) saddle dolomite, (3) anhydrite – solid bitumen II, and (4) calcite-I – elemental sulfur. Scale bar in E = 1cm. Abbreviations: An = Anhydrite; C-I = calcite-I; Md = matrix dolomite; PB I = solid bitumen; PB II = solid bitumen II; S = elemental sulfur; SD = saddle dolomite.

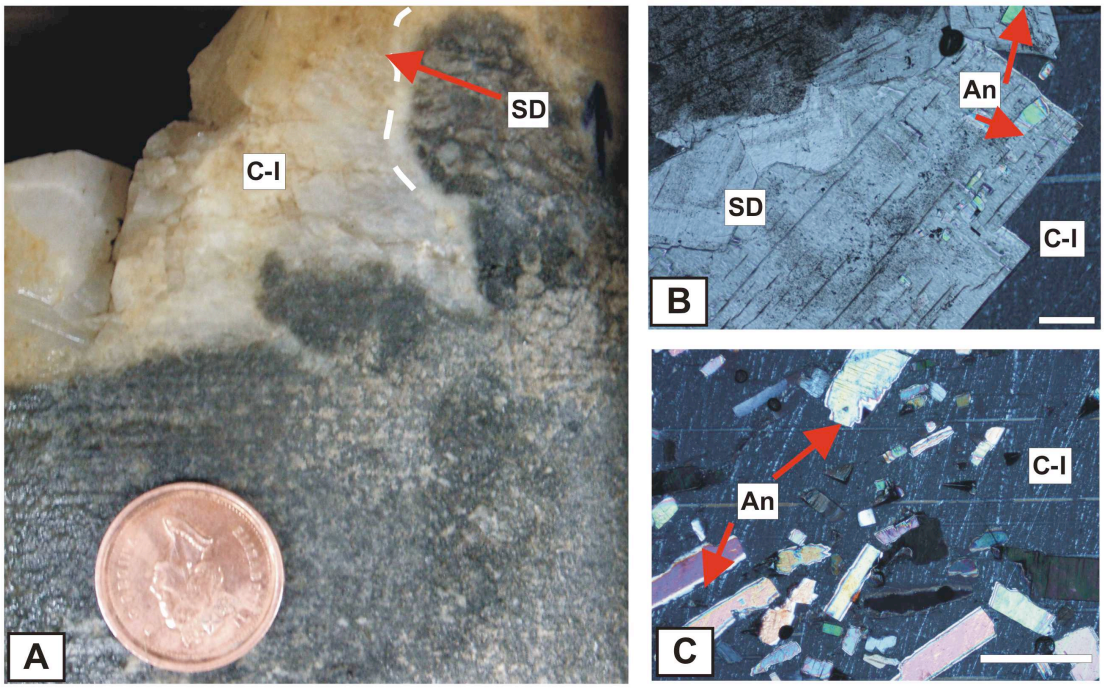

Figure 2.4. Core sample and photomicrographs of calcite-I. Sample NAIV. Location: 3-26-49-20W5. Depth: 4577m. **(A)** Hand sample showing saddle dolomite and calcite-I (in large vug (A). **(B-C)** Photomicrographs of calcite-I. **(B)** Remnant anhydrite in saddle dolomite (SD), and **(C)** Calcite-I showing poikilotopic texture, which is indicated by enclosing medium to coarse crystalline anhydrite with corroded rims. Scale bar = 0.5mm. Abbreviations: An =anhydrite; C-I = calcite-I; SD = saddle dolomite.

2.2.1.2. Calcite-II

Calcite-II consists of subhedral to massive, milky-white colored to “limpid” crystals, characteristically occurring as a fracture-filling phase (**Figure 2.1**). Crystal size varies from medium to very coarse (0.5 – 2 mm) and sporadically reaches 2 cm in diameter; larger crystals are developed towards the centers of these fractures. Under cross-polarized light the crystals show normal to slightly undulose extinction, and orange-red luminescence under by CL (**Figure 2.2**). Calcite-II occurs in association with coarse, subhedral saddle dolomite, where the latter is the first phase lining the fractures and calcite-II overlies it. Cathodolominescence microscopy of this saddle dolomite reveals well-developed zonation of alternating dull red and orange luminescent layers (**Figure 2.2**). No petrographic evidence showing co-occurrence of calcite-I and II has been recorded in the samples analyzed during this study. Thus, it is not possible to establish a relative age relationship between calcite-I and calcite-II on the basis of paragenesis.

2.2.2. Solid bitumen petrography

Solid bitumen usually occurs as pore-lining and pore-filling cements as follows: (1) lining matrix dolomite (Bitumen I), (2) lining saddle dolomite, interstitial to anhydrite and predating calcite-I (Bitumen II), and (3) partially filling fractures, predating calcite-II (Bitumen III). Less commonly, bitumen (I) occurs as < 2 mm-wide black seams and filling open spaces within brecciated host rock (matrix dolomite). Macroscopically, most of the bitumen appears dark brown in color, and glossy-black in some samples. According to the mineral associations found and with a descriptive purpose, three assemblages have been differentiated:

Assemblage I: Matrix dolomite-bitumen I (pre-TSR assemblage)

Assemblage II: Saddle dolomite-anhydrite-bitumen II-calcite-I (TSR assemblage)

Assemblage III: Bitumen III-calcite-II (post-TSR assemblage)

The dolomite of Assemblage I **(Figures 2.5A, 2.6)** is representative of Stage II (Dolomite III, **Figure 1.4**) of the paragenetic sequence described by Machel and Buschkuehle (2008), whereas Assemblage II is part of the paragenesis from Stage IV (**Figure 1.4**). Due to the intimate linkage between solid bitumen, anhydrite, elemental sulfur, and calcite-I **(Figures 2.5B, 2.7, 2.8)** Assemblage II is interpreted as formed during TSR. Calcite-II of Assemblage III **(Figures 2.5C, 2.9)** appears infilling fractures, and postdating a third phase of solid bitumen (PB III); thus, bitumen II and III may be paragenetically coeval. However, no major constraints about the origin of the solid bitumen of Assemblages I and III have been determined.

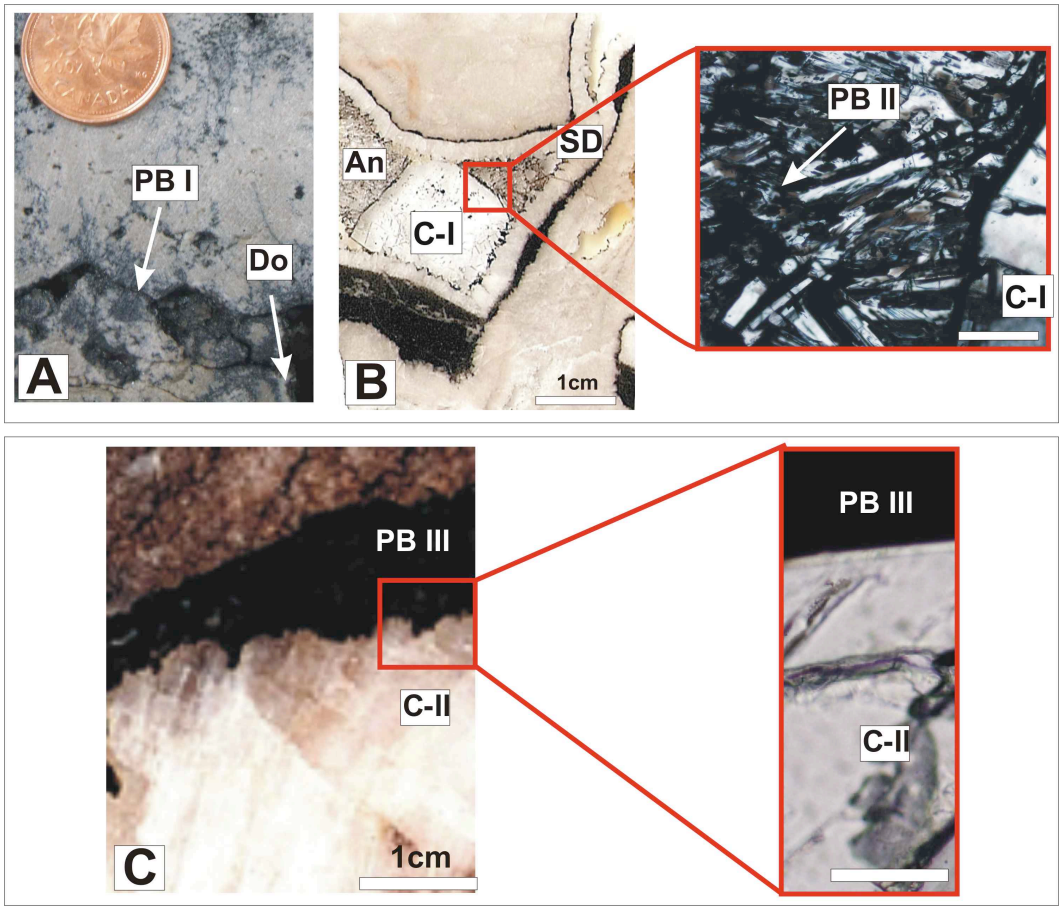

Figure 2.5. Solid bitumen assemblages. (**A**) Bitumen I of Assemblage I coating dolomite (Dolomite III) in vugs. (**B**) Assemblage II: bitumen II coating saddle dolomite, and anhydrite, adjacent to calcite-I. Pyrobitumen II enclosing anhydrite crystals is detailed. (**C**) Calcite-II postdating bitumen III. Detail of the contact between solid bitumen III and calcite-II; scale bar = 320µm.
(A) NA 321-08. Location: 6-34-57-21W5. Depth: 3434.4m. **(B)** Sample: NA 311. Location: 9-17-53-19W5. Depth: 3695.4m. **(C)** NA 322-08. Location: 6-16-55-18W5. Depth: 3319.3m.
Abbreviations: An = anhdyrite; C-I = calcite-I; C-II = calcite-II; Do = dolomite; PB I= solid bitumen I; PB II= solid bitumen II; PB III= solid bitumen III; SD = saddle dolomite.

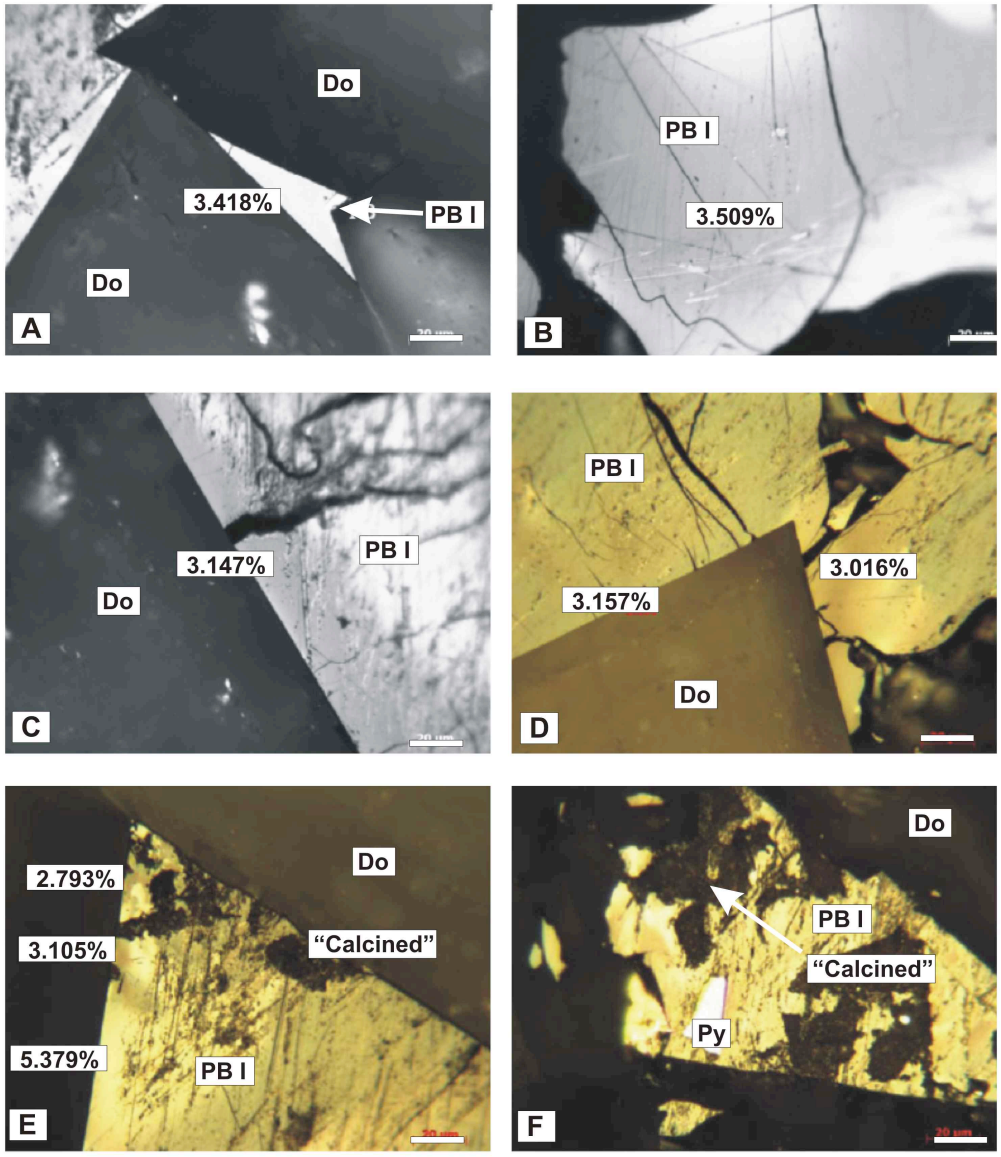

Figure 2.6. Bitumen petrography of sample NA 321-08. Location: 6-34-57-21W5. Depth: 3434.4m. Photomicrographs of pyrobitumen from the SCCC corresponding to **Assemblage I.** Reflected light, oil immersion objective. Scale bar = 20µm.
(**A-D**) High reflecting anisotropic coarse-flow mosaic pyrobitumen within matrix dolomite **(A**), to anisotropic domain mosaic proximal to dolomite crystals **(B - D**), anisotropic domain mosaic pyrobitumen showing signs of calcination **(E-F)**.
Abbreviations: Do = dolomite; PB I = solid bitumen I; Py = pyrite. All numbers represent $\%R_0$ and indicate location of measurement.

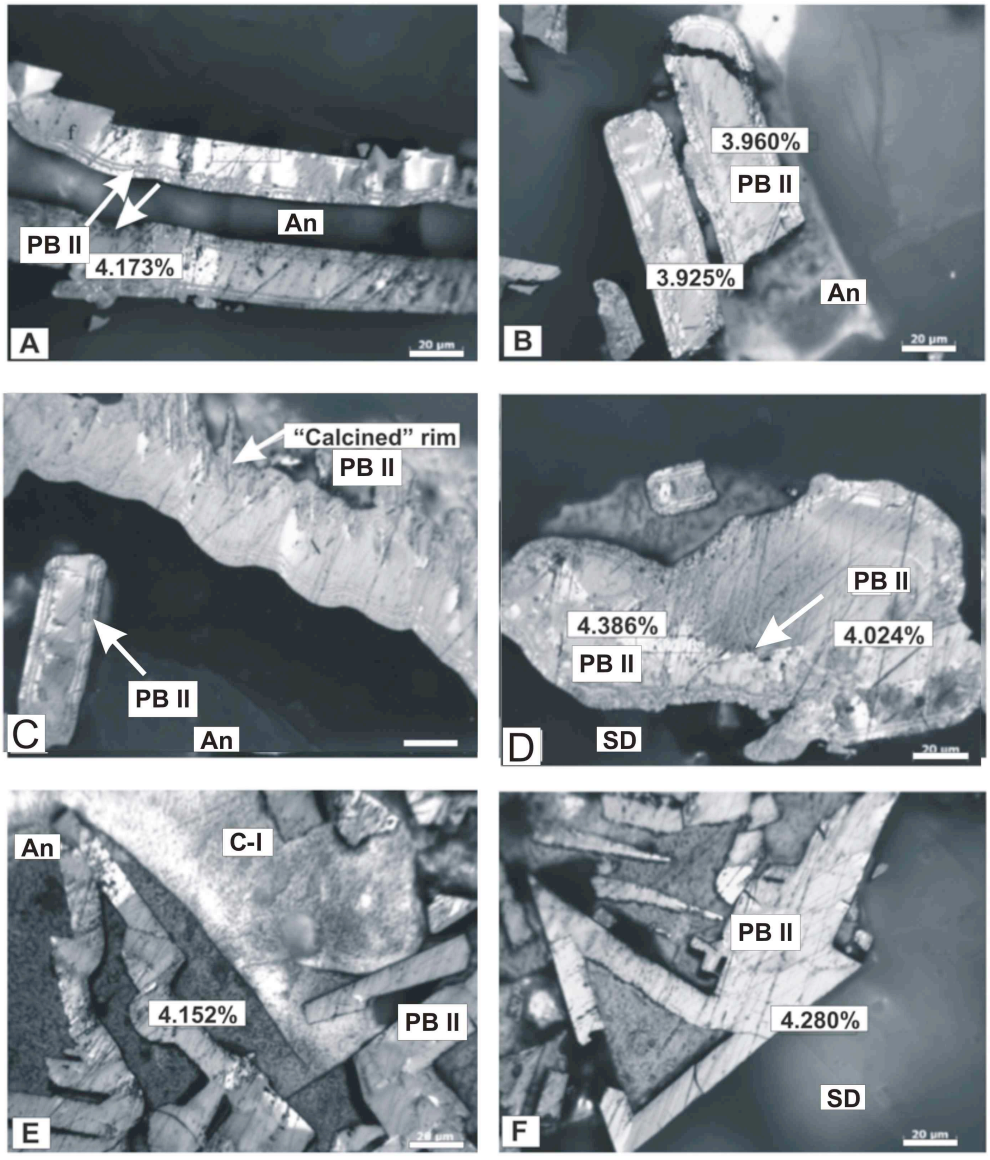

Figure 2.7. Bitumen petrography of sample NA 317-08. Location: 2-14-50-22W5. Depth: 4581.75m. Photomicrographs of anisotropic coarse flow to domain mosaic pyrobitumen from the SCCC corresponding to **Assemblage II.** Reflected light, oil immersion objective. Scale bar = 20µm.
High-reflective pyrobitumen (**A-F**) Coarse-flow mosaic pyrobitumen with striped anisotropy showing very fine to fine fibrous rim bands in a groundmass of anhydrite (**A, B and C)**, with **(C)** showing signs of calcination. Anisotropic coarse-flow mosaic pyrobitumen (bottom left of the images) in transition to domain mosaic pyrobitumen (upper right of the image) also with very fine fibrous rim bands. Angular fractured anisotropic coarse-flow and domain mosaic pyrobitumen filling the micro pores and fractures of calcite-I (C-I) and corroded dolomite (arrowed) **(E)** and saddle dolomite (arrowed) **(F)**. Abbreviations: C-I = calcite-I; PB II = solid bitumen II; SD = saddle dolomite. All numbers represent $\%R_0$ and indicate location of measurement.

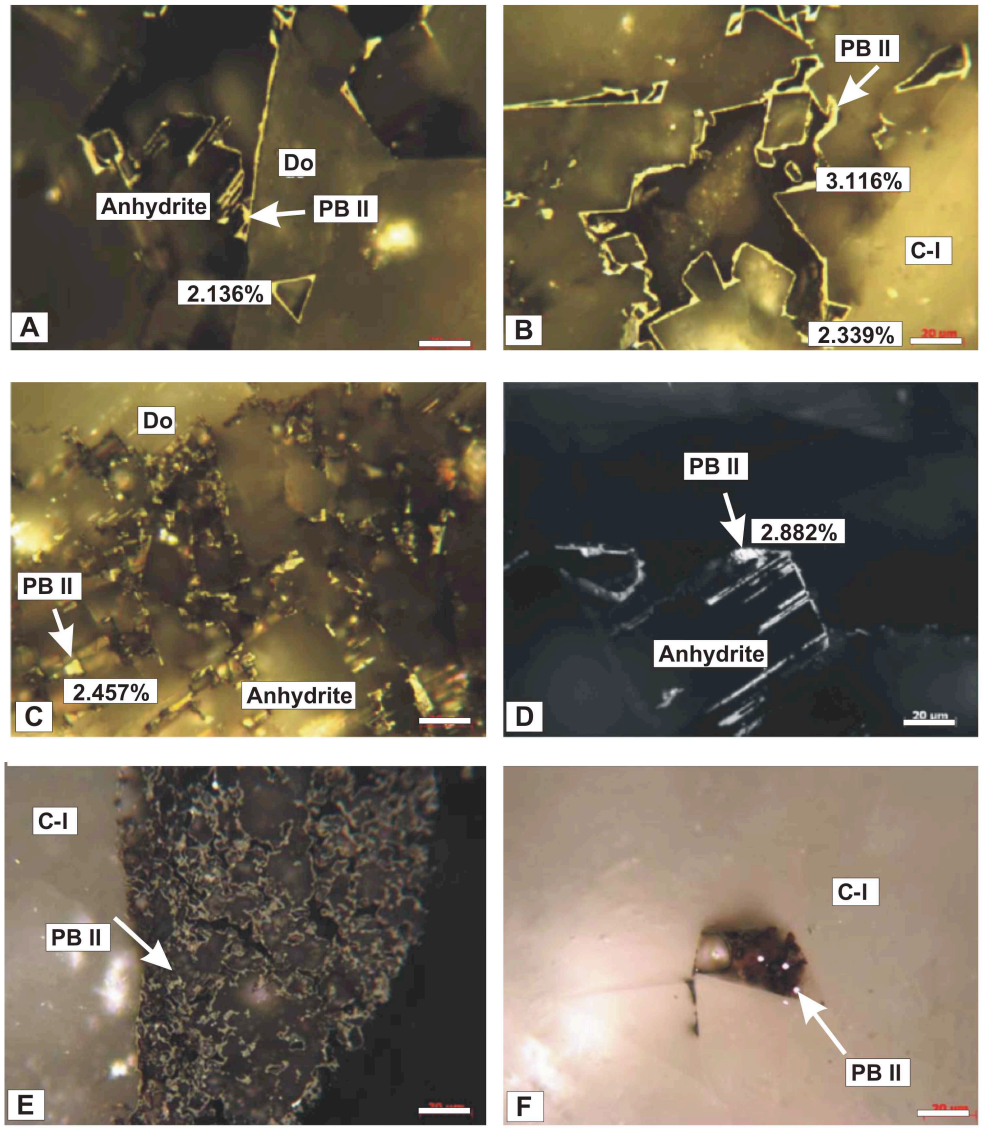

Figure 2.8. Bitumen petrography of sample NA 319-08. Location: 13-15-60-16W5. Depth: 2563m. Photomicrographs of pyrobitumens from the SCCC corresponding to **Assemblage II.** Reflected light, oil immersion objective. Scale bar = 20µm.
Photomicrograph of low-reflective fine-grained mosaic pyrobitumen migrated in to the pores of the carbonate matrix **(A)**. High reflecting anisotropic very fine to fine fibrous pyrobitumen migrated to dolomite and calcite, dolomite and anhydrite and saddle dolomite **(B, C, and D, r**espectively**)** micropores and fractures. Needle-like pyrobitumen (arrowed) and fine fibrous pyrobitumen adjacent to calcite-I (**E**). Cenospheric texture in pyrobitumen "within" micro fractures of calcite-I **(F).** Abbreviations: C-I = calcite-I; Do = dolomite; PB II = solid bitumen II. All numbers represent $\%R_0$ and indicate location of measurement.

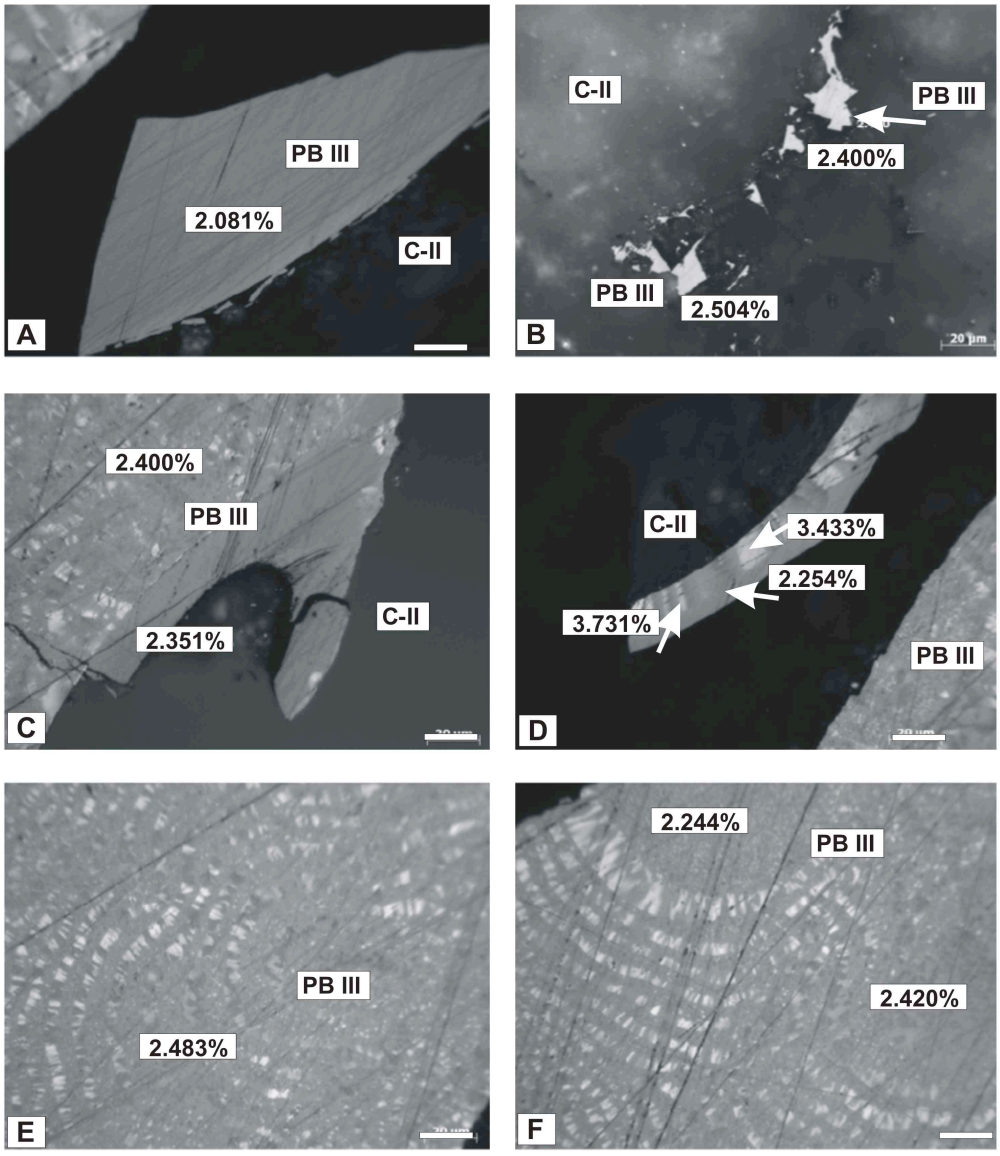

Figure 2.9. Bitumen petrography of sample NA 322-08. Location: 6-16-55-18W5. Depth: 3319.3m. Photomicrographs of pyrobitumens from the SCCC corresponding to **Assemblage III.** Reflected light, oil immersion objective. Scale bar = 20µm. (**A-B**) Low-reflecting isotropic pyrobitumen macerals. (**C**) High-reflectance and low-reflective bitumen in the same sample. (**D**) Pyrobitumen exhibiting 'striped' anisotropy and (**E-F**) transition from fine-grained anisotropic pyrobitumen to coarse-grained and coarse flow mosaics. All the pyrobitumen samples are adjacent to calcite-II (uniform grey colors). Abbreviations: C-II = calcite-II; PB III = solid bitumen III. All numbers represent $\%R_0$ and indicate location of measurement.

Based on the mineral and solid bitumen petrographic observations presented in **section 2.2.1** and **2.2.2**, the paragenetic sequence for the SCCC from Buschkuehle (2003) is modified and expanded (**Figure 2.10**). Because no petrographic evidence showing co-occurrence of calcite-I and II has been recorded, both cements and their associated phases are tentatively place in the same stage of the diagenetic sequence following the scheme of Machel and Buschkuehle (2008). Furthermore, Phase 18 of Stage III, which denotes hydrocarbon migration into the SCCC, is now expanded to Bitumen I, II, and III, whereby the latter two denote alteration products from the oil that migrated into the SCC during Stage III.

PHASE	→ → → → TIME → → → →	STAGE
1	Micrite envelopes	I
2	Anhydrite I, Dolomite I	
3	Dissolution I	
4	Pyrite I	
5	Calcite I	
6	Calcite II	
7	Calcite III	
8	Calcite IV	
9	Dolomite II	II
10	Dissolution II	
11	Pressure solution ----------	
12	Dolomite III ----------	
13	Pyrite II	
14	Fractures I	
15	Calcite V ----------	
16	Secondary anhydrite	
17	Fractures II /	III
18	Hydrocarbons/ Bitumen I (?)	
19	Dissolution III	IV
20	Saddle dolomite	
21	Anhydrite	
22	Solid Bitumen II (TSR)	
23	Calcite-I (TSR) --	
24	Elemental sulfur	
25	Fractures	
26	Solid bitumen III	
27	Calcite-II----------	
29	Fractures IV, anhydrite	V

Figure 2.10. Proposed paragenetic sequence modified from Buschkuehle (2003).

2.2.3. Carbonate Geochemistry

2.2.3.1. Stable C and O isotopic compositions

Carbon and oxygen isotope values of calcites I and II and associated saddle dolomite cements are listed in **Appendix I** and illustrated in **Figure 2.11.** The isotopic signatures of each type of calcite are distinct. The $\delta^{18}O_{VPDB}$ values of calcite-I span a narrow range from -7.8 to -11.8‰, whereas $\delta^{13}C_{VPDB}$ values range from -0.7 to -28.8‰. $\delta^{18}O_{VPDB}$ values of calcite-II are similar to those in calcite-I (–6.3 to –12.9‰), whereas $\delta^{13}C_{VPDB}$ values range from 0.6‰ to -8.1‰. Because the saddle dolomite associated with calcite-I is largely bitumen-coated, only a few samples could be analyzed. Saddle dolomite $\delta^{18}O$ and $\delta^{13}C$ values range from -4.7 to -6‰, and 1.7 to – 4.3‰, respectively.

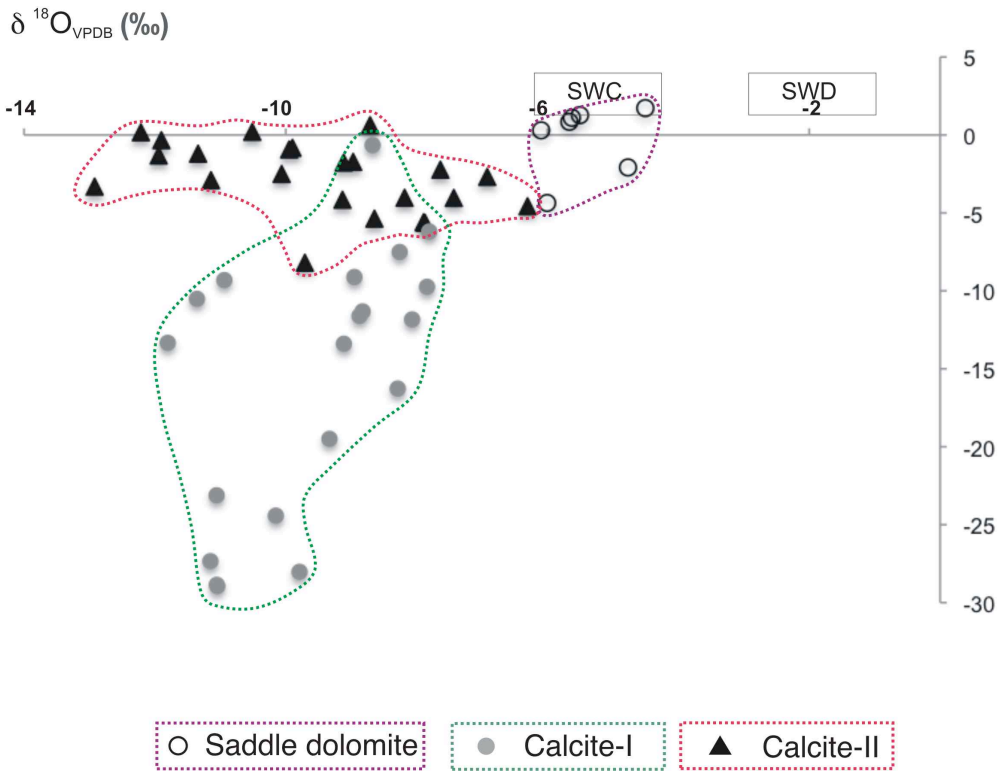

Figure 2.11. Stable isotope plot for late-diagenetic cements from the SCCC. The boxes indicate estimated ranges for marine calcite (SWC) and dolomite (SWD) that would have formed in equilibrium with Late Devonian seawater (Land, 1985; Carpenter and Lohmann, 1989; Hurley and Lohmann, 1989).

2.2.3.2. Sr isotopic compositions

In situ (laser ablation) and solution methods were applied to obtain Sr isotopic values of single crystals. In order to avoid contamination, the former was used in cases where both fine-grained and bitumen-coated crystals were present. Regardless of the method employed, when analyzed conjunctly it is clear that both display overall similar ranges.

Strontium isotope results (solution methods) of calcite I and II are listed in **Appendix IIa**. Calcite-I $^{87}Sr/^{86}Sr$ ratios range between 0.7084 and 0.7224, whereas calcite-II ranges between 0.7122 and 0.7199 (**Figure 2.12**). In situ Sr isotope analyses were conducted on both types of calcite (2 samples of calcite-I and 2 samples of calcite-II) and also in the associated diagenetic phases (**Figure 2.13, 2.14, Appendix IIb)**.

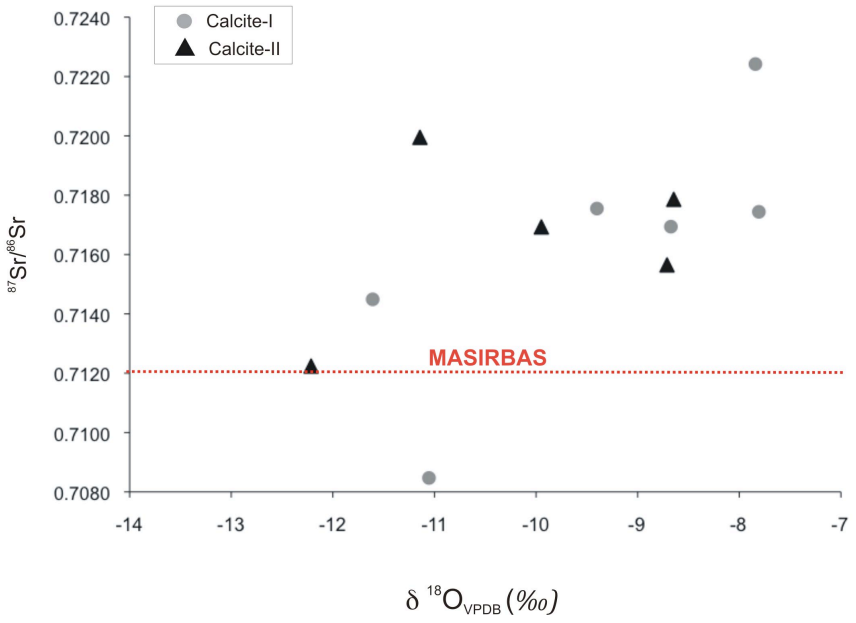

Figure 2.12. $^{87}Sr/^{86}Sr$ values (solution mode) versus $\delta^{18}O_{VPDB}$ (‰) for calcites I and II. A weak trend of increasing $\delta^{18}O$ ratios with increasing Sr isotopic values is evident in both types of calcite. MASIRBAS index (0.7120) represents the maximum strontium isotopic ratio that could be derived from basinal shales (Machel and Cavell, 1999). Almost all calcite values are higher than MASIRBAS.

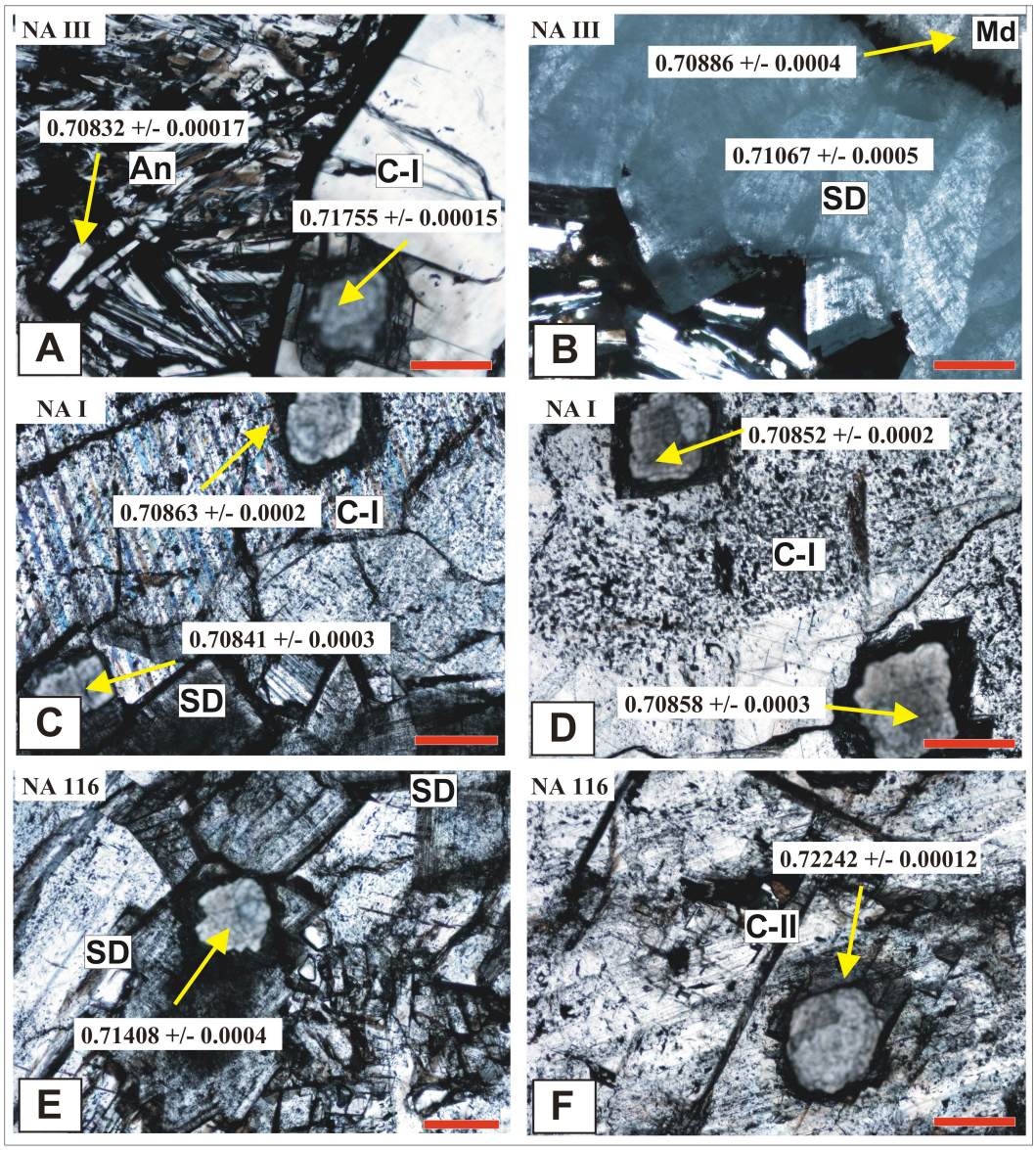

Figure 2.13. In situ $^{87}Sr/^{86}Sr$ results. Calcite-I **(A; C; D)**, and related anhydrite **(A)**, and saddle dolomite **(B; C).** Matrix dolomite value in **(B).** Saddle dolomite **(E)** related to calcite-II **(F)**.
Abbreviations: An = anhydrite; C-I = calcite-I; C-II = calcite-II; SD = saddle dolomite. Scale bar = 320µm. Pits are location of LA-ICP-MS analyses.
Sample NA III. Location: 16-22-58-19W5. Depth: 3375.4m. Sample NA I: Location: 11-29-59-16W5. Depth: 2734.4m. Sample NA 116. Location: 11-29-59-16W5. Depth: 2734.4m.

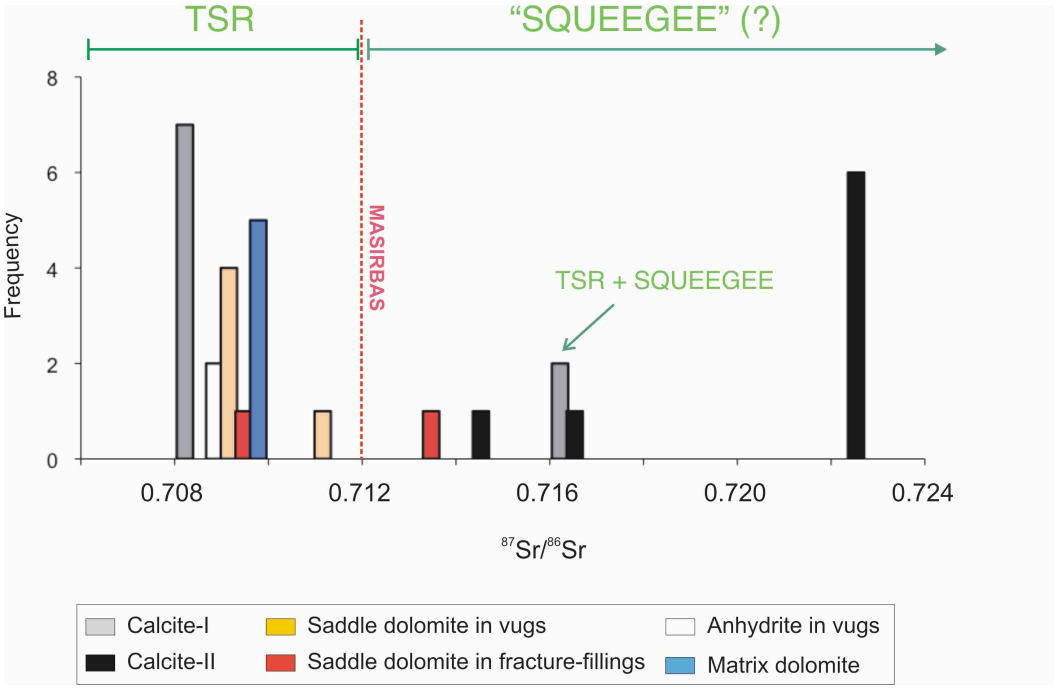

Figure 2.14. Histogram showing the laser ablation ICP-MS strontium isotope results. Frequency equals number of pits. Samples analyzed: 2 calcite-I, 2 calcite-II, 1 anhydrite, 3 saddle dolomite, 3 matrix dolomite.

2.2.4. Fluid Inclusion Petrography

Fluid inclusions hosted in calcites occur in primary, pseudosecondary, and secondary settings according to the criteria of Roedder (1984) and Van den Kerkhof and Hein (2001). Fluid inclusion assemblages were investigated in terms of location, inclusion shape, consistency of liquid/vapor ratios, and consistency of microthermometric results (Goldstein and Reynolds, 1994). Inclusions indicative of necking down or stretching were avoided during microthermometric measurements.

Primary inclusions appear in isolation, in small clusters, or are concentrated along growth zones (**Figure 2.15A**). Most of the primary inclusions display negative crystal shapes or irregular morphologies, and range in size between 5 and 40μm. Secondary inclusions typically possess nearly rectangular, flattened morphologies, smaller sizes (5 to 10 μm), and lie along healed fractures. Both types of calcite are inclusion-rich; however, large inclusions are common only in calcite-I. Five varieties of inclusions have been recognized at room temperature, namely: (I) two-phase aqueous inclusions (**Type A**); (II) H_2S-bearing aqueous inclusions (**Type B**); (III) liquid-only aqueous inclusions (**Type C**); (IV) liquid oil and vapor inclusions (**Type D**); and (V) CO_2-H_2O-bearing inclusions (**Type D**). Fluid inclusions in calcite-I are either type A or type B inclusions, whereas type A inclusions are the dominant type in calcite-II.

Type A: Two-phase (L-V) aqueous inclusions (**Figure 2.15A**) consist of a liquid and a vapor phase with a degree of fill of 90 to 95 vol. % (liquid). These inclusions are colorless to grayish, irregular in shape, and commonly from 5 to 40 μm in size. Two-phase inclusions are mostly primary but also occur as secondary trails with a size of around 10 μm or less in diameter. Some of these inclusions

show signs of leaking and necking, which is indicated by the presence of an unusually large vapor bubble.

Type B: H_2S-bearing inclusions (**Figure 2.15B**) consist of an aqueous liquid, a vapor bubble containing H_2S, and commonly a solid pseudo-daughter phase, and range in size from 5 to 50 μm. Elemental sulfur pseudo-daughter crystals were detected by Raman spectroscopy in well 2-14-50-22w5, and are found in calcite-I. Type B inclusions are only found in calcite-I.

Type C: Monophase (liquid-only) inclusions are scarce. They range in size from 5 to 15μm, and are commonly related to Type A inclusions in both types of calcites. Probably Type C inclusions are Type A inclusions that have not nucleated a vapor bubble.

Type D: The vapor bubble fills less than 15 vol. %. Hydrocarbon fluids are preserved as fluorescing oil-bearing fluid inclusions (**Figure 2.15C**). They are liquid oil-vapor inclusions seldom exceeding 15 μm in diameter and only occur as secondary inclusions along healed fractures in calcite-II.

Type E: CO_2-H_2O-bearing inclusions are primary in origin and range in size from 5 – 20 μm, representing about 15% of the inclusions studied. They are usually irregular in shape and commonly associated with Type A inclusions (**Figure 2.15D**).

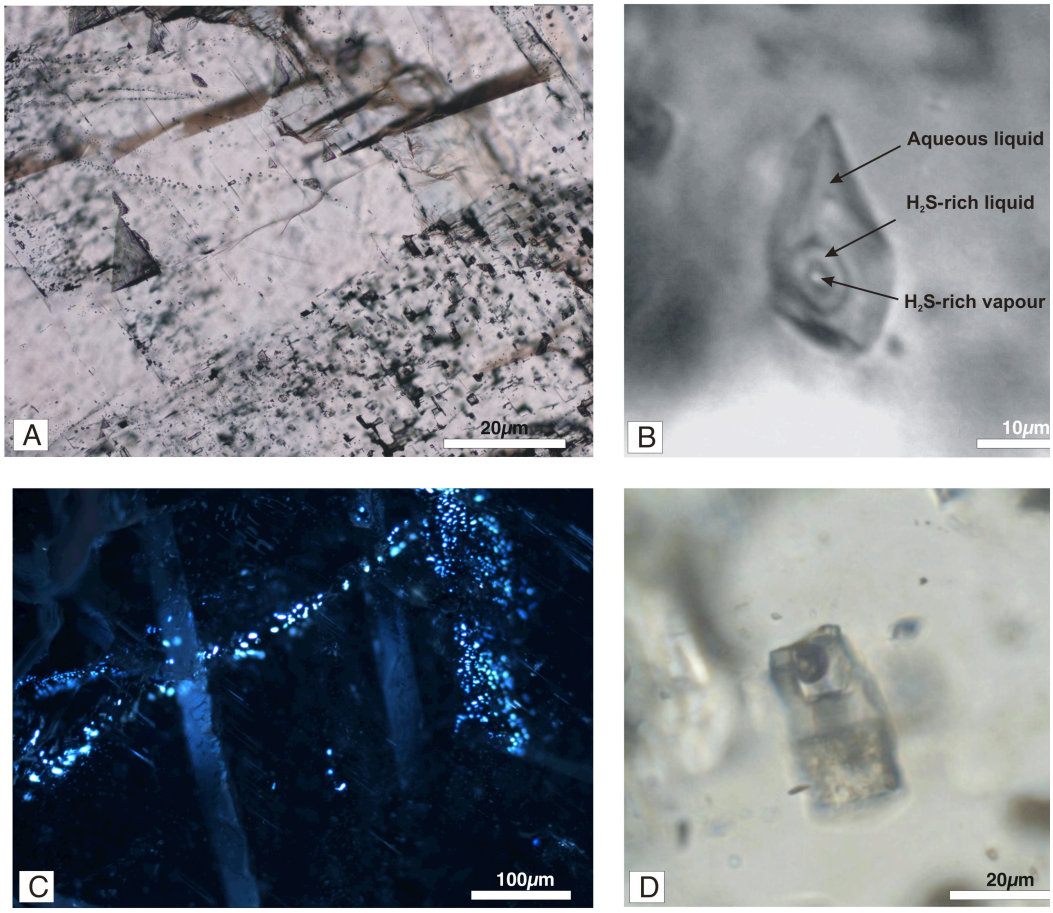

Figure 2.15. Photomicrographs illustrating the main types of fluid inclusion observed in this study. **(A)** Sample NA 270. Location: 5-25-21-22W5. Depth: 4468m. Relatively inclusion-free rim on calcite-II surrounding a core containing abundant primary two-phase aqueous inclusions (type A). **(B**) Sample NA 297. Location: 2-14-50-22W5. Depth: 3918.5m. H_2S-bearing inclusions (type B) in calcite-I. Inner phase is H_2S-rich vapor, the middle phase is H_2S-rich liquid (for further detail see Raman section). **(C)** Sample NA 320. Location: 16-18-61-15W5. Depth: 2768.5m.Type D fluorescent oil-bearing inclusions occurring along healed fractures in calcite-II. **(D)** Sample NA 123. Location: 6-16-55-18W5. Depth: 3319.3m.CO_2-H_2O-bearing inclusions (type E) in calcite-I.
To document H_2S-rich vapor and liquid components, photomicrograph **(B)** was taken during heating at +65.3˚C (for further explanations see section 2.3.4.2.).

2.2.5. Microthermometry

Over seven hundred individual fluid inclusions from eighteen samples of calcite from seventeen locations have been studied. Temperature measurements were focused on linked clusters of inclusions with visually similar phase ratios and shapes (Goldstein and Reynolds, 1994). In order to evaluate alterations postdating crystallization, several secondary inclusions occurring along trails were analyzed and the results were compared to primary inclusions. Microthermometric analyses were focused mostly on two-phase aqueous and H_2S-bearing inclusions, in which several phase changes were recorded. Few measurements were conducted in type D and E inclusions. In the majority of the inclusions total homogenization was observed upon heating through the disappearance of vapor into the liquid phase in both types of calcite. The small size of the fluid inclusions (<5 μm) in saddle dolomite inhibited the determination of homogenization and ice melting temperatures in that mineral. No microthermometric measurements were conducted on type C inclusions.

2.2.5.1. Type A inclusions

2.2.5.1.1. Calcite-I

The minimum and maximum values of homogenization temperatures (Th) of type A inclusions in calcite-I are between 92˚ and 193˚C with a mean of 141 ± 14˚C (n = 218; **Figure 2.16**). Final ice melting temperatures show a bimodal distribution with maximum and minimum values ranging from -20.5˚ to -4.3˚C, with a mean value of -14.4 ± 0.4˚C (n = 204; **Figure 2.17**), With few exceptions (samples NA 297 and NA 254), total freezing took place below −80°C, where the liquid changed into a brownish mass with no identifiable crystal structures. During heating, initial melting was observed between −56°C and −49°C with a mode of

-53 to -54°C (**Figure 2.18**). These eutectic temperatures indicate that the fluids are $CaCl_2$-rich aqueous solutions (Crawford, 1981).

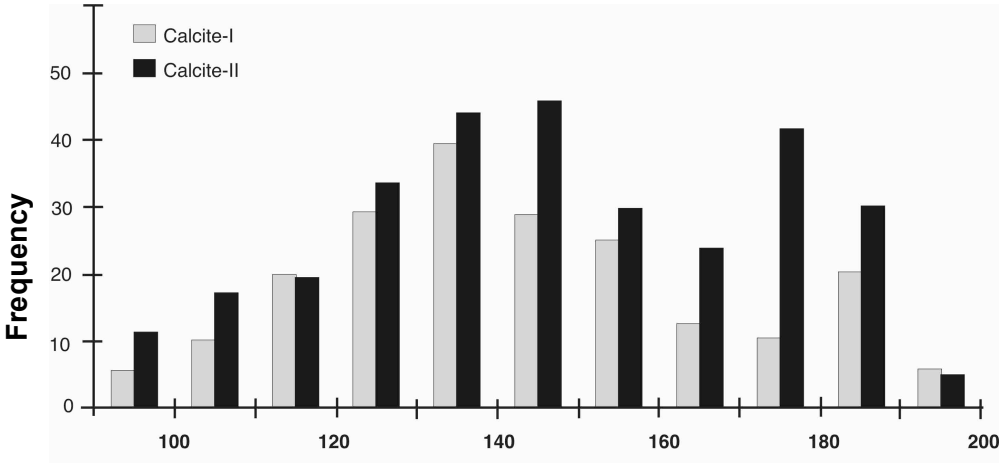

Figure 2.16. Histogram of homogenization temperatures obtained for Type A (liquid-vapor) inclusions hosted in calcite-I and II from the Marlboro-Windfall section. Range = 10˚C.

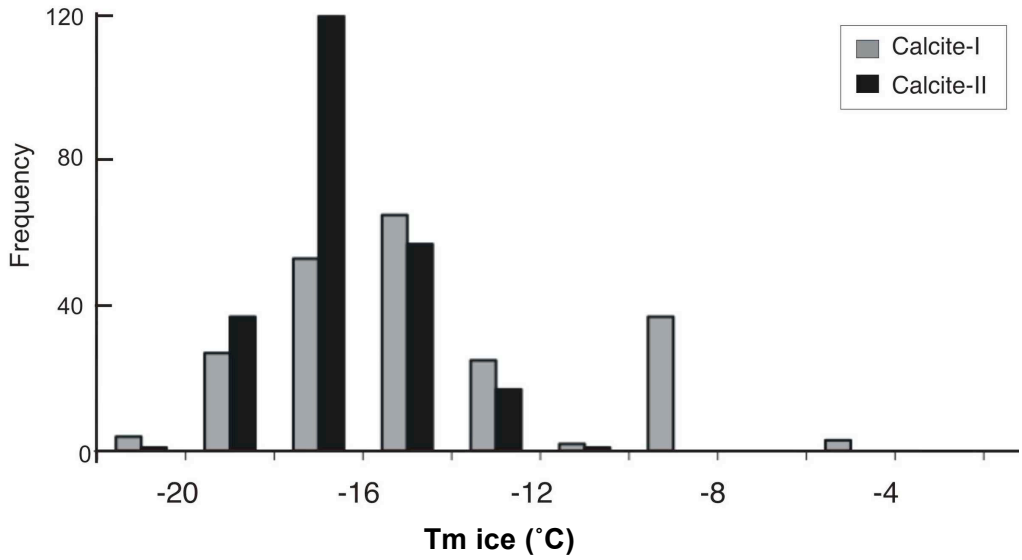

Figure 2.17. Distribution of final ice melting temperatures in Type A (liquid-vapor) inclusions from the Marlboro-Windfall section (n = 493). Note the weak bimodal character of salinities in calcite-I. Range = -2˚C.

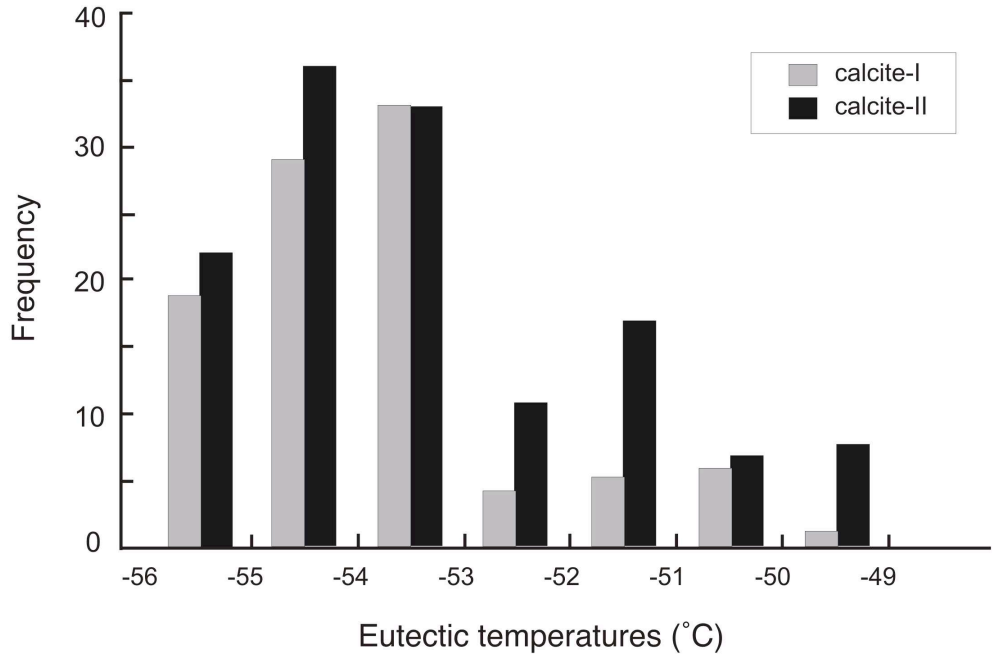

Figure 2.18. Histogram of eutectic temperatures in Type A (liquid-vapor) inclusions from calcite-I and II. Range = -1˚C.

Consequently, salinities were calculated as equivalent weight % $CaCl_2$ according to the equation of Zhang and Frantz (1987). Salinities range between 22.1 and 6.9 eq. wt.% $CaCl_2$, with a mean of 17.7 ± 0.4 eq. wt.% $CaCl_2$ (n = 204). There is no noticeable difference in eutectic temperatures between the measured primary and secondary inclusions.

Carbonic gases (most likely CO_2 with some CH_4) are present in a number of type A inclusions, as detected by clathrate melting at temperatures between -5°C and +12°C. These carbonic gases are mostly confined to inclusions in calcite-I (5 samples).

2.2.5.1.2. Calcite-II

Type A fluid inclusions in calcite-II, display homogenization temperatures from 91˚ to 198˚C, with a mean value of 147 ± 13˚C (n = 323; **Figure 2.16**) and

melting temperatures from -20.2ºC to -11.8ºC with a mean of -16.8 ± 0.6˚C (n = 289; **Figure 2.17**), with corresponding salinities ranging between 21.8 and 16.0 eq. wt.% $CaCl_2$ (mean of 19.8 ± 1.2). Two samples show evidence of carbonic components; clathrate melting was observed between –5°C and +8°C, although the temperature was difficult to record with absolute certainty. Initial ice melting temperatures are similar to those in calcite-I, and consequently typical for eutectic melting in the H_2O-NaCl-$CaCl_2$ system (**Figure 2.18**).

2.2.5.2. Type B inclusions

Type B inclusions were only observed in calcite-I. At low temperature, these fluid inclusions consist of an "outer" immiscible aqueous liquid phase, and an "inner" bubble of H_2S-rich liquid. The transition L to L+V to V in the "inner" bubble (Beny et al., 1982) has been observed in sample NA 297: upon heating, an "inner" vapor bubble appears in the vapor phase at around +55˚C and then disappears at temperatures circa 90˚C. These partial homogenization temperatures for the H_2S phase range between 80˚ and 99˚C, with a mean of 90˚ ± 4.7˚C (n = 45). Complete homogenization between the aqueous liquid and H_2S-rich vapor phase occurs at temperatures between 166˚ and 200˚C with a mean of 184.5 ± 8.5˚C (n = 45). Upon cooling, the system started melting at around -95˚C (eutectic temperatures). The latter, in addition to the partial homogenization values and the observation of the phase transitions, indicate the presence of H_2S, which is corroborated by Raman spectroscopy (see below). Final ice melting temperatures fall between -12 to -4.1˚C, revealing a wide range of salinities from 16 to 6.7 eq. wt.% CaCl. Disappearance of hydrates was recorded during heating after freezing at temperatures between +25 and +29˚C, consistent with the

presence of H_2S-hydrates, which melt at 29.5˚C (Pascal, 1960). Raman spectroscopic analyses were conducted in this sample to determine composition of the phases present.

2.2.5.3. Type D inclusions

Type D inclusions only occur in calcite-II. Homogenization temperatures (L_{oil} + V to L) in oil-bearing inclusions from two samples range between 92˚C and 115˚C, with a mean of 103.4± 5.1˚C (n = 23).

2.2.5.4. Type E inclusions

Partial homogenization temperatures (Th_{CO2}) were measured in calcite-II and range between 28.5 and 32˚C (29.6 ± 1.2˚C, n = 9), whereas homogenization temperatures vary between 127 to 160˚C, with a mean value of 146.7 ± 10.8˚C (n = 12).

2.2.5.5. Pressure correction

Determining if pressure correction should be applied is an important aspect in the interpretation of the fluid inclusion data. In this study, there is no direct evidence for two-phase (vapor + liquid) trapping conditions in the fluid inclusions record of calcite-I and II. Consequently, homogenization temperatures will be minimum estimates of the true temperature, and a pressure correction may be needed. However, Type B and E inclusions contain significant amounts of dissolved H_2S and CO_2, suggesting high gas partial pressures, possibly close to or at saturation levels, and thus, homogenization temperatures would reflect the entrapment conditions. Most hydrocarbon systems, especially during TSR, are in fact gas-saturated, so the SCCC system likely was also, despite the lack of direct evidence for gas-rich (vapor-phase) fluid inclusions. Based on these arguments, and under the assumption that the system is gas-saturated, no pressure correction of the fluid inclusion data was applied, and homogenization temperatures are taken to approximate trapping temperature values.

2.2.6. Raman Spectroscopy

Type A (liquid-vapor) inclusions and type B (H_2S-bearing) inclusions in four samples (3 calcites-I, and 1 calcite-II) were analyzed. Liquid and gaseous H_2S as well as elemental sulfur were detected in type B inclusions hosted in calcite-I (**Figure 2.19**). The calcite-I, type B inclusions are methane-free but contain CO_2 and H_2S in the gas bubble; none of these gases were detected in type A fluid inclusions in calcite-II.

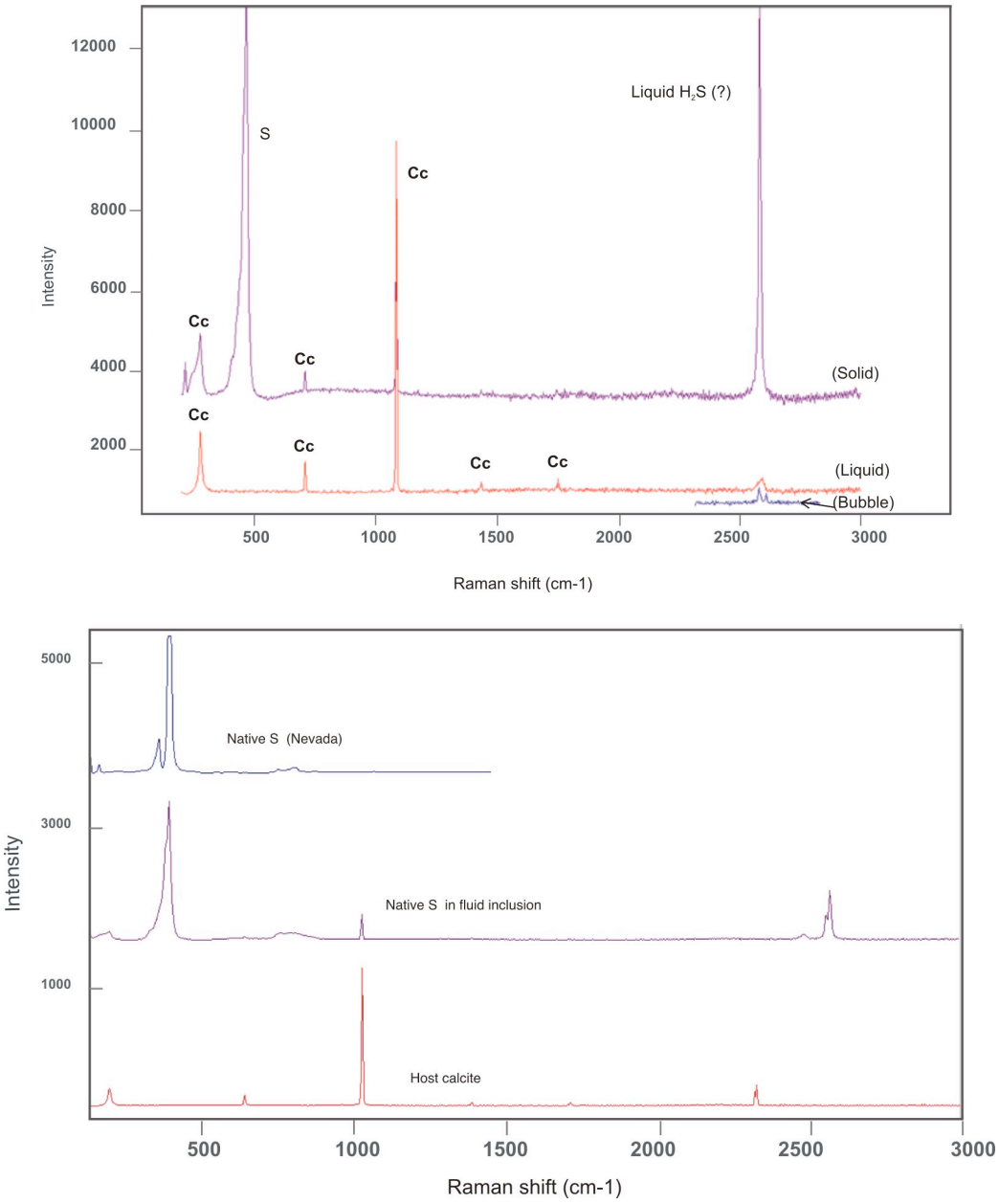

Figure 2.19. Raman spectra of type B fluid inclusions hosted in calcite-I. Abbreviations: Cc = calcite; S = elemental sulfur.

2.2.7. Bitumen Reflectance Values

Solid bitumen reflectance ($\%R_0$) was measured on eight samples from two statigraphic intervals: the Leduc and Nisku Formations (**Table 2.1, Appendix IV**). Owing to its reflectivity, most of the bitumen in the studied samples was identified as pyrobitumen of the meso- to cata-impsonite type (Jacob, 1989). Reflectance measurements are presented in **Figure 2.20**, and show a heterogeneous distribution of reflectance values in different wells at various depths.

Leduc and Nisku Formations reflectance values range from 1.62 to 6.61%, and 1.69 to 3.71%, respectively. A more detailed analysis shows a bimodal distribution of the reflectance values for the Assemblage I ranging from 2.15 to 5.89%, with a mean value of 3.26 ± 0.51%. The same bimodal distribution is seen in the Assemblage II, where reflectance values range from 1.6 to 6.61% with a calculated mean of 2.84 ± 0.83%. Assemblage III displays values between 2.4 and 5.24%, and a mean value of 2.71 ± 0.76% (**Figure 2.20**).

In order to calculate the maximum temperatures of maturity, the measured bitumen reflectance values were converted into vitrinite reflectance equivalent (%VRr) according to the method of Schoenherr et al. (2007). Vitrinite reflectance values were used to estimate peak temperatures (Tpeak) by applying the equation for burial overprint of Barker and Pawlewicz (1994) (see **Appendix IV**).

Table 2.1. Summary of bitumen reflectance data. Abbreviations: %Ro = bitumen reflectance value; N = number of measurements; SD = standard deviation.

Sample	Location	Depth	Unit	Organic type	Mean %Ro	SD	N
97/003 316-08	10-32-44-19w5	5326.6	Leduc	21-23	3.45	0.28	49
97/003 316-08	10-32-44-19w5	5326.6	Leduc	24	4.61	0.25	4
97/003 316-08	10-32-44-19w5	5326.6	Leduc	25	5.83	0.45	3
NA I 317-08	2-14-50-22w5	4581.75	Leduc	21	3.63	0.17	7
NA I 317-08	2-14-50-22w5	4581.75	Leduc	22-23	4.02	0.22	48
NA I 317-08	2-14-50-22w5	4581.75	Leduc	24	4.66	0.01	2
NA I 317-08	2-14-50-22w5	4581.75	Leduc	25-26	6.22	0.34	4
NA 160 318-08	9-17-53-19W5	3696.6	Leduc	2	2.72	0.23	16
NA 160 318-08	9-17-53-19W5	3696.6	Leduc	21	3.44	0.22	22
NA 2563 319-08	13-15-60-16w5	2563	Nisku	21	2.14	0.17	41
NA 2563 319-08	13-15-60-16w5	2563	Nisku	22-23	2.56	0.13	9
NA 208 320-08	11-29-59-16w5	2734.4	Nisku	2	1.77	0.06	37
NA 208 320-08	11-29-59-16w5	2734.4	Nisku	21-23	2.25	0.21	8
NA 208 320-08	11-29-59-16w5	2734.4	Nisku	25-26	3.23	0.20	5
NA 3434 321-08	6-34-57-21w5	3434.4	Leduc	21	3.21	0.24	46
NA 3434 321-08	6-34-57-21w5	3434.4	Leduc	25	4.45	0.50	9
NA 123 322-08	6-16-55-18w5	3319.3	Leduc	21-23	2.28	0.18	50
NA 123 322-08	6-16-55-18w5	3319.3	Leduc	25-26	3.86	0.32	8
9-20/005 323-08	9-21-58-19w5	3375	Leduc	21-24	3.06	0.34	47
9-20/005 323-08	9-21-58-19w5	3375	Leduc	24-26	4.79	0.61	8

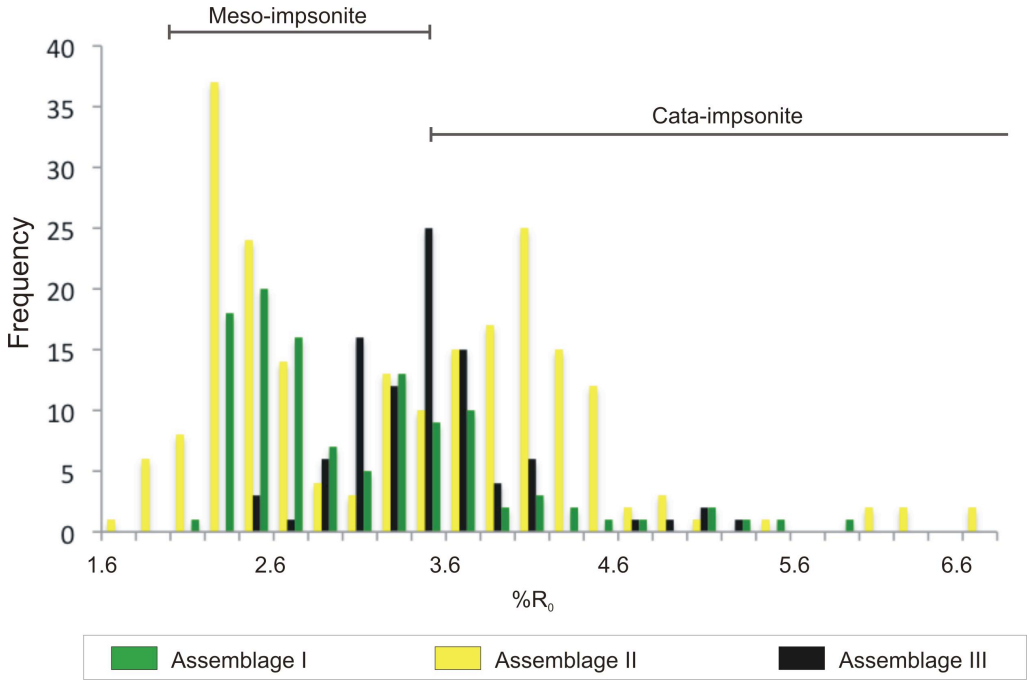

Figure 2.20. Reflectance histograms illustrating ranges of the bitumen reflectance values according to assemblage. Bitumen classification (meso-impsonite, and cata-impsonite type) is based on Jacob (1989).

CHAPTER 3

DISCUSSION

The petrographic and geochemical data of the SCCC presented in this study have shown the existence of two generations of late-diagenetic calcites (calcite-I and calcite-II). In order to constrain the chemistry of the paleofluids involved during calcite precipitation, and differentiate TSR calcites from probable "squeegee" calcites, the geochemical characteristics of the two types of late-diagenetic calcites is compared. Finally, petrography and maturity data of solid bitumen is integrated with microthermometric data to unravel the relative timing of late-diagenetic calcite precipitation and the thermal evolution of the SCCC.

3.1. Carbon and oxygen isotopic composition of calcites

Previous geochemical studies have shown that $\delta^{13}C_{VPDB}$ and $\delta^{18}O_{VPDB}$ isotope values of early marine cements in the study area vary between +2‰ and +1‰, and -6.0‰ and +1‰, respectively (Kaufman et al., 1989; Green, 1999; Buschkuehle, 2003) and fall within the range of late Devonian seawater calcites ($\delta^{13}C_{VPDB}$ = 2.5 ± 1‰, and $\delta^{18}O_{VPDB}$ = -4.5 ± 1‰; Hurley and Lohmann, 1989). In this study, $\delta^{13}C_{VPDB}$ values of late-diagenetic calcite cements show two well-defined signatures: (1) calcite-I with $\delta^{13}C$ values ranging between -0.7 to -28.8‰; and (2) calcite-II with values ranging between +0.6 to -8.1‰ (**Figure 2.11**).

Most calcite-I samples are significantly depleted in $\delta^{13}C$, which can only be explained as a result of organic matter oxidation. Possible sources of organic carbon include: biogenic methane (-70 to -50‰), gas condensates (-45 to -20‰), and crude oil (-30 to -20‰) (Machel et al., 1995). Accordingly, the lowest $\delta^{13}C$ values reported in this work would indicate that the isotopic carbon signature of calcite-I results from the thermal oxidation of any of these possible sources. Furthermore, most of these calcites are located in sour gas pools, they occur as cements in late-diagenetic vugs and/or as replacements of late-diagenetic anhydrite. Similar textures and $\delta^{13}C$ signatures formed via TSR are known from other reservoirs (Krouse et al., 1988; Heydari and Moore, 1989; Machel, 2001). Thus, calcite-I is herewith interpreted to be a by-product of TSR.

One sample of calcite-I does not have a negative $\delta^{13}C$ signature (NAIV $\delta^{13}C_{VPDB}$ = +0.7‰). This sample formed after saddle dolomite and shows partial replacement of anhydrite (**Figure 2.4**) which is typical for TSR calcite (Machel, 2001). However, little organic carbon was available at the time of NAIV precipitation. Overall, the wide range of carbon isotopic variations in calcite-I is best explained by different "extent" of TSR. When TSR began, calcite could precipitate from pore water whose carbon is dominated by matrix dolomite (rock-dominated system), with $\delta^{13}C$ ratios similar to Late Devonian marine values (see above). As TSR proceeded, carbon derived from hydrocarbon oxidation increasingly dominated the pore water (Machel et al., 1995), and was buffered to variable degrees by marine carbon (fluid-dominated system). Accordingly, the variable carbon isotopic signatures of calcite-I could be explained by the mixing of organic carbon with dissolved inorganic carbon. The range in $\delta^{13}C$ values of calcite-II can be explained in an analogous manner except that the total amount

of oxidized organic carbon was much smaller. This suggests that calcite-II may have been formed either before or after TSR, when very little oxidized organic carbon was available.

The oxygen isotopic values of calcite-I overlap with the range of values of calcite-II, and both are more depleted relative than marine values than oxygen isotopic signatures of early-diagenetic phases and saddle dolomite. It is well known that the oxygen isotopic ratio of solids varies as function of both temperature and the oxygen isotopic composition of the water from which the mineral precipitated (Hudson, 1975; Anderson and Arthur, 1983). Accordingly, it is reasonable to explain the observed oxygen isotopic ranges by these two controlling factors. The oxygen isotope ratio may be used to distinguish the type of water (*e.g.*, meteoric, marine, or evaporitic in origin) that was involved in mineral precipitation during diagenesis. The $\delta^{18}O$ signature of the water that was in equilibrium with calcite precipitated from it can be calculated from the Friedman and O'Neil (1977) calcite-water fractionation equation by using: (1) the mean fluid inclusion homogenization temperatures of each sample, assuming that Th equals trapping temperature, and (2) the corresponding $\delta^{18}O$ values of each calcite assuming that these values reflect isotopic equilibrium with the fluid from which the fluid inclusions formed. Accordingly, the $\delta^{18}O_{water\text{-}VSMOW}$ values of calcite-I (individual minimum value = +6.4‰ ± 1.1; individual maximum value = +10.5‰ ± 0.5) overlap with the range defined by calcite-II (individual minimum value = +2.7‰ ± 2; individual maximum value = +10.6‰ ± 0.9; **Figure 3.1**). These oxygen isotopic ranges are significant higher than those of present Devonian formation water from other parts of the Alberta Basin ($\delta^{18}O_{VSMOW}$ = -14 to +8‰; Hitchon and Friedman, 1969; Hitchon et al., 1971), and meteoric water (-

20 to -16‰; Connolly et al., 1990) suggesting that the majority of the late-diagenetic calcites did not form from these fluids. Instead, calculated oxygen isotopic values are in agreement with those of the present formation waters ($\delta^{18}O_{V\text{-}SMOW}$ = +4.0 to +8.7‰; Buschkuehle, 2003), suggesting that present-day formation waters are in equilibrium with both types of calcites. This finding supports the earlier conclusion that the SCCC is and was hydrologically closed relative to meteoric water, and probable has been closed hydrologically at least since sour gas formation during the Late Cretaceous (Machel and Cavell, 1999; Buschkuehle, 2003; Machel and Buschkuehle, 2008).

Considering that both calcite-I and II analyzed here are late-diagenetic in origin, and that the current formation waters have similar $\delta^{18}O$ values for calcite-I and II, it is reasonable to attribute the depleted $\delta^{18}O$ values to an elevated temperature range of precipitation. Given the temperature dependence of the oxygen isotopic fractionation, late-diagenetic calcites generated during normal burial conditions should display progressively lower oxygen values (Choquette and James, 1987). However, the distribution of $\delta^{18}O$ values with respect to the present-day reservoir depths does not exhibit a strong correlation (**Figure 3.2**). Nevertheless, the regression line displayed for calcite-I (r^2 = 0.59) intersects the axes close to the origin (0,0), suggesting a gradual depletion of oxygen isotopic values associated with depth, and consequently with temperature. In addition, the depleted $\delta^{18}O$ signatures documented in calcite-I can be also explained by water formed as a by-product of TSR (Machel et al., 1995). The lack of a strong correlation between $\delta^{18}O$ and depth is thus best explained as an hybrid of downdip T-increase and water formed from TSR. For calcite-II, the scatter of

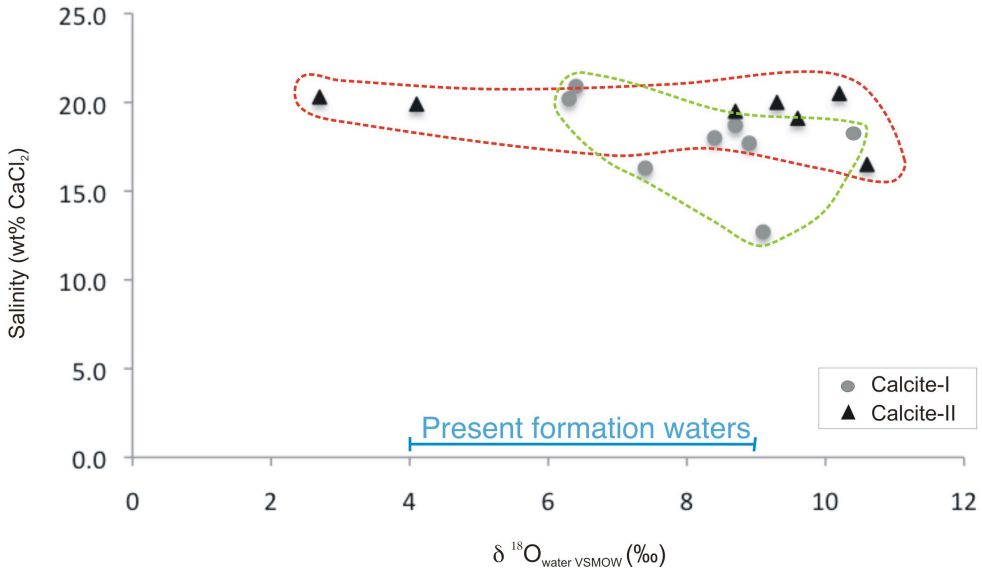

Figure 3.1. Cross-plot of $\delta^{18}O_{water\ V\text{-}SMOW}$ (‰) and salinity values of type A fluid inclusions of late stage calcites from the Marlboro-Windfall section. The calculated $\delta^{18}O_{water}$ values are much higher than that of present or Paleozoic seawater but are consistent with seawater evaporated to salinities between gypsum and halite saturation. Such brines are presently contained as formation waters in the SCC (Michael et al., 2003). Present formation water data from Buschkuehle (2003).

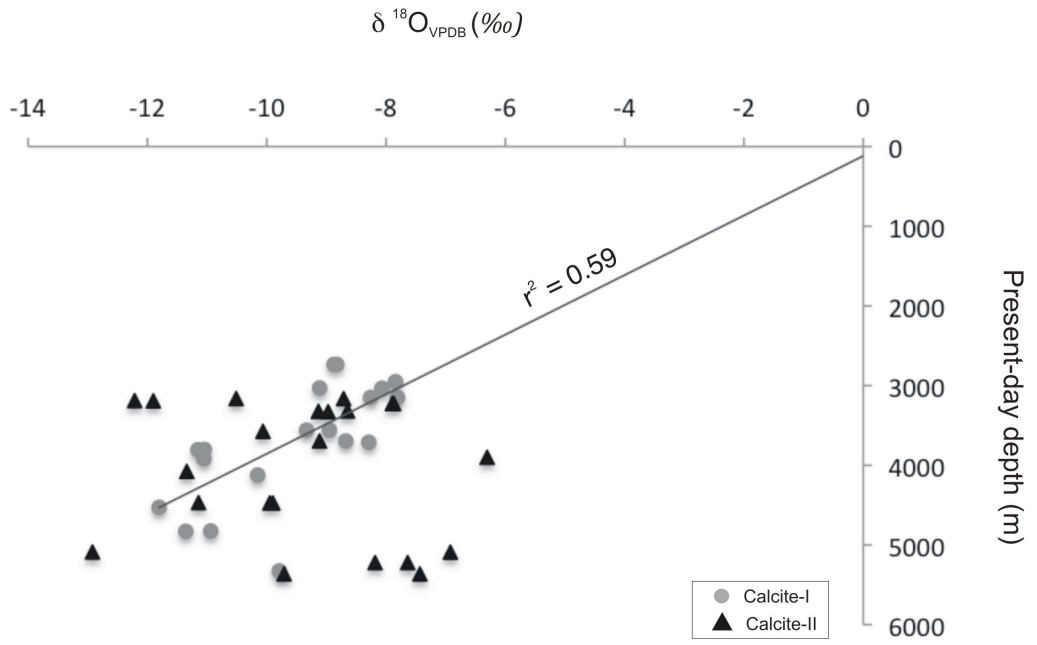

Figure 3.2. Cross-plot of $\delta^{18}O$ versus present-day depth. Trend line is indicated for calcite-I.

$\delta^{18}O$ values with depth suggests that there is no apparent correlation between these two parameters.

3.2. Fluid inclusions analysis of calcite-I and II

Several lines of evidence suggest the influence of TSR during the precipitation of calcite-I. For example, minimum and maximum homogenization temperatures are between 92˚C and 193˚C (assuming Th = Tt), respectively, with the majority of temperatures falling between 125˚ and 155˚C (mean = 141 ± 13.7˚C, n = 218), which is in agreement with the temperature limits at which TSR occurs (100 to 200˚C; Machel, 2001). Likewise, this range coincides with the idea of TSR taking place close or at maximum burial depths in the SCCC (6000 to 7000m; Machel et al., 1996; Green, 1999; Smith, 2001; Yang et al., 2001; Buschkuehle, 2003). This, in addition to the presence of elemental sulfur as pseudo-daughter inclusions and H_2S in fluid inclusions (type B inclusions), in conjunction with the highly depleted carbon isotopic values of calcite-I, suggests that TSR occurred during the precipitation of calcite-I.

Salinity values of fluid inclusions in calcite-I do not show a clear correlation with homogenization temperatures (**Figure 3.3**) and depth (**Figure 3.4**). Low salinity values were recorded in sample NA 297 (mean value of NA 297 = 12.7 ± 1.8 wt.% $CaCl_2$ eq.). However, as previously discussed, there is no evidence of mixing between parental fluids and meteoric waters. In this regard, TSR is believed to produce the dilution of formation water by up to 50% locally and up to 30% on reservoir scale (Worden and Smalley, 1996; Worden et al., 1996; Yang et al., 2001) but, according to Machel (2001), the amount of water generated would be negligible at regional scale.

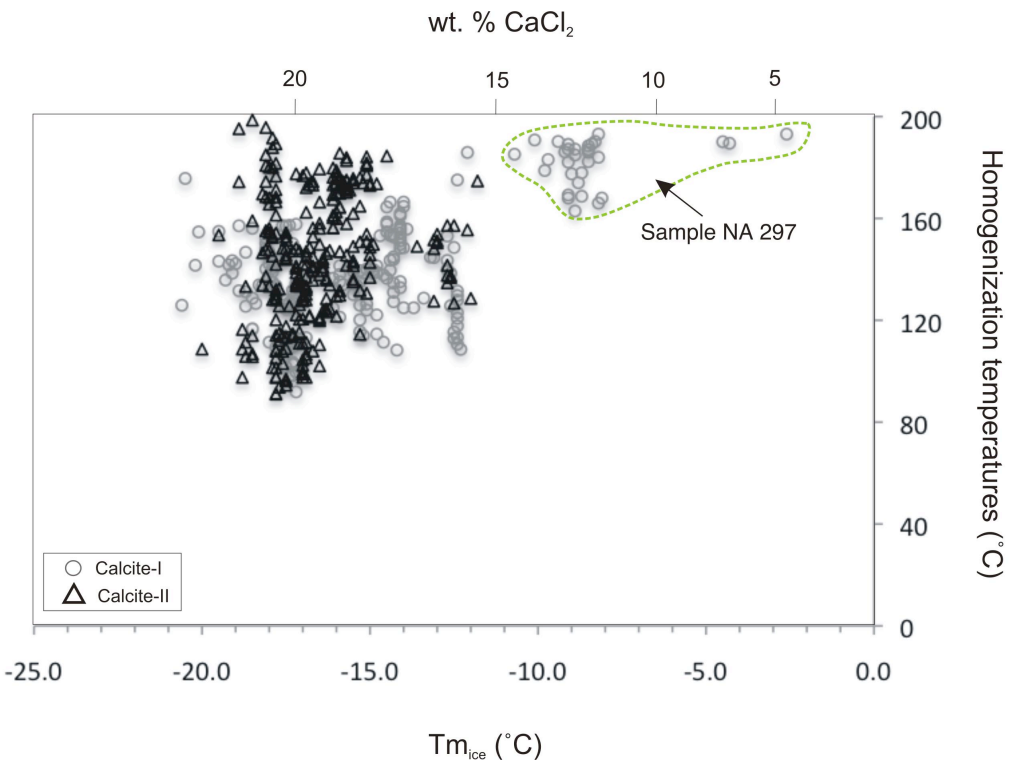

Figure 3.3. Cross-plot of homogenization temperatures of type A fluid inclusions from calcite-I and II versus final ice melting temperatures, and salinities calculated as equivalent wt. % $CaCl_2$.

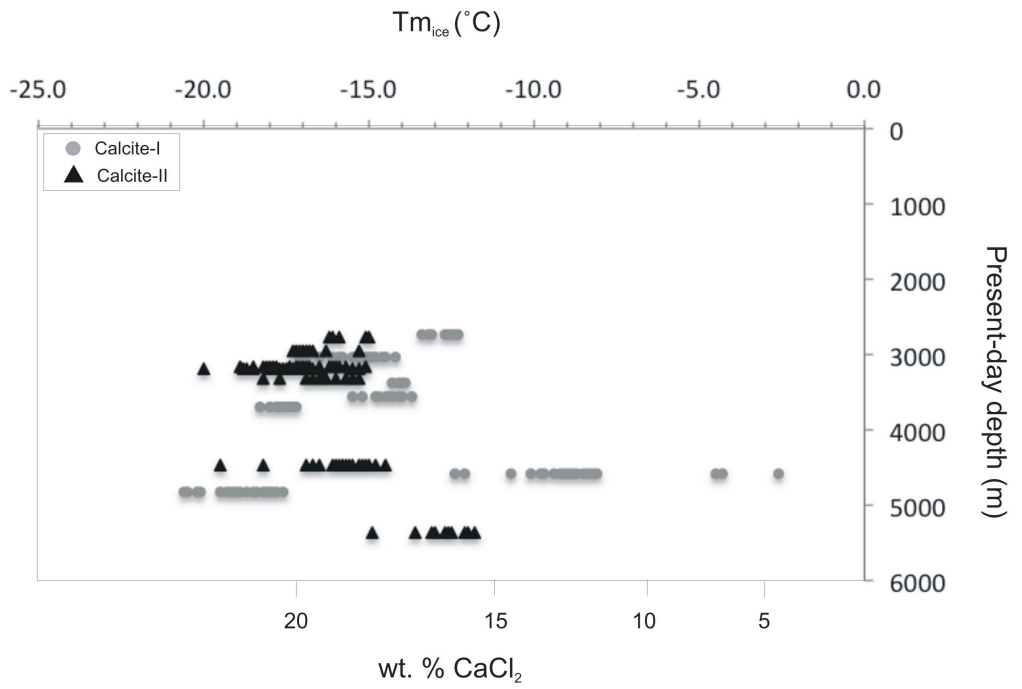

Figure 3.4. Plot of final ice melting temperatures and salinity calculated as equivalent wt. % $CaCl_2$ of type A inclusions from calcite-I and II versus present-day depth.

Thus, water may form due to TSR and could result in the local dilution of the formation water at or near the reaction site (*e.g.*, Worden and Smalley, 1996; Worden et al., 1996). Following the reasoning of Worden and Smalley (1996), the low salinity of the aqueous fluid inclusions of sample NA 297 paired with the highly depleted carbon isotopic values (NA 297), and the presence of H_2S-bearing fluid inclusions and elemental sulfur (detected also by Raman) could suggest that some of the water generated during TSR may indeed have been incorporated into the formational waters. Furthermore, this interpretation could explain the weak bimodal distribution in the final ice melting temperatures for fluid inclusions in calcite-I, and also indicates that TSR water locally diluted the formation waters in the SCCC.

Homogenization temperatures of aqueous inclusions in calcite-II have a mean value of 146.6 ± 12.9˚C (n = 323), and show a weakly bimodal distribution **(Figure 2.16).** One population (n = 256) has minimum and maximum homogenization temperatures between ~135˚C and 198˚C, with a mode of ~165˚C, whereas a small population (n = 67) displays minimum and maximum homogenization values between 91˚C and 135˚C, with a mode of 115˚C. As shown in **Figure 3.5**, such scattered distribution of homogenization temperatures values in calcite-II might be explained by the lack of correlation between Th and depth. Thus, the variable Th of calcite-II along the regional cross section would depend upon fracturing rather than on the geothermal gradient.

A very slight trend of decreasing ice melting temperatures of fluid inclusion with depth is seen in calcite-II (**Figure 3.4**). Geochemical analysis of Devonian formation brines from the sae study area has shown that heavier brines are located progressively farther updip (Michael, 2002; Michael et al., 2003).

Such pattern has been proposed to be consequence of the injection of metamorphic waters (which have relatively low salinity) in the Devonian aquifers due to tectonic forces (Michael, 2001; Machel and Buschkuehle, 2008). Even though both trends could be correlative, more data is needed to statistically corroborate a possible salinity trend in the fluid inclusion data of calcite-II.

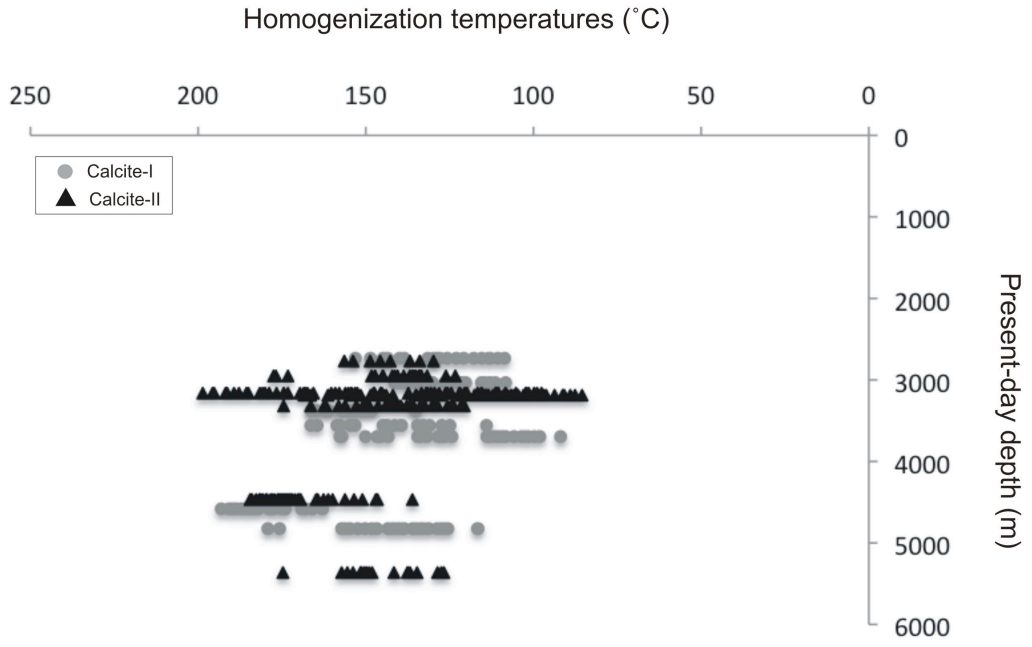

Figure 3.5. Present-day reservoir depth versus homogenization temperature of fluid inclusions for calcite-I and II. There is a weak pattern of decreasing temperature with decreasing depth in calcite-I; however, the same trend is not recorded in calcite-II.

On the other hand, microthermometric measurements of final ice melting temperature performed on calcite-II consistently reveal elevated salinities. Significantly, the distribution of final ice melting temperatures in the majority of fluid inclusions from calcite-I (except NA 297) and II (**Figure 2.17**), with mean

values of -14.4 ± 0.4˚C (n = 204) and -16.8 ± 0.6˚C (n = 289), respectively, suggests that salinity did not fluctuate widely during calcite precipitation.

One of the key arguments supporting squeegee-type fluid flow in the SCCC relies on fluid inclusions homogenization temperatures of late-diagenetic calcites (Machel and Cavell, 1999; Machel and Buschkuehle, 2008). Homogenization temperatures of calcite-I and II reported in the present study do not show a strong correlation with depth (**Figure 3.5**). Additionally, a trend of final ice melting temperatures in late-diagenetic calcites from deep (*e.g.,* Dalehurts field) to shallow reservoirs (*e.g.*, Marlboro field) would be expected if brine flow occurred from the downdip to updip ends along the study area. However, no clear correlation of increasing Tm with Th (calcite-I r^2 = 0.47; calcite-II r^2 = 0.050) or depth exists (**Figure 3.4**). Thus, the interpretation of tectonically-driven fluids influencing late-diagenetic calcite is not supported by the fluid inclusion data presented in this work, albeit “squeegee” flow is consistent with the data.

3.3. Strontium isotopic distribution

The isotopic ratios determined for the late-diagenetic calcites can be compared to the Maximum Strontium Isotope Ratio in Basinal Shales (MASIRBAS; Machel and Cavell, 1999). The MASIRBAS index defines the highest strontium ratio that can be derived from basinal Devonian shales under normal diagenetic conditions in the Alberta Basin. If the MASIRBAS index ($^{87}Sr/^{86}Sr$ = 0.7120) corresponds to the maximum Sr isotopic ratio of acid-extractable Sr from Devonian shales (Machel and Cavell, 1999), then strontium with values higher than 0.7120 could not have been sourced from these shales. Thus, the strontium isotope ratios can be used to determine if the fluids

responsible for late-diagenetic calcite cementation interacted with old, high Rb source rocks (*e.g.*, Precambrian granites, clastic sedimentary rocks, metamorphic rocks). Accordingly, signatures higher than MASIRBAS suggest the injection of radiogenic Sr from such sources.

Calcite-I in the SCCC exhibits both radiogenic (above MASIRBAS) and non-radiogenic (below MASIRBAS) Sr isotopic signatures. As an example, some calcite-I samples from the deepest part of the Marlboro-Windfall section ($^{87}Sr/^{86}Sr$ = 70852, #2-14-50-22w5; $^{87}Sr/^{86}Sr$ = 0.71098, #7-18-52-24w5) do not show evidence of a radiogenic strontium origin. Strontium isotopic signatures of the immediately preceding saddle dolomite (0.70841 ± 0.0003) and calcite-I (NA 297; $^{87}Sr/^{86}Sr$ = 0.70852 ± 0.0002) are similar to that of the precursor matrix dolomite (0.70814 ± 0.0006).

In the Windfall and Marlboro fields, radiogenic values are more common in calcite-I and vary depending on the mineral paragenesis. Sr isotopic values of both saddle dolomite (0.71067 ± 0.0005) and anhydrite (0.70832 ± 0.00017) display relatively non-radiogenic signatures, although when compared the latter shows slightly lower values. Conversely, the paragenetically linked calcite-I exhibits more radiogenic signatures (0.71755 ± 0.00015). The Sr isotopic values in these anhydrites are comparable to those of the early diagenetic matrix dolomite, and are similar to Devonian seawater values (0.7082-0.7084; Denison et al., 1997), which suggests local redistribution of early diagenetic anhydrite with "inherited" Sr-isotope ratios.

On the other hand, Sr isotopic values of calcite-II are all more radiogenic than MASIRBAS, whereas no systematic variations either with depth or along the section could be identified (**Figures 3.6, 3.7**). Radiogenic strontium was injected

into the fluid system during precipitation of calcite-I and II. Thus, Sr-bearing fluids may have been continuously injected into the aquifer, or they could be injected in two or more pulses coincident with the precipitation of both calcites. Based on the Sr isotopic composition of anhydrites, injection of Sr-bearing fluids in several pulses is the most likely scenario because Sr isotopic signatures of anhydrites are slightly lower than the paragenetically younger saddle dolomite and the later formed calcite-I (see **Figure 2.3E**). Low radiogenic Sr isotopic values in secondary anhydrites have been explained as a consequence of the dissolution of Middle Devonian depositional anhydrites (evaporites) and subsequent reprecipitation in the Swan Hills and Leduc reservoirs (Kaufman et al., 1990; Green, 1999). However, the intimate linkage between solid bitumen and anhydrite, in addition to the depleted carbon isotopic values of the postdating calcite-I, challenge this interpretation. Lowering of the Sr signal of the formation waters by dissolution of primary anhydrites does not completely explain the elevated Sr isotopic signatures of calcite-I (formed at expense of the anhydrite), and the elevated Sr isotopic signature reported in some secondary anhydrite from the SCCC (Smith, 2001; Buschkuehle, 2003). Accordingly, some reservoirs appear to have been exposed to radiogenic Sr-bearing fluids during TSR as previously shown by Machel and Bsuchkuehle (2008).

The influence of tectonically-driven fluids on late-diagenetic calcites from the Southesk-Cairn Carbonate Complex (SCCC) was first proposed by Machel et al. (1996). Evidence supporting this contention comes from anomalous homogenization temperatures in late-diagenetic calcite cements showing higher values than those estimated to have occurred during maximum burial (Machel and Buschkuehle, 2008) plus Sr-isotope ratios in late-diagenetic calcites higher

than MASIRBAS (Machel and Cavell, 1999). Furthermore, a general northeastward flow direction through the complex had been interpreted from updip decreasing $^{87}Sr/^{86}Sr$-ratios in late-diagenetic calcite cements (Machel and Cavell, 1999). Thus, tectonic compression was proposed as a mechanism that drove fluid flow in the SCCC (Bachu, 1995; 1999; Machel et al., 1996; Machel and Cavell, 1999; Buschkuehle, 2003; Machel and Buschkuehle, 2008).

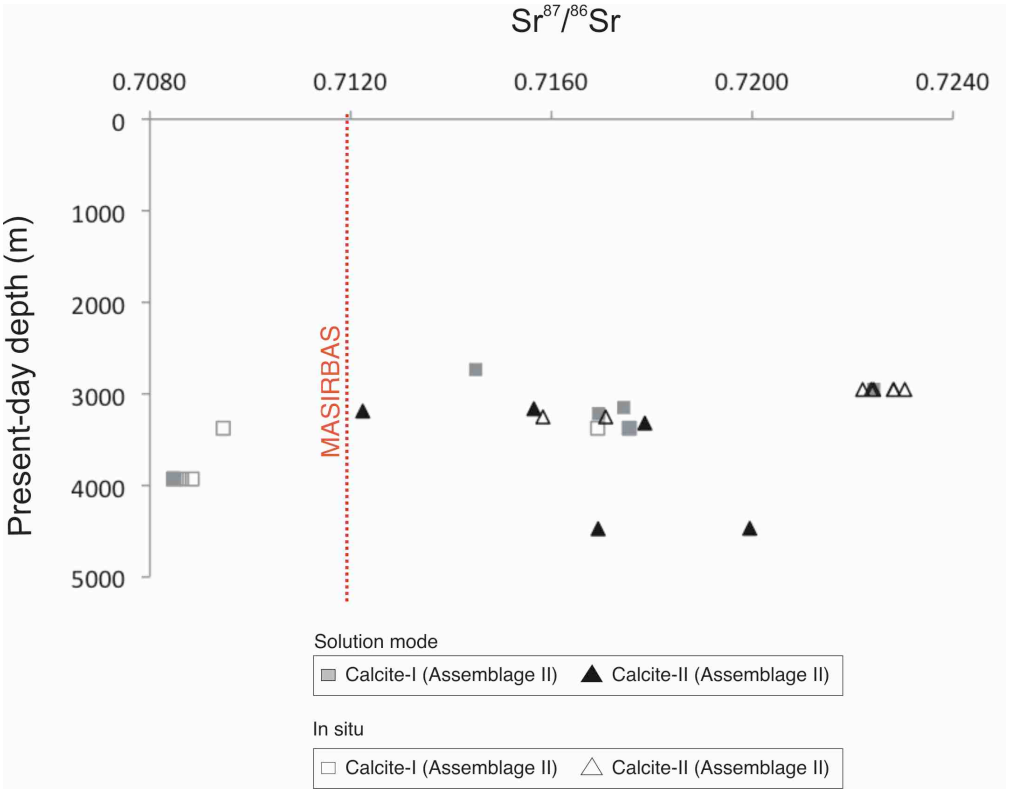

Figure 3.6. Strontium isotopic values of calcite-I and II versus present-day depth.

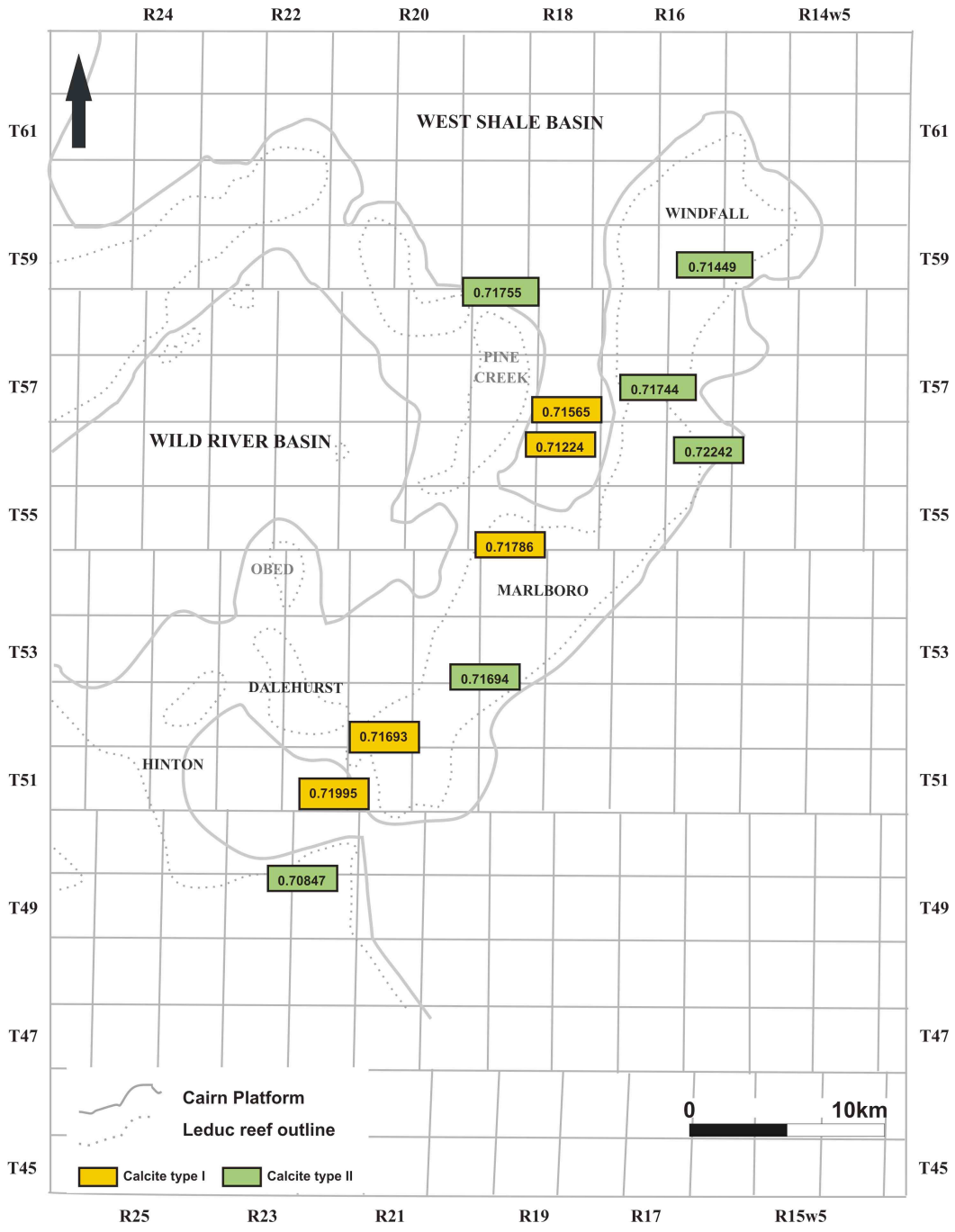

Figure 3.7. Distribution of $^{87}Sr/^{86}Sr$ values in calcite-I and II (from this study) along the Marlboro-Windfall section.

In this study, no discernible pattern in Sr isotopic values of late-diagenetic calcites (calcite-I and II) is observed along the Marlboro-Windfall section (**Figure 3.6, 3.7**). Instead, Sr isotopic compositions vary widely at any given depth, suggesting non-uniform fluid flow. Lateral fluid flow in combination with vertical flow along fractures and faults best explains the observed distribution of the Sr isotopic values of both types of calcites across the study area (see also, Green, 1999; Smith, 2001; Machel and Buschkuehle, 2008). Fractures could be generated during tectonic compression connecting different stratigraphic intervals through which fluids could have been injected into the formational waters.

3.4. Maturity data and burial constraints

Along the section (depicted in **Figure 1.2)**, the lowest bitumen reflectance values correspond to samples located at shallow depths, whereas maxima were recorded in the deepest part of the area (**Figure 3.8**). Overall, the reflectance values of bitumen associated with assemblages I, II, and III show a linear depth-thermal maturity trend (r^2=0.8; **Figure 3.9**).

Calculated equivalent %VRr yield a range of: (a) 1.82 to 3.53% for Assemblage I bitumen; (b), 1.45 to 4.46% for Assemblage II bitumen; and (3) 1.86 to 3.88% for Assemblage III (**Figure 3.10**). Additionally, Green (1999) reported reflectance values (2.19 and 2.69%) and equivalent %VRr (1.75 and 2.06%) for two isotropic bitumens, which are similar to the ranges recorded in this study. All these ranges are plotted in **Figure 3.11** and are consistent with the thermal maturation of the wet to dry gas zone (Powell and Snowdon, 1983; Taylor et al., 1997).

Minimum and maximum temperatures estimated from %VRr yield a Tpeak ranging from 184˚ to 219˚C for Assemblage I (probable thermal cracking bitumen), 154˚ to 256˚C for Assemblage II (probable TSR bitumen), and 169˚ to 244˚C for Assemblage III (bitumen related to calcite-II). Using peak temperatures, and considering a paleogeothermal gradient of 30˚C/km (previously suggested as normal geothermal gradient for the Alberta Basin; Hitchon, 1984; Suggate, 1998; Buschkuehle, 2003), the maximum burial depth can be estimated as: (1) 6840-6900 ± 300m for bitumens of Assemblage I; (2) 6020-7370 ± 250m for bitumens of Assemblage II; and (3) 6170-6790 ± 430m for bitumens of Assemblage III. Given that present-day depths in the study area are *ca.* 2700 and 5500m, and the above-mentioned estimated maximum burial is between 6000 and 7900m, a sediment pile of around 2500 would appear to have been eroded away during uplift. The latter estimate is in agreement with the thermal modeling presented in some previous studies (Hitchon, 1984; Nurkowski, 1984; Green, 1999). Based on the bitumen reflectance data, peak temperatures up to ~260˚C were reached in the SCCC during burial (**Table 3.1**; **Figure 3. 12**), which is significantly above the regional theoretical estimates for the Complex (~220˚C, see Machel and Buschkuehle, 2008). Considering that these values are higher than the mean homogenization temperatures recorded in any type of late-diagenetic calcite (I or II), it is clear that none of those cements were formed at maximum burial.

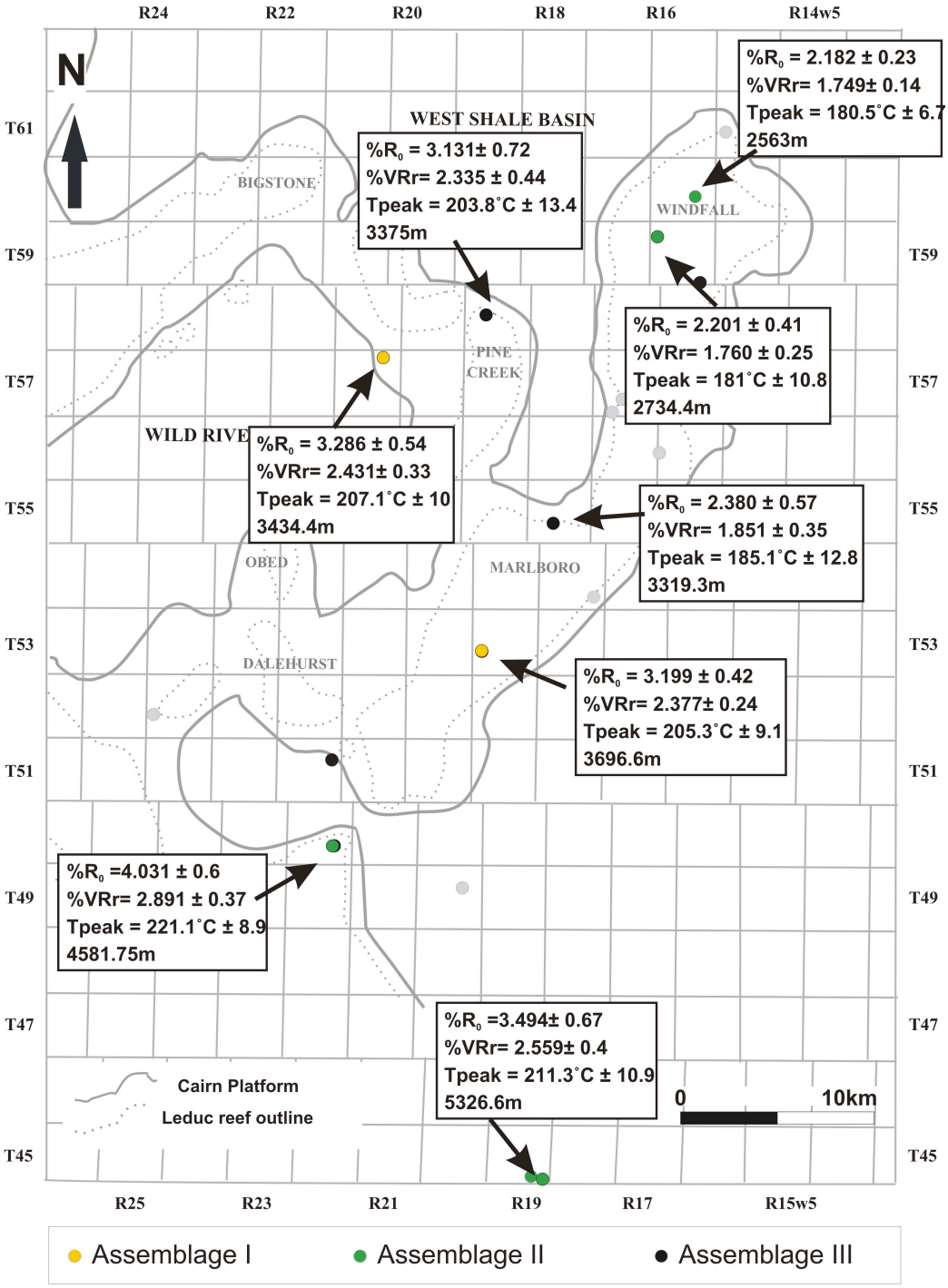

Figure 3.8. Distribution of bitumen reflectance values ($\%R_0$) and calculated vitrinite reflectance (%VRr), and peak temperatures (Tpeak) along the Marlboro-Windfall section.

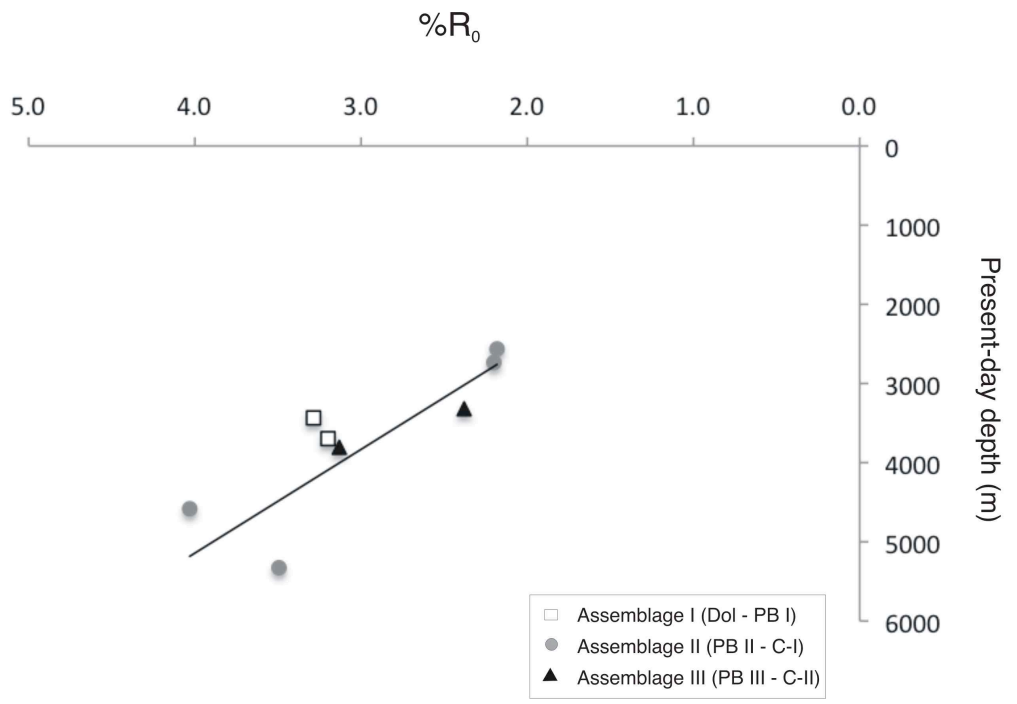

Figure 3.9. Cross-plot showing the distribution of mean bitumen reflectance values (%R_0) versus present-day depth.

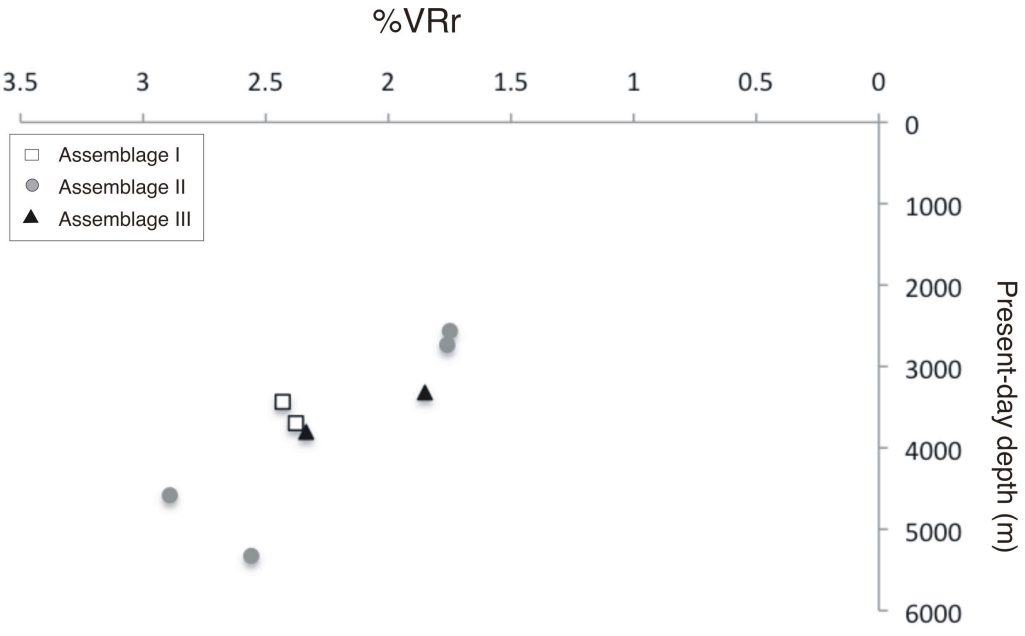

Figure 3.10. Plot of calculated mean vitrinite reflectance values (%VRr) versus present-day depth.

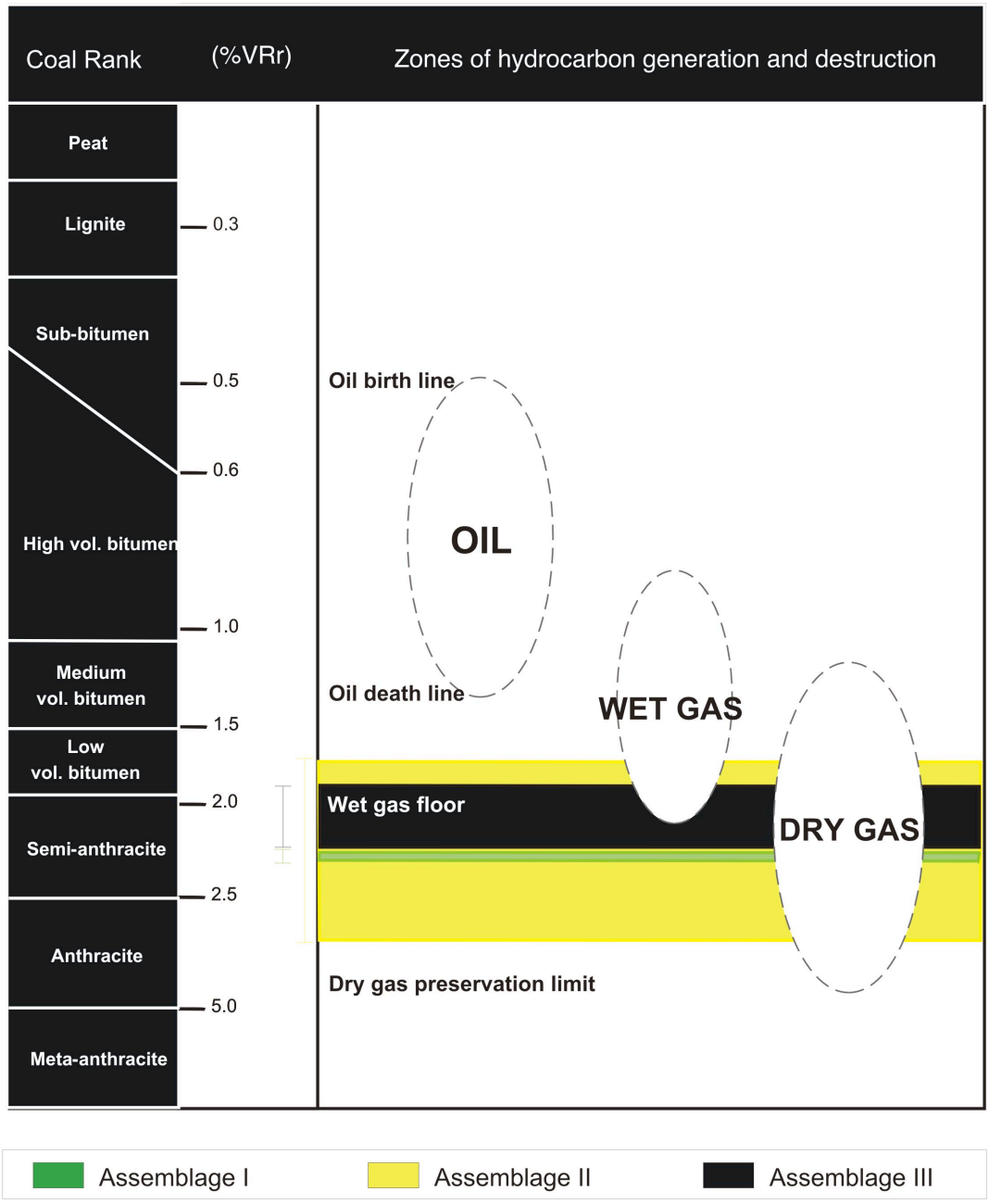

Figure 3.11. Correlation between coal rank stages, oil and gas maturity rank with corresponding vitrinite reflectance values. The rectangles indicate the mean vitrinite reflectance values calculated from $\%R_0$ data for each association described in this work. Modified from Taylor et al. (1998), and Koester et al. (2008).

Table 3.1. Summary of mean peak temperatures data. Abbreviation: N = number of measurements; SD = standard deviation.

Sample	Location	Depth	Assemblage	Mean peak temperature (˚C)	SD	N
NA 3434 321-08	6-34-57-21w5	3434.4	I	207.1	10	55
NA 160 318-08	9-17-53-19W5	3696.6	I	205.3	9.1	38
NA 2563 319-08	13-15-60-16w5	2563	II	180.5	6.7	50
NA 208 320-08	11-29-59-16w5	2734.4	II	181	10.8	50
NA I 317-08	2-14-50-22w5	4581.75	II	221.10	8.8	61
97/003 316-08	10-32-44-19w5	5326.6	II	211.3	10.9	56
NA 123 322-08	6-16-55-18w5	3319.3	III	185.1	12.8	58
9-20/005 323-08	9-21-58-19w5	3375	III	203.8	13.4	55

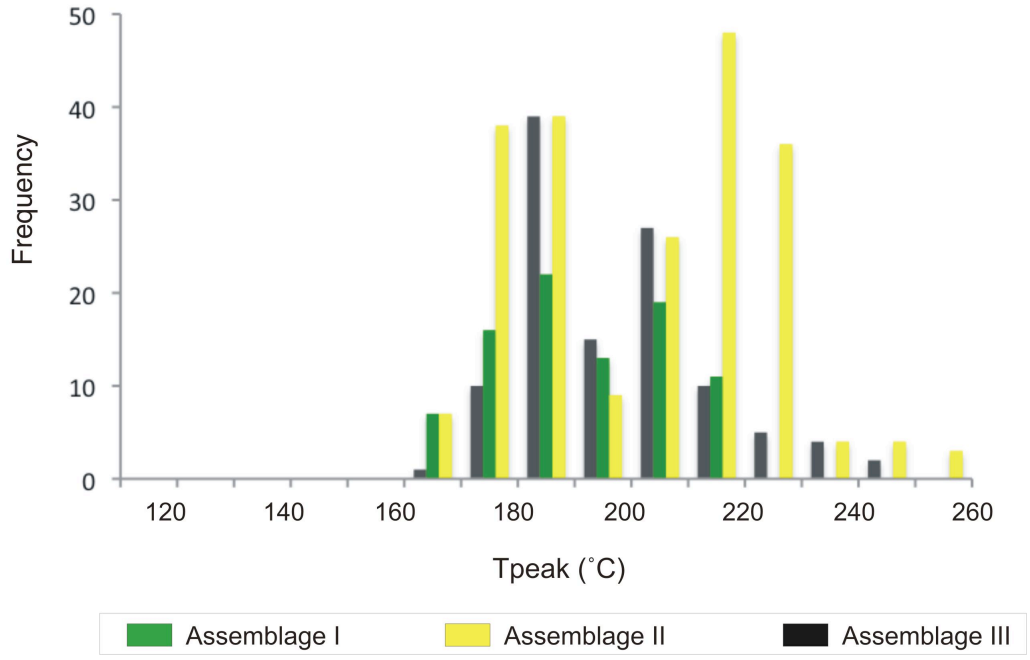

Figure 3.12. Distribution of peak temperatures of the different solid bitumen Assemblages.

3.5. Analysis of solid bitumen textures and reflectance data

Solid bitumen with variable reflectance values in the same sample can be attributable to: (1) different sources and more than one oil migration episode (*e.g.*, Gentzis and Goodarzi, 1990); (2) different origins (e.g. in situ thermal cracking, en route-migration- thermal cracking, and TSR; Parnell, 1996; Stasiuk, 1997); (3) differentiation on reservoir scale (*e.g.* Wilson, 2000), and (4) analytical error. Considering that there is an unique source of oil in the Devonian system (see e.g. Mossop and Shetsen, 1994), and that this system remained hydrologically closed since the Tertiary (e.g. Michael, 2001) option (1) is discarded. In addition and although variable, analytical error does not alter the interpretation.

The relatively wide scatter of bitumen reflectance values in the SCCC (about 1.7% up to 6.2 $\%R_0$, **Figure 2.20**) reflects the anisotropic character of bitumen, and also the elevated maturity levels of the organic matter. Furthermore, a range of textures of solid bitumen has been recognized in this study but only a few of them are indicative of the precursor material (Nandi et al., 1978; Schoenherr et al., 2007). Some samples contain more than one type of solid bitumen, which are recognized by their texture, reflectance, and paragenetic position. For example, solid bitumen in sample NA 319-08 has a low reflectance but also occurs as cenospheric pyrobitumen within fractures in the matrix dolomite (**Figure 2.8F**). On the other hand, increasing anisotropy is commonly shown in bitumens from Assemblage II where the existence of coarse-grained mosaic to flow-like textures could indicate sudden thermal alteration (Barker and Bone, 1995). Hence, low- and high-reflective solid bitumen occurring at the same depth reveals that at least two different processes were involved in the reservoir during burial.

Bitumen matured by normal burial would tend to produce a rather regular distribution histogram and relatively low reflectance values (*e.g.,* Wilson, 2000). The bimodal distribution in the reflectance values of the pyrobitumen from Assemblage II (**Figure 2.20**) seems to indicate that fluids at elevated temperatures overprinted the original distribution of some samples, increasing the reflectance values, and the anisotropic character of solid bitumen. However, inherited compositional differences within the bitumen could have also promoted a variation in the anisotropy (Stasiuk, 1997). Whether the development of anisotropy in solid bitumen is attributable to the chemistry of the original source material (*e.g.,* Stasiuk, 1997) or to an anomalous heating rate (Goodarzi et al., 1993; Gize, 1999), is beyond the scope of this study. However, from the elevated radiogenic Sr isotopic values found in some of calcite-I linked to pyrobitumen of Assemblage II (**Figure 3.6**), the influence of "external" fluids during the their precipitation is most likely involved. Thus, a heating event of short duration may not have allowed sufficient time for thermal equilibration of the pyrobitumen throughout the reservoir(s), but could have locally raised the bitumen reflectance, as evidenced by the presence of cenospheric textures in pyrobitumen associated with Assemblages II and III.

The coke-like bitumen textures found in Assemblage III exhibit a strong anisotropy, which correlates with the elevated reflectance ranges shown along the regional cross section (up to around 6%R_0). Such textures are prone to develop when bitumen undergoes high temperatures as a consequence of burial or a hydrothermal event (*e.g.*, Goodarzi et al., 1993). However, the scatter shown by the maturity data with depth in pyrobitumen associated with fracture-filling calcites (Assemblage III) is better explained as a result of local alteration of the solid bitumen, likely generated by the entry of external and localized "hot fluids"

into the reservoirs, perhaps along fractures. In addition, the elevated radiogenic strontium isotopic signal of the calcite cements (calcite-II; **Figure 3.6**) supports the idea of fluids ascending from the basement. Hence, the heterogeneity of the reflectance values in addition to the presence of coke-like textures in the bitumens related to calcite-II (Assemblage III) argues in favour of a local thermal event causing the anisotropy.

The relatively low-reflectance values, mineral association (with intermediate-diagenetic cements), and textures found in solid bitumen linked to Assemblage I leads to the conclusion that deasphalting processes are responsible for its formation (see also Buschkuehle, 2003).

3.6. Homogenization temperatures versus peak temperatures

One of the main questions is whether reservoir bitumen has been derived from the transformation of the organic matter at spatially locallized elevated temperatures (*e.g.* around faults) or is reflecting progressive burial conditions. In this regard, microthermometric data on coexisting calcite with solid bitumen may be utilized to better constrain the thermal history. Thus, fluid inclusion microthermometry along with bitumen reflectance analysis provide a better idea on the relationship between maximum temperature ranges reached in the reservoir, and temperature of calcite precipitation.

As depicted in **Figure 3.5**, a very slight trend of increasing homogenization temperatures of fluid inclusions in calcite-I with depth exists along the section. In addition, the peak temperatures recorded in the bitumen associated with those calcites (Assemblage II) reflect a similar pattern, and when plotted against paleodepths, most of the values are congruent with a regional geothermal gradient of ~30˚C/km (**Figure 3.13**). Such a relationship, between

homogenization temperatures, paleotemperatures, and depth, could suggest precipitation of calcite-I under two different scenarios: normal sedimentary burial, or “squeegee” conditions. With the exception of a few samples, the distribution of mean homogenization temperatures versus depth in calcite-I shows that most of the Th values follow close to a geothermal gradient of 30˚C/km. If “squeegee” fluid flow generates temperatures of precipitation higher than the values expected during “normal” burial (see for example Machel and Buschkuehle, 2008), the congruence of homogenization temperatures with a normal geothermal gradient could not be explained.

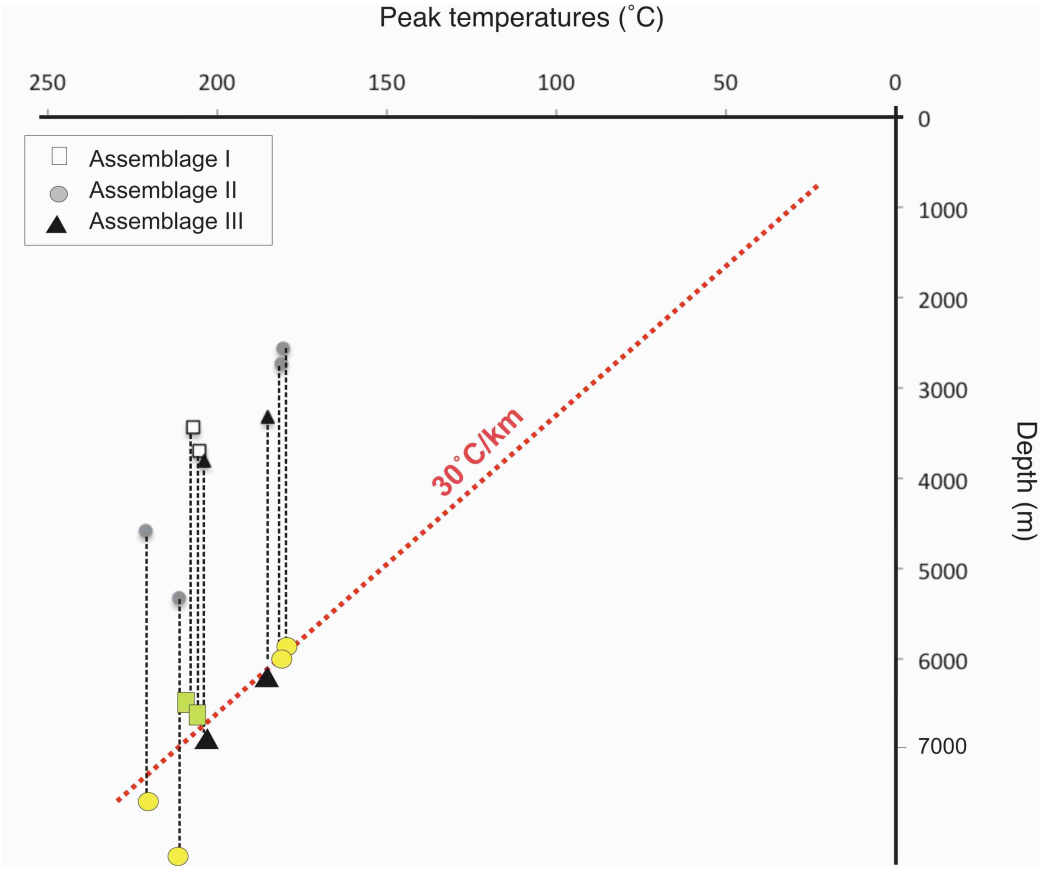

Figure 3.13. Cross-plot of peak temperature values at present-day depth reservoir (grey-scale symbols) and reconstructed peak temperatures values based on the calculated ca. 2500m of eroded sediment pile.

Therefore, the most likely scenario would be the majority of calcite-I being precipitated under normal burial conditions (see also carbon and oxygen isotopic composition of calcites section).

The timing and thermal history of calcite-I can be assessed by combining bitumen petrography, peak temperatures, and fluid inclusion homogenization temperatures. Whereas the highest homogenization temperature value recorded is around 200˚C (mean = 184.5 ± 8.5˚C), the highest peak temperature value in the same calcite corresponds to 255˚C (mean = 221.1 ± 8.8˚C). Accordingly, calcite-I seems to have formed before maximum burial. If normal burial conditions are inferred during calcite-I precipitation, the same conditions have to be reflected in the associated bitumen because both are TSR by-products. The transition from isotropic to anisotropic textures in addition to increasing bitumen reflectance values within the same sample are the result of progressive increase of temperature. However, whether the variation of Th and the calculated Tpeak in calcite-I were due to normal burial or squeegee fluid flow is difficult to demonstrate. If higher temperatures than normal burial were present during “squeegee” fluid flow (Machel and Buschkuehle, 2008), then calcite-I most likely precipitated under normal burial conditions. Alternatively, if the temperature of “squeegee” fluids was similar to that found in normal burial conditions, then the process responsible for the Th signature of calcite-I would be difficult to recognize.

The fluid inclusion homogenization temperatures show that the onset of the cementation of calcite-I took place at temperatures near 100˚C and was progressive during burial, with the bulk of cementation occurring between 125˚ and 155˚C. Assuming that the paleogeothermal gradient has remained the same as today (except during Late Paleocene and Eocene), this interval intersects the

subsidence curve suggesting that the bulk cementation is Late Cretaceous in age (**Figure 3.14**).

Calcite-II seems to have formed in a different context; *i.e.,* occurring as a fracture-filing phase and showing no major influence of TSR. Even though the homogenization temperatures recorded are lower than the peak temperatures of the bitumen (Bitumen III of Assemblage III), the occurrence of calcite-II postdating solid bitumen (**Figure 2.5D**) might be suggesting the post-maximum burial character of this cement. However, no conclusive evidence supporting that view has been found, and consequently, the paragenetic relationship between calcite-I and II remains uncertain.

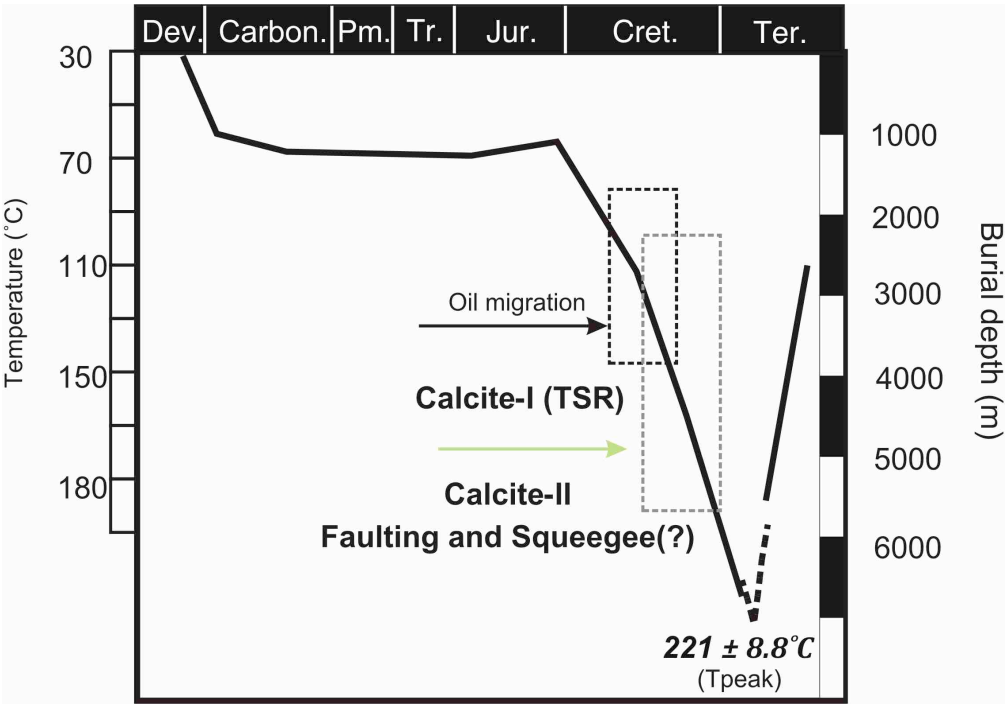

Figure 3.14. Burial curve for the Devonian carbonate sequence in the SCCC (modified from Machel and Buschkuele, 2008). Temperature curve is for a geothermal gradient of 30˚C/km (as suggested by bitumen reflectance data). Temperature ranges for calcite-I and II were determined from fluid inclusion data. Maximum burial temperature calculated from bitumen reflectance data.

CHAPTER 4

CONCLUSIONS

From the foregoing discussion the following conclusions can be drawn:

(1) Two late-diagenetic calcites have been petrographically recognized: calcite-I and calcite-II. Calcite-I is paragenetically linked with saddle dolomite, anhydrite, solid bitumen, and elemental sulfur, and occurs filling vugs and molds. Conversely, calcite-II characteristically appears as a fracture-filling phase, postdating solid bitumen and occasionally occurs in association with saddle dolomite, which is the first pore-lining phase.

(2) Carbon and oxygen isotopic values of both calcites show two distinct groups. Calcite-I displays moderately to highly depleted $\delta^{13}C_{VPDB}$ values (-0.7 to -28.8‰) in a $\delta^{18}O_{VPDB}$ range of -7.8 to -11‰. Calcite-II shows $\delta^{13}C$ values between +0.6 to -8.1‰, and $\delta^{18}O$ signatures ranging between -6.3 and -13‰. The significant content of organically derived carbon in calcite-I, and its petrographic association with anhydrite, elemental sulfur, and solid bitumen, is interpreted to result from thermochemical sulfate reduction (TSR). Pairing the carbon and oxygen isotopic values of calcite-II with those of the associated saddle dolomite suggests that calcite-II was precipitated at higher temperatures, after TSR, when no or little oxidized organic carbon was present.

(3) The calculated oxygen isotopic composition of the fluids from which calcite-I and II precipitated show no dependence on salinity and have oxygen isotopic values overlapping with those of the present-day formation waters, suggesting a source with relatively constant oxygen isotope composition. Therefore, fluids that were involved in the formation of the SCCC calcites were likely similar to the present-day formation waters in terms of $\delta^{18}O$.

(4) Homogenization temperatures in calcite-I range between 92˚C to 193˚C and are coincident with the temperature limits at which TSR occurs, and with the idea of TSR taking place close to maximum burial depths in the SCCC. The homogenization temperatures measured in calcite-I and II are identical within the margin of error (Th of calcite-II varies between 91˚ and 198˚C), which suggest that none of the fluids responsible for their precipitation were hotter than ambient formation temperatures.

(5) The local decrease in salinity of the aqueous fluid inclusions along with the highly depleted carbon isotopic composition of the host calcite-I, and the presence of TSR by-products (H_2S-bearing fluid inclusions, elemental sulfur) suggest that water has been locally generated during TSR in the SCCC.

(6) Most of the calcite-I and all the calcite-II have highly radiogenic strontium isotope ratios (above the MASIRBAS index = 0.7120) with a random distribution along the study area. This would indicate that radiogenic strontium was injected into the fluid system during precipitation of calcite-I and II. Lateral fluid flow in combination with vertical flow along fractures can explain the random distribution

of the Sr isotopic values. The extent of “squeegee” might be determined by considering the distribution of calcite-I and II and their correspondent geochemical signature along the section (**Figure 4.1**). However, distinguishing between faulting and “squeegee” signal at core scale is difficult.

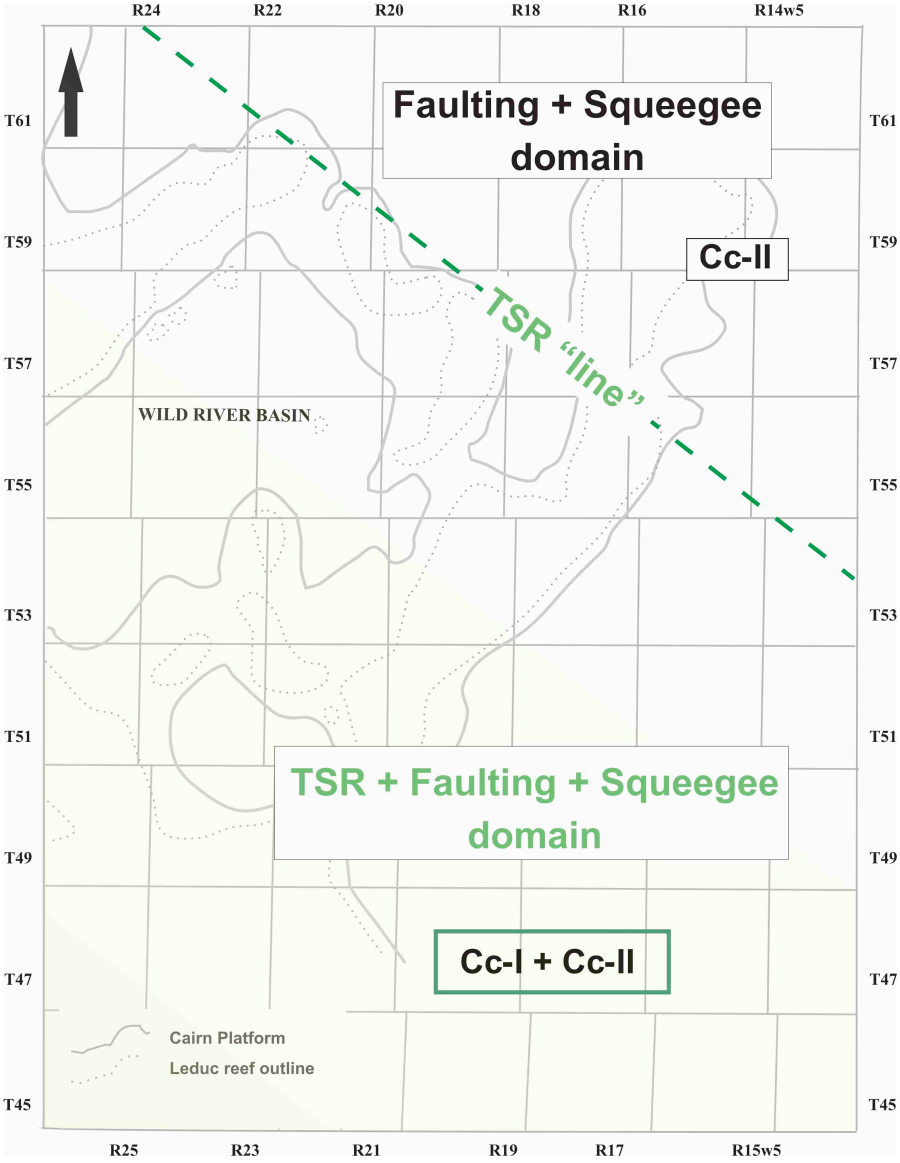

Figure 4.1. The distribution of calcite-I denotes the influence of TSR in the reservoir. Thus, presence of both calcite-I (Cc-I) and calcite-II (Cc-II) determine the TSR+faulting+”Squeegee” domain indicating that these three processes occurred at reservoir scale. Conversely, the absence of calcite-I implies the absence of TSR.

(7) Solid bitumen analysis shows a wide scatter of reflectance values: 1.6 to 6.6%, which reflects the variable anisotropy of the solid bitumen and the elevated maturity of the organic matter. Temperature calculations based on reflectance data indicate that sediments reached maximum temperatures up to 255˚C (with a mean value of 221 ± 8.8˚C). These values are essentially identical (within the margin of error) to the regional temperatures previously estimated for the study area (~220˚C).

(8) Calcite-I was most likely formed before maximum burial. This assumption is supported by the range of precipitation temperatures, which is considerably lower (up to 40˚C) than those recorded in the associated bitumen. The occurrence of some calcite-II postdating bitumen-III provides some, but not conclusive, evidence of its post-maximum burial character and further evidence is needed to draw definitive conclusions.

(9) The change from isotropic to anisotropic textures, increasing bitumen reflectance values, and the very slight trend of increasing homogenization temperatures of fluid inclusions in calcite-I with depth are interpreted to be the result of progressive increase of temperature during burial.

(10) The local thermal alteration of the solid reservoir bitumen can be explained by fluid flow through fractures, which would facilitate the precipitation of calcite-II from “hot” (but cooler than maximum burial temperatures) and Sr-bearing fluids (with values above MASIRBAS) ascending from the basement through the Devonian sequence.

(11) The differentiation of two types of late-diagenetic calcites by means of petrography and geochemistry has been one of the major findings of this work. The following table summarizes the main characteristics of each type of calcite identified in this study.

Remarks	Calcite-I	Calcite-II
Occurrence	Vugs and moldic pores	Fractures
Mineral association	Saddle dolomite ± anhydrite ± solid bitumen ± elemental sulfur	Saddle dolomite
Petrography	Euhedral to subhedral crystals (0.5 – 2cm). Normal extinction. Non-luminescent under CL (closed system)	Subhedral to massive. Normal to undulose extinction. Orange/red luminescence (open system)
Solid bitumen assemblage	Saddle dolomite ± anhydrite-bitumen II-calcite-I	Bitumen III-calcite-II
Stable Isotopic signature	$\delta^{18}O_{VPDB}$: -7.8 to -11.8‰ $\delta^{13}C_{VPDB}$: -0.7 to -28.8‰	$\delta^{18}O_{VPDB}$: -6.3 to –12.9‰. $\delta^{13}C_{VPDB}$: +0.6‰ to -8.1‰
$^{87}Sr/^{86}Sr$ ratios	Solution mode: 0.7084 to 0.7224 In situ $^{87}Sr/^{86}Sr$: 0.70847 to 0.71755	Solution mode: 0.7122 to 0.7199 In situ $^{87}Sr/^{86}Sr$: 0.71583 to 0.72304
Fluid inclusion petrography	Two-phase (L-V) aqueous inclusions; H_2S-bearing inclusions	Two-phase (L-V) aqueous inclusions; oil-bearing inclusions
Homogenization temperatures (L-V inclusions)	Range: 92˚ to 193˚C Mean: 141 ± 14˚C	Range: 91˚ to 198˚C Mean: 147 ± 13˚C
Salinity (eq. wt.% $CaCl_2$)	17.7 ± 0.4	19.8 ± 1.2
Bitumen reflectance (%R_0)	Range: 1.6 to 6.61% Mean = 2.84 ± 0.83%	Range: 2.4 and 5.24% Mean = 2.71 ± 0.76%
Peak temperatures	196 ± 10˚C (Mean = ~ 220˚C)	194 ± 13˚C (Mean = ~ 200˚C)

4.1. Future work

In order to predict the occurrence and distribution of the calcite-II, future studies on the Southesk-Cairn Carbonate Complex should concentrate on the identification and mapping of fractures in subsurface. This will lead to a better understanding of the processes involved during calcite-II cementation, as well as they will contribute to a better definition of a precise paragenetic timing relationship between calcite-I and II.

Organic geochemical analysis of the solid bitumen will better define the processes operating during the maturation of the organic matter and TSR. More detail on the petroleum history in the SCCC can be obtained by geochemical analysis of individual oil-bearing inclusions. Coupling on-line and off-line analysis with gas chromatography, the characterization of the petroleum trapped in fluid inclusions can be assessed. Comparison between the geochemical signatures of the hydrocarbons hosted in primary and secondary inclusions could be key to determine the existence of single or multiple sources with the aim of unraveling the specific time of oil migration events.

CHAPTER 5

REFERENCES

Allen, P.A., Allen, J.R., 1990. Basin Analysis: Principles and Applications. Blackwell, Oxford, 451 pp.

Ammosov, J.J., Sharkowa, L.S., 1975. Paleotemperatures, lithification and oil and gas occurrence in Jurassic deposits in western Kasakhrstan and central Asia. In: J.V., (Eds), Paleotemperatury zon nefteobrazovanija, 60-69.

Amthor, J.E., Mountjoy, E.W., Machel, H.G., 1993. Subsurface dolomites in Upper Devonian Leduc Formation buildups, central part of Rimbey-Meadowbrook reef trend, Alberta, Canada. Bulletin of Canadian Petroleum Geology, 41, 164-185.

Anderson, T. F., Arthur, M. A., 1983. Stable isotopes of oxygen and carbon and their application to sedimentologic and paleoenvironmental problems, in Arthur, M. A., Anderson, T. F., Kaplan, I. R., Veizer, J., Land, L. S., (Eds.), Stable isotopes in sedimentary geology. Society of Economic Paleontologists and Mineralogists Short Course No 10, 1-151.

Baadsgard, H., 1987. Rb-Sr and K-Ca isotope systematics in minerals from potassium horizons in the Prairie Evaporite Formation, Saskatchewan, Canada. Chemical Geology (Isotope Geoscience Section), 66, 1-15.

Bachu, S., 1995. Synthesis and model of formation-water flow, Alberta Basin, Canada. American Association of Petroleum Geologists Bulletin, 79, 1159-1178.

Bachu, S., 1999. Flow systems in the Alberta Basin: patterns, types and driving mechanisms. Bulletin of Canadian Petroleum Geology, 47, 455-474.

Bailey, N. L., Krouse, H. R., Evans C. R., Rogers M. A., 1973. Alteration of crude oil by waters and bacteria - Evidence from geochemical and isotope studies. American Association of Petroleum Geologists Bulletin, 57, 1276-1291.

Barker, C.E., Bone, Y., 1995. The minimal response to contact metamorphism by the Devonian Buchan Caves Limestone, Buchan Rift, Victoria, Australia. Organic Geochemistry, 22, 151-164.

Barker, C.E., Goldstein, R.H. 1990. Fluid-inclusion technique for determining maximum temperature in calcite and its comparison to the vitrinite reflectance geothermometer. Geology, 18, 1003-1006.

Barker, C.E., Pawlewicz, M.J., 1994. Calculation of vitrinite reflectance from thermal histories and peak temperatures. A comparison of methods. In: Mukhopadhyay, P.K., Dow, W.G., (Eds.), Vitrinite reflectance as a maturity

parameter: applications and limitations. ACS Symposium series 570, 216-229.

Bechtel, A., Sun, Y., Püttmann, W., Hoernes, S., Hoefs, J., 2001. Isotopic evidence for multi-stage base metal enrichment in the Kupferschiefer from the Sangerhausen basin. Chemical Geology, 176, 31-49.

Beny, C., Guilhamou, N., Touray, J.C., 1982. Native-sulphur-bearing fluid inclusions in the CO2-H2S-H2O-S system - Microthermometry and raman microprobe (mole) analysis – Thermochemical interpretations. Chemical Geology, 37, 113-127.

Buschkuehle, B. E., Machel, H.G., 2002. Diagenesis and paleofluid flow in the Devonian Southesk-Cairn carbonate complex in Alberta, Canada. Marine and Petroleum Geology, 19, 219-227.

Buschkuehle, B.E., 2003. Geology, diagenesis, and paleofluid flow in the Devonian Southesk-Cairn Carbonate Complex in west-central Alberta, Canada. Unpub. Ph.D. Thesis, University of Alberta, Edmonton, Alberta, 320 pp.

Carpenter, S.J., Lohmann, K.C., 1989. δ18O and δ13C variations in Late Devonian marine cements from the Golden Spike and Nevis reefs, Alberta Canada. Journal of Sedimentary Petrology, 59, 792-814.

Choquette, P.W., James, N.P., 1987. Diagenesis in limestones-3. The deep burial environment. Geoscience Canada, 14, 3-35.

Claypool, G.E., Mancini, E.A., 1989. Geochemical relationships of petroleum in Mesozoic reservoirs to carbonate source rocks of Jurassic Smackover formation, southwestern Alabama. American Association of Petroleum Geologists Bulletin, 73, 904-924.

Connolly, C.A., Walter, L.M., Baadsgaard, H., Longstaffe, F.J., 1990. Origin and evolution of formation waters, Alberta Basin, Western Canada Sedimentary Basin: I. Chemistry. Applied Geochemistry, 5, 375-395.

Connolly, C.A., Walter, I.M., Baadsgaard, H., Longstaffe, F., 1990. Origin and evolution of formation waters, Alberta Basin, Western Canada Sedimentary Basin – II. Applied Geochemistry, 5, 397-413.

Cox, S., 1999. Deformation controls on the dynamics of fluid flow in mesothermal gold systems. In: McCaffery, K.J.W., Lonergan, L., Wilkinson, J.J., (Eds.), Fractures, Fluid Flow and Mineralization, 155. Geological Society of London Special Publications. 123-139 pp.

Crawford, M.L., 1981. Phase equilibria in aqueous fluid inclusions. In: Hollister, L.S. and Crawford, ML., (Eds.), Mineralogical Association of Canada. Short course in fluid inclusions. Applications to Petrology, 6, 75-100.

Curiale, J. A. 1986. Origin of solid bitumens with emphasis on biological marker results, Advance in Organic Geochemistry, 10, 559-580.

Denison, R.E., Koepnick, R.B., Burke, W.H., Hetherington, E.A. & Fletcher, A., 1997. Construction of the Silurian and Devonian seawater 87Sr/86Sr curve. Chemical Geology, 140, 109-121.

Dolphin, D.R., Klovan, J. E., 1970. Stratigraphy and paleoecology of an Upper

Devonian carbonate bank, Saskatchewan River Crossing, Alberta. Bulletin of Canadian Petroleum Geology, 18, 289-331.

Dubessy, J., Boiron, M.-C., Moissette, A., Monnion, C., Sretenskaya, N., 1992. Determination water, hydrates and pH in fluid inclusions by micro-Raman spectrometry. European Journal of Mineralogy, 4, 885-894.

Duggan, J.P., 1997. Sedimentology and diagenesis of Swan Hills Simonette oil field, west-central Alberta basin. Unpub. M.Sc. Thesis, McGill University, Montreal, 177 pp.

Duggan, J.P., Mountjoy, E.W., and Stasiuk, L.D. 2001. Fault-controlled dolomitization at Swan Hills Simonette oil field (Devonian), deep basin west-central Alberta, Canada. Sedimentology, 48, 301-323.

Etheridge, M.A., Wall, V.J. & Vernon, R.H., 1983. The role of the fluid phase during regional metamorphism. Journal of Metamorphic Geology, 1, 205-226.

Friedman, I. O'Neil, J.R., 1977. Compilation of stable isotope fractionation factors of geochemical interest. *USGS Prof. Pap*., 440KK, 12.

Ge, S., Garven, G., 1989. Tectonically Induced Transient Groundwater Flow in Foreland Basins. In: Beck, A.E., Garven, G., Stegena, I., (Eds.), The Origin and Evolution of Sedimentary Basins and Their Energy and Mineral Resources. Amer. Geoph. Union Geodyn. Ser. Monograph, 48, 145-157.

Gentzis, T., Goodarzi, F., 1990. A review of the use of bitumen reflectance in hydrocarbon exploration with examples from Melville Island, Arctic Canada, In: Nuccio, V.F., Barker, C.E., (Eds.), Applications of Maturity Studies to Energy Exploration, reservoir quality. American Association of Petroleum Geologists Bulletin, 76, 1137-1152.

Gize, A., 1999. Organic alteration in hydrothermal sulfide ore deposits. Economic Geology, 94, 967-980.

Goldstein, R.H., Reynolds, T.J., 1994. Systematics of fluid inclusions in diagenetic minerals. SEPM Short course 31, 199 pp.

Goldstein, T.P., and Aizenshtat, Z., 1994. Thermochemical sulfate reduction: a review. Journal of Thermal Analysis, 42, 241-290.

Goodarzi, F., Gentzis, T., Jackson, G., Macqueen, R.W., 1993. Optical characteristics of heat-effected bitumens from the Nanisivik mine, N.W. Baffin Island, Arctic Canada. In: Goodzari, F., Macqueen, R.W. Ž., (Eds.), Geochemistry and Petrology of Bitumen with Respect to Hydrocarbon Generation and Mineralization, Energy Sources, 15, 359-376.

Gratier, J.P., Jenatton, L., 1984. Deformation by solution- deposition, and re-equilibration of fluid inclusions in crystals depending on temperature, internal pressure and stress. Journal of Structural Geology, 6, 189-200.

Green D.G., 1999. Dolomitization and deep burial of the Devonian of west-central Alberta deep basin: Kaybob South and Fox Creek (Swan Hills Formation) and Pine Creek fields (Leduc and Wabamun Formations). Unpub. Ph.D. Thesis, McGill University, Montreal, 267 pp.

Grint, A., Marsh, H., 1981. Carbonization of coal blends mesophase formation.

Fuel, 60, 1115-1120.

Heydari, E., Moore, C.H., 1989. Burial diagenesis and thermochemical sulfate reduction, Smackover formation, southeastern Mississippi salt basin. Geology, 17, 1080- 1084.

Hitchon, B., 1984. Geothermal gradients, hydrodynamics, and hydrocarbon occurrences, Alberta, Canada. American Association of Petroleum Geologists Bulletin, 68, 713- 743.

Hitchon, B., Billings, G.K., Klovan, J.E. 1971. Geochemistry and origin of formation waters in the western Canada sedimentary basin -III. Factors controlling chemical composition. Geochimica et Cosmochimica Acta, 35, 567-598.

Hitchon, B., Friedman, I. 1969. Geochemistry and origin of formation waters in the western Canada sedimentary basin -- I. Stable isotopes of hydrogen and oxygen. Geochimica et Cosmochimica Acta, 33, 1321-1349.

Hudson, J.D., 1975. Carbon isotopes and limestone cement. Geology, 3, 19-22.

Hunt, J.M., 1996. Petroleum Geochemistry and Geology, Second Edition. W.H. Freeman and Company, 743 pp.

Hurley, N.F., Lohmann, K.C., 1989. Diagenesis of Devonian reefal carbonates in the Oscar Range, Canning basin, Western Australia. Journal of Sedimentary Petrology, 59, 127-146.

Jacob, H. 1989. Classification, structure, genesis and practical importance of natural solid oil bitumen ('migrabitumen'). International Journal of Coal Geology, 11, 65-79.

Kaufman, J., Meyers, W.J., Hanson, G.N., 1990. Burial cementation in the Swan Hills Formation (Devonian), Rosevear Field, Alberta, Canada. Journal Sedimentary Petrology, 60, 918-939.

Köster, J., Littke, R., Machel, H.G., 2008. Devonian carbonates of the Nigel Peak area, Rocky Mountains, Canada: a fossil petroleum system? Journal of Petroleum Geology, 31, 283-302.

Krouse, H.R., Viau, C.A., Eliuk, L.S., Ueda, A., Halas, S., 1988. Chemical and isotopic evidence of thermochemical sulfate reduction by light-hydrocarbon gases in deep carbonate reservoirs. Nature, 333, 415-419.

Land, L.S., 1985. The origin of massive dolostone. Journal of Geological Education, 33, 112-125.

Leventhal J.S., 1990. Organic matter and thermochemical sulfate reduction in the Viburnum Trend, southeast Missouri. Economic Geology, 85, 622-632.

Machel, H.G., 2001. Bacterial and thermochemical sulfate reduction in diagenetic settings – old and new insights. Sedimentary Geology, 140, 143-175.

Machel, H.G., Buschkuehle, B.E., 2008. Diagenesis of the Devonian Southesk-Cairn Carbonate Complex, Alberta, Canada: marine cementation, burial dolomitization, thermochemical sulfate reduction, anhydritization, and squeegee fluid flow. Journal of Sedimentary Research, 78, 366-389.

Machel, H.G., Cavell, P.A., 1999. Low-Flux, Tectonically Induced Squeegee Fluid

Flow (“Hot Flash”) into the Rocky Mountain Foreland Basin. Bulletin of Canadian Petroleum Geology, 47, 510-533.

Machel, H.G., Cavell, P.A., Patey, K.S., 1996. Isotopic evidence for carbonate cementation and recrystallization, and for tectonic expulsion of fluids into the Western Canada Sedimentary Basin. Geological Society of America Bulletin, 108, 1108-1119.

Machel, H.G., Krouse, R.H., Riciputi, L.R., Cole, D.R., 1995. Devonian Nisku sour gas play, Canada: A unique natural laboratory for study of thermochemical sulfate reduction. In: Vairavamurthy, M.A. and Schoonens, M.A.A., (Eds), American Chemical Society Symposium Series No. 612, 439-454.

Machel., H. G., Krouse HR, Sassen, R. 1995. Products and distinguishing criteria of bacterial and thermochemical sulfate reduction. Applied Geochemistry, 10, 373- 389.

Manzano, B.K., Fowler, M.G., Machel, H.G., 1997. The influence of thermochemical sulfate reduction on hydrocarbon composition in Nisku reservoirs, Brazeau River area, Alberta, Canada. Organic Geochemistry, 27, 507-521.

McCrea, J.M., 1950. On the isotopic chemistry of carbonates and a paleothermometer scale. Journal of Chemical Physics, 5, 48-51.

Mckenzie, A.S., Mckenzie, D., 1983. Isomerization and aromatization of hydrocarbons in sedimentary basins formed by extension. Geol. Mag. 120/5, 417-528.

McKenzie, M.C., 1999. Carbonates of the Upper Devonian Leduc Formation, southwestern Peace River Arch, Alberta: Indications for tectonically induced fluid flow. Unpub. M.Sc. Thesis, University of Alberta, Edmonton, Alberta, 131 pp.

Michael, K., 2002. Flow of formation water in the Alberta Basin adjacent to the Rocky Mountains thrust and fold belt, west-central Alberta, Canada. Unpub. Ph.D. Thesis, University of Alberta, Edmonton, Alberta, 332 pp.

Michael, K., Machel, H.G., and Bachu, S., 2003. New insights into the origin and migration of brines in deep Devonian aquifers, Alberta, Canada. Journal of Geochemical Exploration, 80, 193-219.

Mossop, G., Shetsen, I., 1994. Geological Atlas of the Western Canada Sedimentary Basin, 510 pp.

Munz, I.A., 2001. Petroleum inclusions in sedimentary basins: systematics, analytical methods and applications. Lithos, 55, 195-212.

Nandi, B.N., Belinko, K., Ciavaglia, L.A., Pruden, B.B., 1978. Formation of coke during thermal hydrocracking of Athabasca bitumen. Fuel, 57, 265-268.

Nöth, S., 1997. High H2S contents and other effects of thermochemical sulfate reduction in deeply buried carbonate reservoirs: a review. Geol. Rundsch., 86, 275-287.

Nurkowski, J.R., 1984. Coal quality, coal rank variation and its relation to reconstructed overburden, Upper Cretaceous and Tertiary Plains Coals,

Alberta, Canada. American Association of Petroleum Geologists, Bulletin, 68, 285–295.

Oliver, J., 1986. Fluids expelled tectonically from orogenic belts: their role in hydrocarbon migration and other geologic phenomena. Geology, 14, 99-102.

Orr, W.L., 1974. Changes in sulfur content and isotope ratios of sulfur during petroleum maturation study of Big Horn basin Paleozoic oils. American Association of Petroleum Geologists, Bulletin, 11, 2295-2318.

Orr, W.L., 1977. Geologic and geochemical controls on the distribution of hydrogen sulphide in natural gas. In: Campos, R., and Goni, I., (Eds), Advances in Organic Geochemistry, 571-597.

Parnell, J., 1996. Phanerozoic analogues for carbonaceous matter in Witwatersrand ore deposits. Economic Geology, 91, 55-62.

Pascal, P., 1960. Nouveau traite de chimie minerale, XIII. Masson, Paris, 1037 pp.

Patey, K.S., 1995. Upper Devonian carbonates in the Obed area. Unpub. M.Sc. Thesis, University of Alberta, Edmonton, Alberta, 147pp.

Powell, T. G., Snowdon, L. R., 1983. A composite hydrocarbon generation model: implications for evaluations of basins for oil and gas. Erdol Erd61 und Kohle 36, 163-170.

Powell, T.G., Macqueen R.W. 1984. Precipitation of sulfide ores and organic matter: Sulfate reactions at Pine Point, Canada. Science, 224, 63-66.

Prezbendowki, D.R., and Larese, R.E. 1987. Experimental stretching of fluid inclusions in calcite - Implications for diagenetic studies. Geology, 15, 333-336.

Price, R.A., 1994. Cordilleran tectonics and the evolution of the Western Canada Sedimentary Basin. In: Geologic Atlas of the Western Canada Sedimentary Basin; Mossop, G.D. and Shetsen, I., (Eds), Canadian Society of Petroleum Geologists and Alberta Research Council, 13-24.

Rock, L., 1999. Sedimentology, diagenesis and reservoir characteristics of the Devonian Simonette (Leduc Formation) and Ante Creek (Swan Hills Formation) fields: a comparison between a limestone and dolomite field, west-central Alberta. Unpub. M.Sc. Thesis, McGill University, Montreal, 168 pp.

Roedder, E., 1984. Fluid inclusions. Mineralogical Society of America. Reviews in Mineralogy, 12, 646 pp.

Sassen, R., 1988. Geochemical and carbon isotopic studies of crude oil destruction, bitumen precipitation, and sulfate reduction in the deep Smackover formation. Organic Geochemistry, 12, 351-361.

Schmidberger, S.S., Simonetti, A. Francis, D. 2003. Small-scale Sr isotope investigation of clinopyroxenes from peridotite xenoliths by laser ablation MC-ICP-MS – implications for mantle metasomatism. Chemical Geology, 199, 317-329.

Schoenherr, J., Littke, R., Urai, J.L, Kukla, P.A., Rawahi, Z. 2007. Polyphase

thermal evolution in the Infra-Cambrian Ara Group (South Oman Salt Basin) as deduced by maturity of solid reservoir bitumen. Organic Geochemistry, 38, 1293-1318.

Simpson, G., Yang, C., Hutcheon, I., 1996. Thermochemical sulphate reduction: a local process that does not generate thermal anomalies. In: 1995 Alberta Basement Transects Workshop, Lithoprobe Report #51, Lithoprobe Secretariat, University of British Columbia, G.M. Ross, comp. 241-245.

Smith, S.G.W., 2001. The origin and timing of late-stage carbonate cements in Devonian carbonates of the deep Alberta basin: based on fluid inclusion and isotopic evidence. Unpub. M.Sc. Thesis, McGill University, Montreal, 116 pp.

Stasiuk, L.D., 1997. The origin of pyrobitumens in Upper Devonian Leduc Formation gas reservoirs, Alberta, Canada; An optical an EDS study of oil to gas transformation: Marine and Petroleum Geology, 14, 915-929.

Suggate, R.P., 1998. Relations between depth of burial, vitrinite reflectance and geothermal gradient. Journal of Petroleum Geology, 21, 5-32.

Switzer, S.B., Holland, W.G., Christie, P.S., Graf, G.C., Hedinger, A.S., McAnley, R.J., Wierzbicki, R.A., Packard, J.J., 1994. Devonian Woodbend - Winterburn Strata of the Western Canada Sedimentary Basin. In: Mossop, G.D. and Shetsen, I., (Eds.), Geological Atlas of the Western Canada Sedimentary Basin. Canadian Society of Petroleum Geologists and Alberta Research Council, 165-202.

Taylor, G.H., Teichmueller, M., Davis, A., Diessel, C.F.K., Littke, R., Robert, P., 1998. Organic Petrology. Borntraeger, Berlin – Stuttgart, 68.

Teichmuller, R., 1973. Die palaogeographisch - fazielle unol tektonische Entwicklung eines kohlenbeckens am Beispiel des Ruhrkarbons. Z. dt. geol. Ges. 124: 149-165.

Thomson, M.L., Mastalerz, M., Sinclair, A.J., Bustin, R.M., 1992. Fluid source and thermal history of an epithermal vein deposit, Owen Lake, central British Columbia: evidence from bitumen and fluid inclusions. Mineral Deposita, 27, 219-225.

Tissot, B.P., Welte, D.H. 1984. Petroleum formation and occurrence. Springer-Verlag. 699 pp.

Van den Kerkhof, A.M., Hein, U.F., 2001. Fluid inclusion petrography. Lithos, 55, 27-47.

Vandeginste, V., Swennen, R., Gleeson, S., Ellam, R., Osadetz, K., Roure, F., 2008. Thermochemical sulphate reduction in the Upper Devonian Cairn Formation of the Fairholme carbonate complex (South-West Alberta, Canadian Rockies): evidence from fluid inclusions and isotopic data. Sedimentology, 56, 439-460.

Walters, C.C., Kelemen, S.R., Kwiatek, P.J., Pottorf, R.J., Mankiewicz, P.J., Curry, D.J., Putney, K., 2006. Reactive polar precipitation via ether cross-linkage: a new mechanism for solid bitumen formation. Organic Geochemistry, 37, 408-427.

Waples, D.W. 1980. Time and temperature in petroleum formation:application of

Lopatinn's method to petroleum exploration. Bulletin of American Association of Petroleum Geologists, 64, 916-926.

Weissenberger, J.A.W., 1994. Frasnian reef and basinal strata of West Central Alberta: a combined sedimentological and biostratigraphic analysis. Bulletin of Canadian Petroleum Geology, 42, 1-25.

White, J.L., 1976. Mesophase mechanisms in the formation of the microstructure of petroleum coke. In: Ž. Deviney, M.L., O'Grady, T.M., (Eds.), Petroleum Derived Carbons, Am. Chem. Soc. Symposium, Ser. 21, 282-314.

Wilkinson, P.K., 1995. Is Fluid Flow in Paleozoic Formations of West Central Alberta Affected by the Rocky Mountain Thrust Belt?. Unpub. M.Sc. Thesis, University of Alberta, Edmonton, Alberta, 102 pp.

Wilson, N., 2000. Organic petrology, chemical composition, and reflectance of pyrobitumen from the El Soldado Cu deposit, Chile. Coal Geology, 43, 53–82.

Worden, R.H. and Cai, C., 2006. Geochemical characteristics of the Zhaolanzhuang sour gas accumulation and thermochemical sulfate reduction in the Jixian Sag of Bohai Bay Basin by Zhang et al. (Organic Geochemistry 36, 1717-1730): Discussion. Organic Geochemistry, 37, 511-514.

Worden, R.H., Smalley, P.C., 1996. H2S-producing reactions in deep carbonate gas reservoirs: Khuff Formation, Abu Dhabi. Chemical Geology, 133, 157-171.

Worden, R.H., Smalley, P.C., Oxtoby, N.H., 1996. The effects of thermochemical sulfate reduction upon formation water salinity and oxygen isotopes in carbonate gas reservoirs. Geochimica et Cosmochimica Acta, 60, 3925-3931.

Yang, C., Hutcheon, I., Krouse, H.R., 2001. Fluid inclusion and stable isotopic studies of thermochemical sulphate reduction from Burnt Timber and Crossfield East gas fields in Alberta, Canada. Bulletin of Canadian Petroleum Geology, 49, 149-164.

Zhang, S.C., Zhu, G.Y., Liang, Y.B., Dai, J.X., Liang, H.B., Li, M.W., 2005. Geochemical characteristics of the Zhaolanzhuang sour gas accumulation and thermochemical sulfate reduction in the Jixian Sag of Bohai Bay Basin. Organic Geochemistry, 36, 1717-1730.

Zhang, Y., Frantz, J.D., 1987. Determination of the homogenization temperatures and densities of supercritical fluids in the system NaCl–KCl–CaCl2–H2O using synthetic fluid inclusions. Chemical Geology, 64, 335-350.

APPENDIX I

List of stable isotope results

Table A-1. Summary of stable isotope data.

	$^{18}O/^{16}O$ (‰)	$^{18}/^{16}O$ (‰)	$^{13}C/^{12}C$ (‰)	Location	Depth	Remarks
	VSMOW	**VPDB**	**VPDB**			
NA 231	22.37	-8.29	-16.27	16-32-58-24w5	3711	Calcite-I
NA 297	19.51	-11.05	-28.86	2-14-50-22w5	3918.5	Calcite-I
NA 14164	20.45	-10.15	-24.42	10-9-57-24W5	4121.8	Calcite-I
NA 87	18.74	-11.80	-13.33	01-32-57-25w5	4527.8	Calcite-I
NA 005/97	19.41	-11.15	-27.34	09-20-59-22w5	3805.6	Calcite-I
NA 003/97	19.52	-11.05	-28.94	09-20-59-22w5	3802.3	Calcite-I
NA 005/97b	19.51	-11.06	-23.11	09-20-59-22w5	3805.6	Calcite-I
NA 312	21.29	-9.33	-19.49	10-12-54-18w5	3559.45	Calcite-I
NA 208	21.76	-8.87	-11.61	11-29-59-16w5	2734.4	Calcite-I
NA 208b	21.81	-8.83	-11.32	11-29-59-16w5	2734	Calcite-I
NA 322	21.52	-9.11	-13.39	10-23-58-17w5	3030	Calcite-I
NA 254	19.63	-10.94	-9.31	7-18-52-24w5	4825	Calcite-I
NA 256	19.20	-11.36	-10.51	7-18-52-24w5	4829.1	Calcite-I
NA 117	22.83	-7.84	-9.74	1-18-56-16w5	2951.2	Calcite-I
NA 197	22.40	-8.26	-7.51	15-9-57-17w5	3149.5	Calcite-I
NA 323	22.59	-8.07	-11.83	10-23-58-17W5	3033	Calcite-I
NA 330	22.86	-7.81	-6.20	15-9-57-17w5	3149.5	Calcite-I
NA IV	21.97	-8.67	-0.65	9-17-53-19W5	3695.4	Calcite-I
NA 003/97	20.82	-9.79	-28.02	10-32-44-19W5	5326.3	Calcite-I
NA 311	21.68	-8.95	-9.11	10-12-54-18W5	3557.9	Calcite-I
NA 15	23.04	-7.64	-2.23	14-36-52-27w5	5220.8	Calcite-II
NA 3191	18.64	-11.90	-0.33	9-5-57-17W5	3191	Calcite-II
NA 16693'	17.59	-12.92	-3.31	1-16-55-27W5	5088	Calcite-II
NA 125	21.50	-9.13	-4.16	6-16-55-18w5	3323	Calcite-II
NA 211A	22.77	-7.89	-5.60	9-5-57-17W5	3225.5	Calcite-II
NA 314	20.54	-10.06	-2.50	10-12-54-18W5	3574.4	Calcite-II
NA 123	22.00	-8.65	-5.37	6-16-55-18w5	3319	Calcite-II
NA 12124'	21.51	-9.12	-1.77	9-17-53-19w5	3695.4	Calcite-II
NA 290	18.32	-12.21	0.17	9-5-57-17w5	3188	Calcite-II
NA 270	19.42	-11.14	-2.90	5-25-51-22w5	4468	Calcite-II
NA 10915	21.66	-8.97	-1.73	15-29-55-17w5	3327.5	Calcite-II
NA 73	24.41	-6.31	-4.57	9-22-58-24w5	3899.25	Calcite-II
NA 264	23.78	-6.92	-2.69	1-16-55-27w5	5090.16	Calcite-II
NA 15	-18.25	-8.18	-4.03	14-36-52-27w5	5220.8	Calcite-II
NA 201b	19.22	-11.34	-1.20	05-13-54-23w5	4076.6	Calcite-II
NA 271	20.71	-9.90	-0.82	5-25-51-22W5	4473	Calcite-II
NA 272 A	20.65	-9.95	-0.93	5-25-51-22W5	4473	Calcite-II
NA 3225	22.79	-7.87	-5.63	9-5-57-17W5	3225	Calcite-II
NA 200	21.93	-8.71	0.63	2/15-09-57-17W5	3162.75	Calcite-II
NA 333	20.07	-10.51	0.20	15-9-57-17W5	3162	Calcite-II
NA 10	23.25	-7.43	-4.04	10-32-44-19w5	5363.9	Calcite-II
NA 9	22.46	-9.71	-8.20	10-32-44-19w5	5363	Calcite-II
NA 12140	25.11	-5.63	1.10	9-17-53-19w5	3700	saddle dolomite

NA 211	25.99	-4.77	-2.08	11-29-59-16w5	2736.3	saddle dolomite
NA 3223	24.62	-6.10	0.30	9-5-57-17w5	3223	saddle dolomite
NA 290	26.27	-4.51	1.72	9-5-57-17w5	3188	saddle dolomite
NA 240	25.24	-5.50	1.27	7-35-59-24w5	3840	saddle dolomite
NA 89	24.72	-6.01	-4.36	1-32-57-25w5	4261.1	saddle dolomite
NA 201	25.07	-5.67	0.85	05-13-54-23w5	4076.6	saddle dolomite

APPENDIX IIa

List of Sr isotope results (solution method)

Table A-2. Summary of Sr isotope data (solution mode).

Sample	$^{87}Sr/^{86}Sr$	2σ	Location	Depth	Remarks
NA 200	0.71565	0.000020	2/15-09-57-17W5	3162.75	calcite-II
NA 271	0.71693	0.000020	5-25-51-22W5	4473	calcite-II
NA 290	0.71224	0.000020	9-5-57-17W5	3188	calcite-II
NA 270	0.71995	0.000020	5-25-51-22W5	4468	calcite-II
NA 123	0.71786	0.000020	6-16-55-18W5	3319.3	calcite-II
NA 330	0.71744	0.000020	15-9-57-17W5	3153	calcite-I
NA IV	0.71694	0.000020	9-17-53-19W5	3216	calcite-I
NAVI	0.72242	0.000020	1-18-56-16W5	2952	calcite-I
NA 208	0.71449	0.000020	11-2-59-16W5	2734.4	calcite-I
NA 297	0.70847	0.000020	2-14-50-22W5	3918.5	calcite-I
NA III	0.71755	0.000020	16-22-58-19W5	3375.4	calcite-I

APPENDIX IIb

List of Sr isotope results (laser ablation ICP-MS)

Table A-3. Summary of strontium isotope data (laser ablation ICP-MS).

Sample	$^{87}Sr/^{86}Sr$	2σ	Location	Depth (m)	Remarks
NA 116	0.72304	0.0004	1-18-56-16w5	2952.5	calcite-II
NA 116	0.7222	0.00055	1-18-56-16w5	2952.5	calcite-II
NA 116	0.72237	0.00028	1-18-56-16w5	2952.5	calcite-II
NA 116	0.72282	0.00026	1-18-56-16w5	2952.5	calcite-II
NA 116	0.72242	0.00012	1-18-56-16w5	2952.5	calcite-II
NA 116	0.72281	0.0003	1-18-56-16w5	2952.5	calcite-II
NA I	0.70884	0.0004	2-14-50-22w5	3930	calcite-I
NA I	0.70847	0.0002	2-14-50-22w5	3930	calcite-I
NA I	0.70858	0.0003	2-14-50-22w5	3930	calcite-I
NA I	0.70852	0.0005	2-14-50-22w5	3930	calcite-I
NA I	0.70852	0.0002	2-14-50-22w5	3930	calcite-I
NA I	0.70863	0.0002	2-14-50-22w5	3930	calcite-I
NA III	0.71692	0.0002	16-22-58-19W5	3375.4	calcite-I
NA III	0.71755	0.00015	16-22-58-19W5	3375.4	calcite-I
NA III	0.70946	0.0001	16-22-58-19W5	3375.4	calcite-I
NA VII	0.71583	0.0003	9-17-53-19W5	3251.5	calcite-II
NA VII	0.71708	0.0001	9-17-53-19W5	3251.5	calcite-II
NA 116	0.71212	0.0008	1-18-56-16w5	2952.5	saddle dolomite
NA 116	0.70996	0.0004	1-18-56-16w5	2952.5	saddle dolomite
NA I	0.70841	0.0003	2-14-50-22w5	3930	saddle dolomite
NA I	0.70846	0.0005	2-14-50-22w5	3930	saddle dolomite
NA III	0.71067	0.0005	16-22-58-19W5	3375.4	saddle dolomite
NA III	0.70961	0.00055	16-22-58-19W5	3375.4	saddle dolomite
NAIII	0.70935	0.0002	16-22-58-19W5	3375.4	saddle dolomite
NA 116	0.70901	0.0005	1-18-56-16w5	2952.5	matrix dolomite
NA 116	0.70848	0.0004	1-18-56-16w5	2952.5	matrix dolomite
NA I	0.70868	0.0005	2-14-50-22w5	3930	matrix dolomite
NA I	0.70814	0.00055	2-14-50-22w5	3930	matrix dolomite
NA III	0.70886	0.0004	16-22-58-19W5	3375.4	matrix dolomite
NA III	0.70832	0.00017	16-22-58-19W5	3375.4	anhydrite
NA III	0.70826	0.0002	16-22-58-19W5	3375.4	anhydrite

APPENDIX III

List of fluid inclusion microthermometry results

Table A-4. Summary of microthermometric analyses of fluid inclusion.

Sample	Location	Depth (m)	Th (˚C)	Te(˚C)	Tm (˚C)	wt% $CaCl_2$	Remarks	Ty.
NA 254	7-18-52-24W5	4824.5	127.6	-53	-17.8	20.4	calcite-l	A
NA 254	7-18-52-24W5	4824.5	140.5	-53	-17.9	20.5	calcite-l	A
NA 254	7-18-52-24W5	4824.5	142.1	-53	-18.0	20.6	calcite-l	A
NA 254	7-18-52-24W5	4824.5	146.7	-53	-18.0	20.6	calcite-l	A
NA 254	7-18-52-24W5	4824.5	152.4	-53	-18.1	20.6	calcite-l	A
NA 254	7-18-52-24W5	4824.5	140.2	-53	-18.1	20.6	calcite-l	A
NA 254	7-18-52-24W5	4824.5	157.2	-53	-17.6	20.3	calcite-l	A
NA 254	7-18-52-24W5	4824.5	133		-17.9	20.5	calcite-l	A
NA 254	7-18-52-24W5	4824.5	134.9		-17.9	20.5	calcite-l	A
NA 254	7-18-52-24W5	4824.5	139.1		-17.9	20.5	calcite-l	A
NA 254	7-18-52-24W5	4824.5	142.2	-51	-19.0	21.2	calcite-l	A
NA 254	7-18-52-24W5	4824.5	143.2	-50	-19.5	21.5	calcite-l	A
NA 254	7-18-52-24W5	4824.5	148.2	-50	-18.1	20.6	calcite-l	A
NA 254	7-18-52-24W5	4824.5	154.9	-50	-19.5	21.5	calcite-l	A
NA 254	7-18-52-24W5	4824.5	156.1		-18.5	20.9	calcite-l	A
NA 254	7-18-52-24W5	4824.5	138.5		-19.1	21.2	calcite-l	A
NA 254	7-18-52-24W5	4824.5	150.2	-56	-18.1	20.6	calcite-l	A
NA 254	7-18-52-24W5	4824.5	157.1	-50	-18.9	21.1	calcite-l	A
NA 254	7-18-52-24W5	4824.5	175.7		-20.5	22.0	calcite-l	A
NA 254	7-18-52-24W5	4824.5	179.2	-50	-17.9	20.5	calcite-l	A
NA 254	7-18-52-24W5	4824.5	125.9	-49	-20.6	22.1	calcite-l	A
NA 254	7-18-52-24W5	4824.5	126.6	-55	-18.4	20.8	calcite-l	A
NA 254	7-18-52-24W5	4824.5	128.7	-54	-18.5	20.9	calcite-l	A
NA 254	7-18-52-24W5	4824.5	133.7		-18.2	20.7	calcite-l	A
NA 254	7-18-52-24W5	4824.5	116.7		-18.5	20.9	calcite-l	A
NA 254	7-18-52-24W5	4824.5	125.5	-53	-18.7	21.0	calcite-l	A
NA 254	7-18-52-24W5	4824.5	131.6	-53	-18.9	21.1	calcite-l	A
NA 254	7-18-52-24W5	4824.5	141.8	-53	-19.2	21.3	calcite-l	A
NA 254	7-18-52-24W5	4824.5	116.5	-50 (?)	-18.5	20.9	calcite-l	A
NA 254	7-18-52-24W5	4824.5	131.2		-18.7	21.0	calcite-l	A
NA 254	7-18-52-24W5	4824.5	136	-52	-18.0	20.6	calcite-l	A
NA 254	7-18-52-24W5	4824.5	135.8	-51	-19.3	21.4	calcite-l	A
NA 254	7-18-52-24W5	4824.5	143.4	-50	-19.1	21.2	calcite-l	A
NA 254	7-18-52-24W5	4824.5	146.7	-51	-18.7	21.0	calcite-l	A
NA 254	7-18-52-24W5	4824.5	154.7		-20.1	21.8	calcite-l	A
NA 254	7-18-52-24W5	4824.5	141.6	-55	-20.2	21.9	calcite-l	A
NA 254	7-18-52-24W5	4824.5		-55			calcite-l	A
NA 254	7-18-52-24W5	4824.5		-55			calcite-l	A
NA 254	7-18-52-24W5	4824.5					calcite-l	A
NA 254	7-18-52-24W5	4824.5		-56			calcite-l	A
NA 254	7-18-52-24W5	4824.5				20.0	calcite-l	A
NA 323	10-23-58-17W5	3033	124.8	-52	-16.1	19.3	calcite-l	A
NA 323	10-23-58-17W5	3033	122.1		-14.8	18.3	calcite-l	A

NA 323	10-23-58-17W5	3033	121.2	-53	-15.9	19.1	calcite-I	A
NA 323	10-23-58-17W5	3033	125.9	-51 to -50	-15.3	18.7	calcite-I	A
NA 323	10-23-58-17W5	3033	124		-15.1	18.5	calcite-I	A
NA 323	10-23-58-17W5	3033	108.3		-14.2	17.8	calcite-I	A
NA 323	10-23-58-17W5	3033	111.4		-14.6	18.1	calcite-I	A
NA 323	10-23-58-17W5	3033	126.4		-15.1	18.5	calcite-I	A
NA 323	10-23-58-17W5	3033	112.9		-17.1	20.0	calcite-I	A
NA 323	10-23-58-17W5	3033	114.6	-53	-14.8	18.3	calcite-I	A
NA 323	10-23-58-17W5	3033	115.5		-15.3	18.7	calcite-I	A
NA 323	10-23-58-17W5	3033	139.5	-51	-15.3	18.7	calcite-I	A
NA 323	10-23-58-17W5	3033	120.2		-15.3	18.7	calcite-I	A
NA 323	10-23-58-17W5	3033	134.7	-51	-15.5	18.8	calcite-I	A
NA 323	10-23-58-17W5	3033	135	-51	-15.3	18.7	calcite-I	A
NA 323	10-23-58-17W5	3033	130.1	-55 to -52	-15.5	18.8	calcite-I	A
NA 323	10-23-58-17W5	3033	138.9	-53	-14.8	18.3	calcite-I	A
NA 323	10-23-58-17W5	3033	138.6	-53	-14.9	18.4	calcite-I	A
NA 323	10-23-58-17W5	3033	130.2	-53	-15.3	18.7	calcite-I	A
NA 323	10-23-58-17W5	3033	136.5	-53	-16.1	19.3	calcite-I	A
NA 323	10-23-58-17W5	3033	140.1	-53	-15.1	18.5	calcite-I	A
NA 323	10-23-58-17W5	3033	140.6		-15.0	18.4	calcite-I	A
NA 323	10-23-58-17W5	3033	133.8	-54	-15.4	18.7	calcite-I	A
NA 323	10-23-58-17W5	3033	139.8	-54	-14.9	18.4	calcite-I	A
NA 323	10-23-58-17W5	3033	136.5	-54	-14.5	18.0	calcite-I	A
NA 323	10-23-58-17W5	3033	137.8		-14.6	18.1	calcite-I	A
NA 323	10-23-58-17W5	3033	138.5		-15.2	18.6	calcite-I	A
NA 323	10-23-58-17W5	3033	138		-15.9	19.1	calcite-I	A
NA 323	10-23-58-17W5	3033	141.4	-53	-15.9	19.1	calcite-I	A
NA 323	10-23-58-17W5	3033	138.8		-16.5	19.5	calcite-I	A
NA 323	10-23-58-17W5	3033	132.2		-17.0	19.9	calcite-I	A
NA 323	10-23-58-17W5	3033	135.1		-15.9	19.1	calcite-I	A
NA 323	10-23-58-17W5	3033	113.2	-50	-16.9	19.8	calcite-I	A
NA 323	10-23-58-17W5	3033	137.9	-54	-17.0	19.9	calcite-I	A
NA 323	10-23-58-17W5	3033	134	-53	-15.8	19.0	calcite-I	A
NA 323	10-23-58-17W5	3033					calcite-I	A
NA 311	10-12-54-18W5	3557.9	134.6	-53	-14.3	17.9	calcite-I	A
NA 311	10-12-54-18W5	3557.9	132.8		-14.1	17.7	calcite-I	A
NA 311	10-12-54-18W5	3557.9	139.3		-15.5	18.8	calcite-I	A
NA 311	10-12-54-18W5	3557.9	114	-54 to -53	-15.2	18.6	calcite-I	A
NA 311	10-12-54-18W5	3557.9	124.9		-13.7	17.4	calcite-I	A
NA 311	10-12-54-18W5	3557.9	124.9		-14.0	17.6	calcite-I	A
NA 311	10-12-54-18W5	3557.9	131	-54	-14.3	17.9	calcite-I	A
NA 311	10-12-54-18W5	3557.9	134.6	-54	-14.3	17.9	calcite-I	A
NA 311	10-12-54-18W5	3557.9	143.9	-54	-14.3	17.9	calcite-I	A
NA 311	10-12-54-18W5	3557.9	144.9	-53	-14.3	17.9	calcite-I	A
NA 311	10-12-54-18W5	3557.9	127.3	-54	-14.3	17.9	calcite-I	A
NA 311	10-12-54-18W5	3557.9	143.6	-55 to -54	-14.4	18.0	calcite-I	A
NA 311	10-12-54-18W5	3557.9	166.4	-55 to -54	-14.4	18.0	calcite-I	A

NA 311	10-12-54-18W5	3557.9	153.3	-55 to -54	-14.4	18.0	calcite-I	A
NA 311	10-12-54-18W5	3557.9	139.6	-55 to -54	-14.4	18.0	calcite-I	A
NA 311	10-12-54-18W5	3557.9	141.4		-14.8	18.3	calcite-I	A
NA 311	10-12-54-18W5	3557.9	164.5		-14.5	18.0	calcite-I	A
NA 311	10-12-54-18W5	3557.9	157.7		-14.5	18.0	calcite-I	A
NA 311	10-12-54-18W5	3557.9	153.2		-14.7	18.2	calcite-I	A
NA 311	10-12-54-18W5	3557.9	154.7		-14.5	18.0	calcite-I	A
NA 311	10-12-54-18W5	3557.9	158.6		-14.5	18.0	calcite-I	A
NA IV	9-17-53-19W5	3695.4	111.4		-18.0	20.6	calcite-I	A
NA IV	9-17-53-19W5	3695.4	133.9		-18.3	20.7	calcite-I	A
NA IV	9-17-53-19W5	3695.4	109.4		-17.4	20.2	calcite-I	A
NA IV	9-17-53-19W5	3695.4	128.4		-17.3	20.1	calcite-I	A
NA IV	9-17-53-19W5	3695.4	145.5		-17.5	20.2	calcite-I	A
NA IV	9-17-53-19W5	3695.4	150.1		-17.3	20.1	calcite-I	A
NA IV	9-17-53-19W5	3695.4	105.8		-17.5	20.2	calcite-I	A
NA IV	9-17-53-19W5	3695.4	109.3		-17.8	20.4	calcite-I	A
NA IV	9-17-53-19W5	3695.4	102.7		-17.3	20.1	calcite-I	A
NA IV	9-17-53-19W5	3695.4	110.9		-17.3	20.1	calcite-I	A
NA IV	9-17-53-19W5	3695.4	113.3		-17.5	20.2	calcite-I	A
NA IV	9-17-53-19W5	3695.4	127.9		-17.5	20.2	calcite-I	A
NA IV	9-17-53-19W5	3695.4	113.9		-17.6	20.3	calcite-I	A
NA IV	9-17-53-19W5	3695.4	133.6		-17.8	20.4	calcite-I	A
NA IV	9-17-53-19W5	3695.4	134.5		-17.2	20.0	calcite-I	A
NA IV	9-17-53-19W5	3695.4	113.6		-17.3	20.1	calcite-I	A
NA IV	9-17-53-19W5	3695.4	91.9		-17.2	20.0	calcite-I	A
NA IV	9-17-53-19W5	3695.4	113.1		-17.2	20.0	calcite-I	A
NA IV	9-17-53-19W5	3695.4	99.7		-17.2	20.0	calcite-I	A
NA IV	9-17-53-19W5	3695.4	101.6		-17.5	20.2	calcite-I	A
NA IV	9-17-53-19W5	3695.4	103.5		-17.3	20.1	calcite-I	A
NA IV	9-17-53-19W5	3695.4	98.3		-17.3	20.1	calcite-I	A
NA IV	9-17-53-19W5	3695.4	112.2		-17.3	20.1	calcite-I	A
NA IV	9-17-53-19W5	3695.4	126.9		-17.3	20.1	calcite-I	A
NA IV	9-17-53-19W5	3695.4	127		-17.4	20.2	calcite-I	A
NA IV	9-17-53-19W5	3695.4	98.1		-17.4	20.2	calcite-I	A
NA IV	9-17-53-19W5	3695.4	108.3		-17.5	20.2	calcite-I	A
NA IV	9-17-53-19W5	3695.4	109.5		-17.3	20.1	calcite-I	A
NA IV	9-17-53-19W5	3695.4	124.5		-17.3	20.1	calcite-I	A
NA IV	9-17-53-19W5	3695.4	131.8		-17.3	20.1	calcite-I	A
NA IV	9-17-53-19W5	3695.4	157.3		-17.4	20.2	calcite-I	A
NA IV	9-17-53-19W5	3695.4	110.5		-17.3	20.1	calcite-I	A
NA IV	9-17-53-19W5	3695.4	157.1		-17.5	20.2	calcite-I	A
NA IV	9-17-53-19W5	3695.4	157.7		-17.2	20.0	calcite-I	A
NA IV	9-17-53-19W5	3695.4	143.3		-17.7	20.4	calcite-I	A
NA IV	9-17-53-19W5	3695.4	146.6		-17.5	20.2	calcite-I	A
NA IV	9-17-53-19W5	3695.4	113.9		-17.3	20.1	calcite-I	A
NA IV	9-17-53-19W5	3695.4	124.3		-17.4	20.2	calcite-I	A
NA IV	9-17-53-19W5	3695.4	126.4		-17.4	20.2	calcite-I	A

NA IV	9-17-53-19W5	3695.4	124.3		-17.5	20.2	calcite-I	A
NA 208	11-2-59-16w5	2734.4	110.6		-12.4	16.2	calcite-I	A
NA 208	11-2-59-16w5	2734.4	108.6		-12.3	16.1	calcite-I	A
NA 208	11-2-59-16w5	2734.4	120.8		-12.4	16.2	calcite-I	A
NA 208	11-2-59-16w5	2734.4	127.9		-12.4	16.2	calcite-I	A
NA 208	11-2-59-16w5	2734.4	112.9		-12.5	16.3	calcite-I	A
NA 208	11-2-59-16w5	2734.4	117.8		-12.4	16.2	calcite-I	A
NA 208	11-2-59-16w5	2734.4	113.3		-12.4	16.2	calcite-I	A
NA 208	11-2-59-16w5	2734.4	115.4		-12.5	16.3	calcite-I	A
NA 208	11-2-59-16w5	2734.4	123		-12.4	16.2	calcite-I	A
NA 208	11-2-59-16w5	2734.4	148.6		-12.5	16.3	calcite-I	A
NA 208	11-2-59-16w5	2734.4	139.9	-53.0	-12.7	16.5	calcite-I	A
NA 208	11-2-59-16w5	2734.4	144.6	-54 to -53	-13.1	16.9	calcite-I	A
NA 208	11-2-59-16w5	2734.4	144.8	-54 to -53	-13.2	17.0	calcite-I	A
NA 208	11-2-59-16w5	2734.4	153.1	-54 to -53	-12.7	16.5	calcite-I	A
NA 208	11-2-59-16w5	2734.4	143.5	-54 to -53	-12.7	16.5	calcite-I	A
NA 208	11-2-59-16w5	2734.4	128.7	-54 to -53	-13.4	17.1	calcite-I	A
NA 208	11-2-59-16w5	2734.4	125.7	-53	-12.6	16.4	calcite-I	A
NA 208	11-2-59-16w5	2734.4	138.5	-53	-12.6	16.4	calcite-I	A
NA 208	11-2-59-16w5	2734.4	131.5	-53	-12.4	16.2	calcite-I	A
NA 208	11-2-59-16w5	2734.4	129.7	-53	-12.4	16.2	calcite-I	A
NA 303 (NA III)	16-22-58-19W5	3375.4	135.2		-14.1	17.7	calcite-I	A
NA 303 (NA III)	16-22-58-19W5	3375.4	156.7		-14.1	17.7	calcite-I	A
NA 303 (NA III)	16-22-58-19W5	3375.4	148.3		-14.1	17.7	calcite-I	A
NA 303 (NA III)	16-22-58-19W5	3375.4	152.7		-14.3	17.9	calcite-I	A
NA 303 (NA III)	16-22-58-19W5	3375.4	155.6		-14.1	17.7	calcite-I	A
NA 303 (NA III)	16-22-58-19W5	3375.4	153.8		-14.3	17.9	calcite-I	A
NA 303 (NA III)	16-22-58-19W5	3375.4	149.8		-14.1	17.7	calcite-I	A
NA 303 (NA III)	16-22-58-19W5	3375.4	148.5		-14.0	17.6	calcite-I	A
NA 303 (NA III)	16-22-58-19W5	3375.4	166.4		-14.0	17.6	calcite-I	A
NA 303 (NA III)	16-22-58-19W5	3375.4	155.9		-14.1	17.7	calcite-I	A
NA 303 (NA III)	16-22-58-19W5	3375.4	151.2		-14.1	17.7	calcite-I	A
NA 303 (NA III)	16-22-58-19W5	3375.4	152.7		-14.1	17.7	calcite-I	A
NA 303 (NA III)	16-22-58-19W5	3375.4	155.8		-13.9	17.5	calcite-I	A
NA 303 (NA III)	16-22-58-19W5	3375.4	161.9		-14.1	17.7	calcite-I	A
NA 303 (NA III)	16-22-58-19W5	3375.4	154.3		-14.1	17.7	calcite-I	A
NA 303 (NA III)	16-22-58-19W5	3375.4	161		-14.1	17.7	calcite-I	A
NA 303 (NA III)	16-22-58-19W5	3375.4	164.7		-14.0	17.6	calcite-I	A
NA 303 (NA III)	16-22-58-19W5	3375.4	157.1		-14.1	17.7	calcite-I	A
NA 297	2-14-50-22w5	4581.75	189.5	-89	-4.3	6.9	calcite-I	A
NA 297	2-14-50-22w5	4581.75	189.1	-88	-9.1	12.9	calcite-I	A
NA 297	2-14-50-22w5	4581.75	189	-90 to -87	-9.1	12.9	calcite-I	A
NA 297	2-14-50-22w5	4581.75	188.5	-90 to -87	-8.5	12.3	calcite-I	A

NA 297	2-14-50-22w5	4581.75	190.2	-90 to -87	-8.3	12.0	calcite-I	A
NA 297	2-14-50-22w5	4581.75	190.8	-90 to -87	-10.1	14.0	calcite-I	A
NA 297	2-14-50-22w5	4581.75	184.9		-8.9	12.7	calcite-I	A
NA 297	2-14-50-22w5	4581.75	185.9		-8.5	12.3	calcite-I	A
NA 297	2-14-50-22w5	4581.75	187.1		-8.5	12.3	calcite-I	A
NA 297	2-14-50-22w5	4581.75	187.2	-90	-8.9	12.7	calcite-I	A
NA 297	2-14-50-22w5	4581.75	187.2	-90	-9.1	12.9	calcite-I	A
NA 297	2-14-50-22w5	4581.75	187.2	-89	-9.1	12.9	calcite-I	A
NA 297	2-14-50-22w5	4581.75	193.1	-89	-8.2	11.9	calcite-I	A
NA 297	2-14-50-22w5	4581.75	185.2	-92 to -89	-10.7	14.6	calcite-I	A
NA 297	2-14-50-22w5	4581.75	168	-92 to -89	-8.1	11.8	calcite-I	A
NA 297	2-14-50-22w5	4581.75	169.2	-92 to -89	-9.1	12.9	calcite-I	A
NA 297	2-14-50-22w5	4581.75	186.1	-92 to -89	-9.2	13.0	calcite-I	A
NA 297	2-14-50-22w5	4581.75	187		-8.5	12.3	calcite-I	A
NA 297	2-14-50-22w5	4581.75	189.2		-8.4	12.1	calcite-I	A
NA 297	2-14-50-22w5	4581.75	168		-9.1	12.9	calcite-I	A
NA 297	2-14-50-22w5	4581.75	177.9	-89	-8.7	12.5	calcite-I	A
NA 297	2-14-50-22w5	4581.75	193.1	-89	-2.6	4.4	calcite-I	A
NA 297	2-14-50-22w5	4581.75	166	-90	-8.2	11.9	calcite-I	A
NA 297	2-14-50-22w5	4581.75	184	-90	-8.2	11.9	calcite-I	A
NA 297	2-14-50-22w5	4581.75	185.9	-92 to -89	-12.1	16.0	calcite-I	A
NA 297	2-14-50-22w5	4581.75	177.5		-9.0	12.8	calcite-I	A
NA 297	2-14-50-22w5	4581.75	183.1	-92 to -89	-9.7	13.6	calcite-I	A
NA 297	2-14-50-22w5	4581.75	182.1		-9.1	12.9	calcite-I	A
NA 297	2-14-50-22w5	4581.75	175.1		-12.4	16.2	calcite-I	A
NA 297	2-14-50-22w5	4581.75	174		-8.8	12.6	calcite-I	A
NA 297	2-14-50-22w5	4581.75	190.2		-9.4	13.3	calcite-I	A
NA 297	2-14-50-22w5	4581.75	168.7	-94	-8.7	12.5	calcite-I	A
NA 297	2-14-50-22w5	4581.75	190.1	-93	-4.5	7.2	calcite-I	A
NA 297	2-14-50-22w5	4581.75	162.9	-95	-8.9	12.7	calcite-I	A
NA 297	2-14-50-22w5	4581.75	178.8	-90	-9.8	13.7	calcite-I	A
NA 297	2-14-50-22w5	4581.75	182.3	-90	-8.5	12.3	calcite-I	A
NA 297	2-14-50-22w5	4581.75	183.1		-9.7	13.6	calcite-I	A
NA 297	2-14-50-22w5	4581.75	182.1		-9.1	12.9	calcite-I	A
NA 297	2-14-50-22w5	4581.75	175.1		-12.4	16.2	calcite-I	A
NA 297	2-14-50-22w5	4581.75	174		-8.8	12.6	calcite-I	A
NA 297	2-14-50-22w5	4581.75	190.2		-9.4	13.3	calcite-I	A
NA 297	2-14-50-22w5	4581.75	168.7		-8.7	12.5	calcite-I	A
NA 297	2-14-50-22w5	4581.75	190.1		-4.5	7.2	calcite-I	A
NA 297	2-14-50-22w5	4581.75	162.9		-8.9	12.7	calcite-I	A
NA 297	2-14-50-22w5	4581.75	178.8		-9.8	13.7	calcite-I	A
NA 297	2-14-50-22w5	4581.75	182.3		-8.5	12.3	calcite-I	A
NA 200	2/15-09-57-17w5	3162.75	180.8	-55	-18.1	20.6	calcite-II	A
NA 200	2/15-09-57-17w5	3162.75	181.6	-55	-17.8	20.4	calcite-II	A
NA 200	2/15-09-57-17w5	3162.75	180.1	-56	-18.0	20.6	calcite-II	A
NA 200	2/15-09-57-17w5	3162.75	195.7	-56	-18.1	20.6	calcite-II	A
NA 200	2/15-09-57-17w5	3162.75	198.6	-56	-18.5	20.9	calcite-II	A

NA 200	2/15-09-57-17w5	3162.75	195.2	-56	-18.9	21.1	calcite-II	A
NA 200	2/15-09-57-17w5	3162.75	173.2	-56	-16.1	19.3	calcite-II	A
NA 200	2/15-09-57-17w5	3162.75	191.6	-56	-17.9	20.5	calcite-II	A
NA 200	2/15-09-57-17w5	3162.75	176.6	-56	-17.8	20.4	calcite-II	A
NA 200	2/15-09-57-17w5	3162.75	180	-56	-17.9	20.5	calcite-II	A
NA 200	2/15-09-57-17w5	3162.75	165.6		-18.0	20.6	calcite-II	A
NA 200	2/15-09-57-17w5	3162.75	185		-18.1	20.6	calcite-II	A
NA 200	2/15-09-57-17w5	3162.75	147.7		-18.1	20.6	calcite-II	A
NA 200	2/15-09-57-17w5	3162.75	156.1		-18.0	20.6	calcite-II	A
NA 200	2/15-09-57-17w5	3162.75	153.2		-17.9	20.5	calcite-II	A
NA 200	2/15-09-57-17w5	3162.75	125.6	-49	-17.4	20.2	calcite-II	A
NA 200	2/15-09-57-17w5	3162.75	127.6	-49	-17.0	19.9	calcite-II	A
NA 200	2/15-09-57-17w5	3162.75	128	-49	-16.9	19.8	calcite-II	A
NA 200	2/15-09-57-17w5	3162.75	128.4	-49	-17.0	19.9	calcite-II	A
NA 200	2/15-09-57-17w5	3162.75	154.4	-53	-18.0	20.6	calcite-II	A
NA 200	2/15-09-57-17w5	3162.75	168.1	-53	-18.0	20.6	calcite-II	A
NA 200	2/15-09-57-17w5	3162.75	169.6	-53	-18.2	20.7	calcite-II	A
NA 200	2/15-09-57-17w5	3162.75	168.5	-53	-18.1	20.6	calcite-II	A
NA 200	2/15-09-57-17w5	3162.75	174.5	-53	-18.1	20.6	calcite-II	A
NA 200	2/15-09-57-17w5	3162.75	120.5	-51	-17.0	19.9	calcite-II	A
NA 200	2/15-09-57-17w5	3162.75	121.9	-51	-16.8	19.8	calcite-II	A
NA 200	2/15-09-57-17w5	3162.75	152.5	-51	-17.9	20.5	calcite-II	A
NA 200	2/15-09-57-17w5	3162.75	154.2	-51	-17.8	20.4	calcite-II	A
NA 200	2/15-09-57-17w5	3162.75	167.4	-49	-16.1	19.3	calcite-II	A
NA 200	2/15-09-57-17w5	3162.75	178.8	-54	-16.0	19.2	calcite-II	A
NA 200	2/15-09-57-17w5	3162.75	185.6	-54	-15.9	19.1	calcite-II	A
NA 200	2/15-09-57-17w5	3162.75	131.6	-53	-15.9	19.1	calcite-II	A
NA 200	2/15-09-57-17w5	3162.75	145.6	-53	-15.7	19.0	calcite-II	A
NA 200	2/15-09-57-17w5	3162.75	157.9	-53	-15.7	19.0	calcite-II	A
NA 200	2/15-09-57-17w5	3162.75	147.4		-16.2	19.3	calcite-II	A
NA 200	2/15-09-57-17w5	3162.75	171.3		-17.8	20.4	calcite-II	A
NA 200	2/15-09-57-17w5	3162.75	155.2	-51 to -53	-18.1	20.6	calcite-II	A
NA 200	2/15-09-57-17w5	3162.75	159.1	-51 to -53	-18.5	20.9	calcite-II	A
NA 200	2/15-09-57-17w5	3162.75	133.4		-18.6	20.9	calcite-II	A
NA 200	2/15-09-57-17w5	3162.75	137.3	-51	-18.1	20.6	calcite-II	A
NA 200	2/15-09-57-17w5	3162.75	160.3	-51	-16.1	19.3	calcite-II	A
NA 200	2/15-09-57-17w5	3162.75	174.4	-51	-18.9	21.1	calcite-II	A
NA 200	2/15-09-57-17w5	3162.75	187.8		-19.1	21.2	calcite-II	A
NA 200	2/15-09-57-17w5	3162.75	128.1		-17.9	20.5	calcite-II	A
NA 200	2/15-09-57-17w5	3162.75	132		-17.9	20.5	calcite-II	A
NA 200	2/15-09-57-17w5	3162.75	145.2	-51	-17.9	20.5	calcite-II	A
NA 200	2/15-09-57-17w5	3162.75	189.3		-17.8	20.4	calcite-II	A
NA 200	2/15-09-57-17w5	3162.75		-54	-17.9	20.5	calcite-II	A
NA 200	2/15-09-57-17w5	3162.75		-49			calcite-II	A
NA 200	2/15-09-57-17w5	3162.75		-51			calcite-II	A
NA 200	2/15-09-57-17w5	3162.75		-54			calcite-II	A
NA 200	2/15-09-57-17w5	3162.75		-51 to -53			calcite-II	A

NA 200	2/15-09-57-17w5	3162.75		-56			calcite-II	A
NA 200	2/15-09-57-17w5	3162.75		-56			calcite-II	A
NA 10	10-32-44-19W5	5363.9	126.7	-51	-12.5	16.3	calcite-II	A
NA 10	10-32-44-19W5	5363.9	127.5		-13.1	16.9	calcite-II	A
NA 10	10-32-44-19W5	5363.9	137.6	-52	-12.7	16.5	calcite-II	A
NA 10	10-32-44-19W5	5363.9	141.6	-53	-12.7	16.5	calcite-II	A
NA 10	10-32-44-19W5	5363.9	149.8	-51	-14.9	18.4	calcite-II	A
NA 10	10-32-44-19W5	5363.9	137.5		-11.7	15.6	calcite-II	A
NA 10	10-32-44-19W5	5363.9	128.6	-50	-11.8	15.7	calcite-II	A
NA 10	10-32-44-19W5	5363.9	155.5	-49	-12.1	16.0	calcite-II	A
NA 10	10-32-44-19W5	5363.9	150.4	-50	-13.0	16.8	calcite-II	A
NA 10	10-32-44-19W5	5363.9	157.2	-50	-12.5	16.3	calcite-II	A
NA 10	10-32-44-19W5	5363.9	157.2	-50	-12.7	16.5	calcite-II	A
NA 10	10-32-44-19W5	5363.9	134.7	-52	-12.7	16.5	calcite-II	A
NA 10	10-32-44-19W5	5363.9	136.8	-52	-12.6	16.4	calcite-II	A
NA 10	10-32-44-19W5	5363.9	153.8	-52	-13.0	16.8	calcite-II	A
NA 10	10-32-44-19W5	5363.9	174.7	-54	-11.8	15.7	calcite-II	A
NA 10	10-32-44-19W5	5363.9	149	-54	-13.6	17.3	calcite-II	A
NA 10	10-32-44-19W5	5363.9	151.2	-54	-13.0	16.8	calcite-II	A
NA 10	10-32-44-19W5	5363.9	148.1	-54	-13.1	16.9	calcite-II	A
NA 10	10-32-44-19W5	5363.9	151.6		-13.1	16.9	calcite-II	A
NA 10	10-32-44-19W5	5363.9					calcite-II	A
NA 273	3-26-49-20w5	4577	126.5				calcite-II	A
NA 273	3-26-49-20w5	4577	133.5				calcite-II	A
NA 273	3-26-49-20w5	4577	147.5				calcite-II	A
NA 273	3-26-49-20w5	4577	157.3				calcite-II	A
NA 273	3-26-49-20w5	4577	152.1				calcite-II	A
NA 273	3-26-49-20w5	4577	158.1				calcite-II	A
NA 273	3-26-49-20w5	4577	159.9				calcite-II	A
NA 116	1-18-56-16w5	2951.2	131.7	-54	-15.3	18.7	calcite-II	A
NA 116	1-18-56-16w5	2951.2	148.3	-54	-17.2	20.0	calcite-II	A
NA 116	1-18-56-16w5	2951.2	136.2	-54	-17.1	20.0	calcite-II	A
NA 116	1-18-56-16w5	2951.2	136.9	-55 to -53	-17.1	20.0	calcite-II	A
NA 116	1-18-56-16w5	2951.2	138.7	-55 to -53	-17.2	20.0	calcite-II	A
NA 116	1-18-56-16w5	2951.2	142.1	-55 to -53	-17.0	19.9	calcite-II	A
NA 116	1-18-56-16w5	2951.2	147.3	-54	-17.1	20.0	calcite-II	A
NA 116	1-18-56-16w5	2951.2	126.1	-54	-17.1	20.0	calcite-II	A
NA 116	1-18-56-16w5	2951.2	134.2		-17.2	20.0	calcite-II	A
NA 116	1-18-56-16w5	2951.2	147.2		-17.3	20.1	calcite-II	A
NA 116	1-18-56-16w5	2951.2	133.5		-17.2	20.0	calcite-II	A
NA 116	1-18-56-16w5	2951.2	173.2		-16.8	19.8	calcite-II	A
NA 116	1-18-56-16w5	2951.2	140.5	-53 to -52	-17.2	20.0	calcite-II	A
NA 116	1-18-56-16w5	2951.2	141.3	-53	-17.2	20.0	calcite-II	A
NA 116	1-18-56-16w5	2951.2	176.8	-53	-17.0	19.9	calcite-II	A
NA 116	1-18-56-16w5	2951.2	177.5		-17.2	20.0	calcite-II	A
NA 116	1-18-56-16w5	2951.2	133.7	-54 to -53	-17.1	20.0	calcite-II	A
NA 116	1-18-56-16w5	2951.2	135.1	-54 to -53	-17.2	20.0	calcite-II	A

NA 116	1-18-56-16w5	2951.2	133.4	-54 to -53	-17.1	20.0	calcite-II	A
NA 116	1-18-56-16w5	2951.2	135.7		-16.7	19.7	calcite-II	A
NA 116	1-18-56-16w5	2951.2	145	-54	-16.9	19.8	calcite-II	A
NA 116	1-18-56-16w5	2951.2	123.3	-54	-16.3	19.4	calcite-II	A
NA 116	1-18-56-16w5	2951.2	144.8	-53	-16.7	19.7	calcite-II	A
NA 271	5-25-51-22w5	4473	136.9				calcite-II	A
NA 271	5-25-51-22w5	4473	142.8				calcite-II	A
NA 271	5-25-51-22w5	4473	132.1				calcite-II	A
NA 271	5-25-51-22w5	4473	139.2				calcite-II	A
NA 271	5-25-51-22w5	4473	141.9				calcite-II	A
NA 271	5-25-51-22w5	4473	149.2				calcite-II	A
NA 271	5-25-51-22w5	4473	146				calcite-II	A
NA 271	5-25-51-22w5	4473	154.1				calcite-II	A
NA 271	5-25-51-22w5	4473	166.0				calcite-II	A
NA 271	5-25-51-22w5	4473	166.5				calcite-II	A
NA 271	5-25-51-22w5	4473	167.3				calcite-II	A
NA 271	5-25-51-22w5	4473	182.5				calcite-II	A
NA 271	5-25-51-22w5	4473	178.7				calcite-II	A
NA 271	5-25-51-22w5	4473	167.0				calcite-II	A
NA 271	5-25-51-22w5	4473	155.9				calcite-II	A
NA 271	5-25-51-22w5	4473	164.0				calcite-II	A
NA 271	5-25-51-22w5	4473	181.0				calcite-II	A
NA 271	5-25-51-22w5	4473	172.8				calcite-II	A
NA 271	5-25-51-22w5	4473	167.3				calcite-II	A
NA 271	5-25-51-22w5	4473	183.1				calcite-II	A
NA 271	5-25-51-22w5	4473	166.4				calcite-II	A
NA 271	5-25-51-22w5	4473	144.4				calcite-II	A
NA 271	5-25-51-22w5	4473	176.5				calcite-II	A
NA 271	5-25-51-22w5	4473	180.9				calcite-II	A
NA 271	5-25-51-22w5	4473	165.9				calcite-II	A
NA 271	5-25-51-22w5	4473	180.3				calcite-II	A
NA 271	5-25-51-22w5	4473	181.2				calcite-II	A
NA 271	5-25-51-22w5	4473	180.9				calcite-II	A
NA 271	5-25-51-22w5	4473	180.8				calcite-II	A
NA 271	5-25-51-22w5	4473	181.8				calcite-II	A
NA 271	5-25-51-22w5	4473	184.1				calcite-II	A
NA 271	5-25-51-22w5	4473	186.9				calcite-II	A
NA 271	5-25-51-22w5	4473	188.7				calcite-II	A
NA 271	5-25-51-22w5	4473	191.2				calcite-II	A
NA 271	5-25-51-22w5	4473	171.2				calcite-II	A
NA 271	5-25-51-22w5	4473	181.8				calcite-II	A
NA 271	5-25-51-22w5	4473	189.0				calcite-II	A
NA 271	5-25-51-22w5	4473	190.1				calcite-II	A
NA 271	5-25-51-22w5	4473	158.9				calcite-II	A
NA 270	5-25-51-22w5	4468	175.1		-15.7	19.0	calcite-II	A
NA 270	5-25-51-22w5	4468	170.2		-15.7	19.0	calcite-II	A
NA 270	5-25-51-22w5	4468	136.1		-15.5	18.8	calcite-II	A

NA 270	5-25-51-22w5	4468	171.9	-53	-15.7	19.0	calcite-II	A
NA 270	5-25-51-22w5	4468	172.5	-54	-15.9	19.1	calcite-II	A
NA 270	5-25-51-22w5	4468	173.9	-54	-15.5	18.8	calcite-II	A
NA 270	5-25-51-22w5	4468	173.9	-54	-15.2	18.6	calcite-II	A
NA 270	5-25-51-22w5	4468	175.7		-15.5	18.8	calcite-II	A
NA 270	5-25-51-22w5	4468	175.6	-53 to -51	-15.9	19.1	calcite-II	A
NA 270	5-25-51-22w5	4468	178.4	-51	-16.0	19.2	calcite-II	A
NA 270	5-25-51-22w5	4468	146.9		-15.9	19.1	calcite-II	A
NA 270	5-25-51-22w5	4468	146.9	-52	-15.9	19.1	calcite-II	A
NA 270	5-25-51-22w5	4468	147	-52	-15.9	19.1	calcite-II	A
NA 270	5-25-51-22w5	4468	161.2	-52	-16.1	19.3	calcite-II	A
NA 270	5-25-51-22w5	4468	173.1	-52	-15.9	19.1	calcite-II	A
NA 270	5-25-51-22w5	4468	174	-53 to -51	-16.0	19.2	calcite-II	A
NA 270	5-25-51-22w5	4468	162.6		-16.0	19.2	calcite-II	A
NA 270	5-25-51-22w5	4468	169.4		-16.1	19.3	calcite-II	A
NA 270	5-25-51-22w5	4468	170		-16.0	19.2	calcite-II	A
NA 270	5-25-51-22w5	4468	159.9	-53	-16.0	19.2	calcite-II	A
NA 270	5-25-51-22w5	4468	170.1	-53 to -51	-16.0	19.2	calcite-II	A
NA 270	5-25-51-22w5	4468	171.1	-53 to -51	-15.6	18.9	calcite-II	A
NA 270	5-25-51-22w5	4468	179.4	-53	-16.5	19.5	calcite-II	A
NA 270	5-25-51-22w5	4468	179.8	-53	-16.1	19.3	calcite-II	A
NA 270	5-25-51-22w5	4468	156.2		-16.1	19.3	calcite-II	A
NA 270	5-25-51-22w5	4468	169.8		-15.9	19.1	calcite-II	A
NA 270	5-25-51-22w5	4468	174.5		-15.8	19.0	calcite-II	A
NA 270	5-25-51-22w5	4468	176.2		-16.1	19.3	calcite-II	A
NA 270	5-25-51-22w5	4468	151		-15.1	18.5	calcite-II	A
NA 270	5-25-51-22w5	4468	164.8		-15.3	18.7	calcite-II	A
NA 270	5-25-51-22w5	4468	182.7		-15.7	19.0	calcite-II	A
NA 270	5-25-51-22w5	4468	184.2		-15.1	18.5	calcite-II	A
NA 270	5-25-51-22w5	4468	147	-53	-16.9	19.8	calcite-II	A
NA 270	5-25-51-22w5	4468	146.5	-53	-18.2	20.7	calcite-II	A
NA 270	5-25-51-22w5	4468	176.3		-16.0	19.2	calcite-II	A
NA 270	5-25-51-22w5	4468	153.5	-53 to -52	-19.5	21.5	calcite-II	A
NA 270	5-25-51-22w5	4468	173.1		-16.7	19.7	calcite-II	A
NA 270	5-25-51-22w5	4468	174.6	-54 to -52	-15.7	19.0	calcite-II	A
NA 270	5-25-51-22w5	4468	175	-53	-15.5	18.8	calcite-II	A
NA 270	5-25-51-22w5	4468	177.9	-53	-16.9	19.8	calcite-II	A
NA 270	5-25-51-22w5	4468	184.5	-54	-14.5	18.0	calcite-II	A
NA 270	5-25-51-22w5	4468	181.8	-54 to -53	-15.1	18.5	calcite-II	A
NA 270	5-25-51-22w5	4468	183.9	-53 to -51	-15.7	19.0	calcite-II	A
NA 270	5-25-51-22w5	4468	164.3	-55 to -53	-15.9	19.1	calcite-II	A
NA 270	5-25-51-22w5	4468	164.5	-54 to -52	-15.9	19.1	calcite-II	A
NA 270	5-25-51-22w5	4468	172.9		-15.0	18.4	calcite-II	A
NA 270	5-25-51-22w5	4468	173.6		-14.8	18.3	calcite-II	A
NA 270	5-25-51-22w5	4468	173.6	-54 to -53	-15.0	18.4	calcite-II	A
NA 270	5-25-51-22w5	4468	176	-54	-15.3	18.7	calcite-II	A
NA 270	5-25-51-22w5	4468	180.7		-15.1	18.5	calcite-II	A

NA 270	5-25-51-22w5	4468	181.3		-15.1	18.5	calcite-II	A
NA 270	5-25-51-22w5	4468	181.5		-15.1	18.5	calcite-II	A
NA 270	5-25-51-22w5	4468	172.1		-16.9	19.8	calcite-II	A
NA 270	5-25-51-22w5	4468	177.2	-54	-15.1	18.5	calcite-II	A
NA 270	5-25-51-22w5	4468	146.9				calcite-II	A
NA 290	9-5-57-17w5	3188	93.7		-17.7	20.4	calcite-II	A
NA 290	9-5-57-17w5	3188	103		-17.6	20.3	calcite-II	A
NA 290	9-5-57-17w5	3188	112.1		-17.7	20.4	calcite-II	A
NA 290	9-5-57-17w5	3188	114.9		-17.7	20.4	calcite-II	A
NA 290	9-5-57-17w5	3188	97.6	-54 to -53	-18.8	21.1	calcite-II	A
NA 290	9-5-57-17w5	3188	105.7	-54 to -53	-18.5	20.9	calcite-II	A
NA 290	9-5-57-17w5	3188	106.8	-54 to -53	-18.5	20.9	calcite-II	A
NA 290	9-5-57-17w5	3188	107.9		-17.8	20.4	calcite-II	A
NA 290	9-5-57-17w5	3188	113.3		-17.5	20.2	calcite-II	A
NA 290	9-5-57-17w5	3188	114.7		-17.3	20.1	calcite-II	A
NA 290	9-5-57-17w5	3188	114.3		-17.3	20.1	calcite-II	A
NA 290	9-5-57-17w5	3188	107.9	-55	-16.7	19.7	calcite-II	A
NA 290	9-5-57-17w5	3188	114.5	-55	-15.3	18.7	calcite-II	A
NA 290	9-5-57-17w5	3188	108.7	-55 to -54	-18.8	21.1	calcite-II	A
NA 290	9-5-57-17w5	3188	111.4	-55	-18.7	21.0	calcite-II	A
NA 290	9-5-57-17w5	3188	113.7	-54	-17.6	20.3	calcite-II	A
NA 290	9-5-57-17w5	3188	114	-54	-18.5	20.9	calcite-II	A
NA 290	9-5-57-17w5	3188	116.4		-18.8	21.1	calcite-II	A
NA 290	9-5-57-17w5	3188	114.1		-17.8	20.4	calcite-II	A
NA 290	9-5-57-17w5	3188	121.3	-54	-16.8	19.8	calcite-II	A
NA 290	9-5-57-17w5	3188	121.5	-54	-16.8	19.8	calcite-II	A
NA 290	9-5-57-17w5	3188	104.5	-55	-17.0	19.9	calcite-II	A
NA 290	9-5-57-17w5	3188	110.9	-54	-17.0	19.9	calcite-II	A
NA 290	9-5-57-17w5	3188	113.6	-54 to -53	-17.3	20.1	calcite-II	A
NA 290	9-5-57-17w5	3188	105.8	-54	-18.7	21.0	calcite-II	A
NA 290	9-5-57-17w5	3188	106.6	-55 to -54	-16.9	19.8	calcite-II	A
NA 290	9-5-57-17w5	3188	107.8	-55 to -54	-17.6	20.3	calcite-II	A
NA 290	9-5-57-17w5	3188	108.7	-55 to -54	-20.1	21.8	calcite-II	A
NA 290	9-5-57-17w5	3188	91		-17.8	20.4	calcite-II	A
NA 290	9-5-57-17w5	3188	91.3	-55 to -54	-17.8	20.4	calcite-II	A
NA 290	9-5-57-17w5	3188	96.9		-17.5	20.2	calcite-II	A
NA 290	9-5-57-17w5	3188	97.5		-17.8	20.4	calcite-II	A
NA 290	9-5-57-17w5	3188	97.9		-17.8	20.4	calcite-II	A
NA 290	9-5-57-17w5	3188	108.9		-17.5	20.2	calcite-II	A
NA 290	9-5-57-17w5	3188	120.2		-17.8	20.4	calcite-II	A
NA 290	9-5-57-17w5	3188	94.5		-17.5	20.2	calcite-II	A
NA 290	9-5-57-17w5	3188	96.2		-17.5	20.2	calcite-II	A
NA 290	9-5-57-17w5	3188	101.3		-17.8	20.4	calcite-II	A
NA 290	9-5-57-17w5	3188	105.2		-17.8	20.4	calcite-II	A
NA 290	9-5-57-17w5	3188	113.4		-17.5	20.2	calcite-II	A
NA 290	9-5-57-17w5	3188	143.9		-17.5	20.2	calcite-II	A
NA 290	9-5-57-17w5	3188	145.6		-17.5	20.2	calcite-II	A

NA 290	9-5-57-17w5	3188	127.5	-55	-17.8	20.4	calcite-II	A
NA 290	9-5-57-17w5	3188	128		-17.8	20.4	calcite-II	A
NA 290	9-5-57-17w5	3188	128.8	-55	-17.8	20.4	calcite-II	A
NA 290	9-5-57-17w5	3188	129.2	-55	-17.6	20.3	calcite-II	A
NA 290	9-5-57-17w5	3188	130.8	-55	-17.5	20.2	calcite-II	A
NA 290	9-5-57-17w5	3188	132	-55	-17.8	20.4	calcite-II	A
NA 290	9-5-57-17w5	3188	132.1	-55	-18.0	20.6	calcite-II	A
NA 290	9-5-57-17w5	3188		-55	-18.0	20.6	calcite-II	A
NA 290	9-5-57-17w5	3188		-55	-17.5	20.2	calcite-II	A
NA 290	9-5-57-17w5	3188			-17.5	20.2	calcite-II	A
NA 290	9-5-57-17w5	3188		-54 to -53	-16.8	19.8	calcite-II	A
NA 290	9-5-57-17w5	3188		-54 to -53	-17.5	20.2	calcite-II	A
NA 290	9-5-57-17w5	3188		-54 to -53	-17.8	20.4	calcite-II	A
NA 290	9-5-57-17w5	3188	117.6	-54 to -53	-17.5	20.2	calcite-II	A
NA 290	9-5-57-17w5	3188	130.2	-54 to -53	-17.8	20.4	calcite-II	A
NA 290	9-5-57-17w5	3188	141.9	-55	-17.8	20.4	calcite-II	A
NA 290	9-5-57-17w5	3188	144.6	-55	-17.5	20.2	calcite-II	A
NA 290	9-5-57-17w5	3188	134.9	-55	-17.2	20.0	calcite-II	A
NA 290	9-5-57-17w5	3188	128.8	-56 to -55	-17.8	20.4	calcite-II	A
NA 290	9-5-57-17w5	3188	131.9	-56 to -55	-17.8	20.4	calcite-II	A
NA 290	9-5-57-17w5	3188	133.3	-56 to -55	-18.7	21.0	calcite-II	A
NA 290	9-5-57-17w5	3188	135.1		-15.5	18.8	calcite-II	A
NA 123	06-16-55-18w5	3319.3	142.8	-56 to -55	-16.4	19.5	calcite-II	A
NA 123	06-16-55-18w5	3319.3	139.5	-56 to -55	-16.4	19.5	calcite-II	A
NA 123	06-16-55-18w5	3319.3	121.6	-56 to -55	-16.0	19.2	calcite-II	A
NA 123	06-16-55-18w5	3319.3	129.5	-56 to -55	-16.0	19.2	calcite-II	A
NA 123	06-16-55-18w5	3319.3	141.6	-56 to -55	-15.7	19.0	calcite-II	A
NA 123	06-16-55-18w5	3319.3	140.9		-16.4	19.5	calcite-II	A
NA 123	06-16-55-18w5	3319.3	128.5	-54 to -53	-16.3	19.4	calcite-II	A
NA 123	06-16-55-18w5	3319.3	121.2	-54	-16.5	19.5	calcite-II	A
NA 123	06-16-55-18w5	3319.3	149.8	-54 to -53	-16.5	19.5	calcite-II	A
NA 123	06-16-55-18w5	3319.3	124.5	-53	-16.3	19.4	calcite-II	A
NA 123	06-16-55-18w5	3319.3	133.7		-18.2	20.7	calcite-II	A
NA 123	06-16-55-18w5	3319.3	152.8		-16.7	19.7	calcite-II	A
NA 123	06-16-55-18w5	3319.3	141.3		-16.7	19.7	calcite-II	A
NA 123	06-16-55-18w5	3319.3	146.3		-16.3	19.4	calcite-II	A
NA 123	06-16-55-18w5	3319.3	174.5	-54 to -53	-16.7	19.7	calcite-II	A
NA 123	06-16-55-18w5	3319.3	136.6		-16.3	19.4	calcite-II	A
NA 123	06-16-55-18w5	3319.3	120.6		-16.5	19.5	calcite-II	A
NA 123	06-16-55-18w5	3319.3	141.8	-55	-16.9	19.8	calcite-II	A
NA 123	06-16-55-18w5	3319.3	158.1	-55	-16.5	19.5	calcite-II	A
NA 123	06-16-55-18w5	3319.3	166.4	-55	-16.5	19.5	calcite-II	A
NA 123	06-16-55-18w5	3319.3	162.4	-55	-16.9	19.8	calcite-II	A
NA 123	06-16-55-18w5	3319.3	137.8		-16.5	19.5	calcite-II	A
NA 123	06-16-55-18w5	3319.3	140.7	-55	-16.7	19.7	calcite-II	A
NA 123	06-16-55-18w5	3319.3	156.2	-56 to -54	-16.7	19.7	calcite-II	A
NA 123	06-16-55-18w5	3319.3	139.6	-56 to -54	-16.7	19.7	calcite-II	A

NA 123	06-16-55-18w5	3319.3	144.1		-16.4	19.5	calcite-II	A
NA 123	06-16-55-18w5	3319.3	156.1		-16.5	19.5	calcite-II	A
NA 123	06-16-55-18w5	3319.3	123.8		-16.4	19.5	calcite-II	A
NA 123	06-16-55-18w5	3319.3	141.4		-15.5	18.8	calcite-II	A
NA 123	06-16-55-18w5	3319.3	142.8		-15.5	18.8	calcite-II	A
NA 123	06-16-55-18w5	3319.3	143.4		-15.5	18.8	calcite-II	A
NA 123	06-16-55-18w5	3319.3	149		-15.5	18.8	calcite-II	A
NA 123	06-16-55-18w5	3319.3	150.8		-15.3	18.7	calcite-II	A
NA 123	06-16-55-18w5	3319.3	161.9		-15.5	18.8	calcite-II	A
NA 123	06-16-55-18w5	3319.3	132.4		-17.7	20.4	calcite-II	A
NA 123	06-16-55-18w5	3319.3	125.6		-17.7	20.4	calcite-II	A
NA 123	06-16-55-18w5	3319.3	130.2		-16.9	19.8	calcite-II	A
NA 123	06-16-55-18w5	3319.3	132.9		-16.9	19.8	calcite-II	A
NA 123	06-16-55-18w5	3319.3	133		-16.9	19.8	calcite-II	A
NA 123	06-16-55-18w5	3319.3	135.8		-16.3	19.4	calcite-II	A
NA 123	06-16-55-18w5	3319.3	136.9		-16.9	19.8	calcite-II	A
NA 123	06-16-55-18w5	3319.3	133.4		-16.9	19.8	calcite-II	A
NA 320	16-18-61-15w5	2768.5	145.7	-50	-15	18.4	calcite-II	A
NA 320	16-18-61-15w5	2768.5	148.7	-53	-15	18.4	calcite-II	A
NA 320	16-18-61-15w5	2768.5	153.8	-51 to -50	-15.1	18.5	calcite-II	A
NA 320	16-18-61-15w5	2768.5	136.8	-52	-15	18.4	calcite-II	A
NA 320	16-18-61-15w5	2768.5	142.7	-52	-15	18.4	calcite-II	A
NA 320	16-18-61-15w5	2768.5	156.4	-49	-16.1	19.3	calcite-II	A
NA 320	16-18-61-15w5	2768.5	129.8	-50	-15.9	19.1	calcite-II	A
NA 320	16-18-61-15w5	2768.5	133.9	-50 to -49	-16.2	19.3	calcite-II	A
NA 333	15-9-57-17w5	3162	99.8	-55 to -54	-17.0	19.9	calcite-II	A
NA 333	15-9-57-17w5	3162	105.2	-55 to -54	-16.9	19.8	calcite-II	A
NA 333	15-9-57-17w5	3162	97.6	-55 to -54	-16.9	19.8	calcite-II	A
NA 333	15-9-57-17w5	3162	111.3	-55 to -54	-16.9	19.8	calcite-II	A
NA 333	15-9-57-17w5	3162	101.4	-54	-17.9	20.5	calcite-II	A
NA 333	15-9-57-17w5	3162	108.3	-54	-17.8	20.4	calcite-II	A
NA 333	15-9-57-17w5	3162	97.6	-54	-17.0	19.9	calcite-II	A
NA 333	15-9-57-17w5	3162	98.9	-54	-17.0	19.9	calcite-II	A
NA 333	15-9-57-17w5	3162	102.3	-54	-17.0	19.9	calcite-II	A
NA 333	15-9-57-17w5	3162	102.1	-53	-16.5	19.5	calcite-II	A
NA 333	15-9-57-17w5	3162	119.8	-53	-16.5	19.5	calcite-II	A
NA 333	15-9-57-17w5	3162	124.5	-53	-16.2	19.3	calcite-II	A
NA 333	15-9-57-17w5	3162	130.6	-53	-15.1	18.5	calcite-II	A
NA 333	15-9-57-17w5	3162	129.5	-55 to -54	-17.0	19.9	calcite-II	A
NA 333	15-9-57-17w5	3162	110.4		-16.5	19.5	calcite-II	A
NA 333	15-9-57-17w5	3162	111	-54	-17.1	20.0	calcite-II	A
NA 333	15-9-57-17w5	3162	115.4	-54	-17.1	20.0	calcite-II	A
NA 333	15-9-57-17w5	3162	120.4	-54	-17.1	20.0	calcite-II	A
NA 333	15-9-57-17w5	3162	122.1	-54	-17.2	20.0	calcite-II	A
NA 297	2-14-50-22w5	89.5	189.5	-89	-4.3	6.9	calcite-I	B
NA 297	2-14-50-22w5	91.1	189.1	-90	-9.1	12.9	calcite-I	B
NA 297	2-14-50-22w5	93.9	189	-90	-9.1	12.9	calcite-I	B

NA 297	2-14-50-22w5	98.8	188.5	-90	-8.5	12.3	calcite-I	B
NA 297	2-14-50-22w5	91.6	190.2	-92 to -89	-8.3	12.0	calcite-I	B
NA 297	2-14-50-22w5	94.2	190.8	-92 to -89	-10.1	14.0	calcite-I	B
NA 297	2-14-50-22w5	88.8	184.9	-92 to -89	-8.9	12.7	calcite-I	B
NA 297	2-14-50-22w5	91.3	185.9	-92 to -89	-8.5	12.3	calcite-I	B
NA 297	2-14-50-22w5	90.1	187.1	-92 to -89	-8.5	12.3	calcite-I	B
NA 297	2-14-50-22w5	90.1	187.2	-92 to -89	-8.9	12.7	calcite-I	B
NA 297	2-14-50-22w5	90.2	187.2		-9.1	12.9	calcite-I	B
NA 297	2-14-50-22w5	90.7	187.2	-92 to -89	-9.1	12.9	calcite-I	B
NA 297	2-14-50-22w5	89.5	193.1	-90	-8.2	11.9	calcite-I	B
NA 297	2-14-50-22w5	89.1	185.2	-90 to -87	-10.7	14.6	calcite-I	B
NA 297	2-14-50-22w5	81.5	168	-90 to -87	-8.1	11.8	calcite-I	B
NA 297	2-14-50-22w5	81.5	169.2	-90 to -87	-9.1	12.9	calcite-I	B
NA 297	2-14-50-22w5	90	186.1	-90 to -87	-9.2	13.0	calcite-I	B
NA 297	2-14-50-22w5	90.7	187		-8.5	12.3	calcite-I	B
NA 297	2-14-50-22w5	90.5	189.2		-8.4	12.1	calcite-I	B
NA 297	2-14-50-22w5	82.2	168		-9.1	12.9	calcite-I	B
NA 297	2-14-50-22w5	90.1	177.9	-90	-8.7	12.5	calcite-I	B
NA 297	2-14-50-22w5	82.8	193.1	-90	-2.6	4.4	calcite-I	B
NA 297	2-14-50-22w5	98.9	166		-8.2	11.9	calcite-I	B
NA 297	2-14-50-22w5	89.2	184		-8.2	11.9	calcite-I	B
NA 297	2-14-50-22w5	89.2	185.9		-12.1	16.0	calcite-I	B
NA 297	2-14-50-22w5	91.3	177.5		-9.0	12.8	calcite-I	B
NA 297	2-14-50-22w5	88.7	183.1		-9.7	13.6	calcite-I	B
NA 297	2-14-50-22w5	90.5	182.1		-9.1	12.9	calcite-I	B
NA 297	2-14-50-22w5	80	175.1		-12.4	16.2	calcite-I	B
NA 297	2-14-50-22w5	82	174		-8.8	12.6	calcite-I	B
NA 297	2-14-50-22w5	91	190.2		-9.4	13.3	calcite-I	B
NA 297	2-14-50-22w5	81	168.7		-8.7	12.5	calcite-I	B
NA 297	2-14-50-22w5	81.4	190.1		-4.5	7.2	calcite-I	B
NA 297	2-14-50-22w5	89.7	162.9		-8.9	12.7	calcite-I	B
NA 297	2-14-50-22w5	92.7	178.8		-9.8	13.7	calcite-I	B
NA 297	2-14-50-22w5	87.6	182.3	-92 to -89	-8.5	12.3	calcite-I	B
NA 297	2-14-50-22w5	88.7	183.1		-9.7	13.6	calcite-I	B
NA 297	2-14-50-22w5	90.5	182.1		-9.1	12.9	calcite-I	B
NA 297	2-14-50-22w5	80	175.1		-12.4	16.2	calcite-I	B
NA 297	2-14-50-22w5	82	174	-92 to -89	-8.8	12.6	calcite-I	B
NA 297	2-14-50-22w5	91	190.2	-94	-9.4	13.3	calcite-I	B
NA 297	2-14-50-22w5	81	168.7		-8.7	12.5	calcite-I	B
NA 297	2-14-50-22w5	81.4	190.1		-4.5	7.2	calcite-I	B
NA 297	2-14-50-22w5	89.7	162.9		-8.9	12.7	calcite-I	B
NA 297	2-14-50-22w5	92.7	178.8		-9.8	13.7	calcite-I	B
NA 297	2-14-50-22w5	87.6	182.3		-8.5	12.3	calcite-I	B
NA 333	15-9-57-17w5	3162	92.0				calcite-II	D
NA 333	15-9-57-17w5	3162	92.0				calcite-II	D
NA 333	15-9-57-17w5	3162	101.5				calcite-II	D
NA 333	15-9-57-17w5	3162	101.0				calcite-II	D

NA 333	15-9-57-17w5	3162	103.0				calcite-II	D
NA 333	15-9-57-17w5	3162	104.9				calcite-II	D
NA 333	15-9-57-17w5	3162	96.7				calcite-II	D
NA 333	15-9-57-17w5	3162	96.7				calcite-II	D
NA 333	15-9-57-17w5	3162	97.0				calcite-II	D
NA 333	15-9-57-17w5	3162	99.7				calcite-II	D
NA 333	15-9-57-17w5	3162	106.9				calcite-II	D
NA 333	15-9-57-17w5	3162	98.5				calcite-II	D
NA 333	15-9-57-17w5	3162	103.4				calcite-II	D
NA 333	15-9-57-17w5	3162	104.0				calcite-II	D
NA 333	15-9-57-17w5	3162	105.1				calcite-II	D
NA 320	16-18-61-15w5	2768.5	97.6				calcite-II	D
NA 320	16-18-61-15w5	2768.5	102.3				calcite-II	D
NA 320	16-18-61-15w5	2768.5	108.3				calcite-II	D
NA 320	16-18-61-15w5	2768.5	112.3				calcite-II	D
NA 320	16-18-61-15w5	2768.5	105.6				calcite-II	D
NA 320	16-18-61-15w5	2768.5	106.9				calcite-II	D
NA 320	16-18-61-15w5	2768.5	112.4				calcite-II	D
NA 320	16-18-61-15w5	2768.5	109.3				calcite-II	D
NA 320	16-18-61-15w5	2768.5	115.4				calcite-II	D
NA 123	06-16-55-18w5	3319.3	28.5	132.5			calcite-II	E
NA 123	06-16-55-18w5	3319.3	29.6	136.9			calcite-II	E
NA 123	06-16-55-18w5	3319.3	29	143.9			calcite-II	E
NA 123	06-16-55-18w5	3319.3	32	146.7			calcite-II	E
NA 123	06-16-55-18w5	3319.3	28.7	127			calcite-II	E
NA 123	06-16-55-18w5	3319.3	30	154.3			calcite-II	E
NA 123	06-16-55-18w5	3319.3	31.2	156.4			calcite-II	E
NA 123	06-16-55-18w5	3319.3	28.9	160.1			calcite-II	E
NA 123	06-16-55-18w5	3319.3	31	141.8			calcite-II	E
NA 123	06-16-55-18w5	3319.3		150.1			calcite-II	E
NA 123	06-16-55-18w5	3319.3		157.6			calcite-II	E

Abbreviations:

Th = homogenization temperatures (˚C)
Tm_{ice} = final ice melting temperatures (˚C)
Ty. = type of fluid inclusions

Type A: two-phase aqueous inclusions
Type B: H_2S-bearing aqueous inclusions
Type C: liquid-only aqueous inclusions
Type D: liquid oil and vapor inclusions
Type E: CO_2-H_2O-bearing inclusions

APPENDIX IV

Bitumen reflectance data

Table A-5. Summary of bitumen reflectance, and calculated vitrinte reflectance and peak temperature data.

Code	Sample	Location	Depth (m)	$\%R_0$	%VRr	Tpeak	Remarks
316-08	97/003	10-32-44-19w5	5326.6	2.946	2.22	199.83	dol/bit
316-08	97/003	10-32-44-19w5	5326.6	2.996	2.25	200.93	dol/bit
316-08	97/003	10-32-44-19w5	5326.6	3.017	2.26	201.39	dol/bit
316-08	97/003	10-32-44-19w5	5326.6	3.024	2.27	201.55	dol/bit
316-08	97/003	10-32-44-19w5	5326.6	3.080	2.30	202.77	dol/bit
316-08	97/003	10-32-44-19w5	5326.6	3.101	2.32	203.22	dol/bit
316-08	97/003	10-32-44-19w5	5326.6	3.101	2.32	203.22	dol/bit
316-08	97/003	10-32-44-19w5	5326.6	3.136	2.34	203.97	dol/bit
316-08	97/003	10-32-44-19w5	5326.6	3.136	2.34	203.97	dol/bit
316-08	97/003	10-32-44-19w5	5326.6	3.150	2.35	204.27	dol/bit
316-08	97/003	10-32-44-19w5	5326.6	3.157	2.35	204.42	dol/bit
316-08	97/003	10-32-44-19w5	5326.6	3.185	2.37	205.02	dol/bit
316-08	97/003	10-32-44-19w5	5326.6	3.220	2.39	205.75	dol/bit
316-08	97/003	10-32-44-19w5	5326.6	3.290	2.43	207.20	dol/bit
316-08	97/003	10-32-44-19w5	5326.6	3.311	2.45	207.63	dol/bit
316-08	97/003	10-32-44-19w5	5326.6	3.325	2.46	207.92	dol/bit
316-08	97/003	10-32-44-19w5	5326.6	3.353	2.47	208.48	dol/bit
316-08	97/003	10-32-44-19w5	5326.6	3.374	2.49	208.91	dol/bit
316-08	97/003	10-32-44-19w5	5326.6	3.381	2.49	209.05	dol/bit
316-08	97/003	10-32-44-19w5	5326.6	3.388	2.49	209.19	dol/bit
316-08	97/003	10-32-44-19w5	5326.6	3.395	2.50	209.33	dol/bit
316-08	97/003	10-32-44-19w5	5326.6	3.402	2.50	209.47	dol/bit
316-08	97/003	10-32-44-19w5	5326.6	3.424	2.52	209.88	dol/bit
316-08	97/003	10-32-44-19w5	5326.6	3.431	2.52	210.02	dol/bit
316-08	97/003	10-32-44-19w5	5326.6	3.459	2.54	210.58	dol/bit
316-08	97/003	10-32-44-19w5	5326.6	3.473	2.55	210.85	dol/bit
316-08	97/003	10-32-44-19w5	5326.6	3.487	2.55	211.13	dol/bit
316-08	97/003	10-32-44-19w5	5326.6	3.494	2.56	211.26	dol/bit
316-08	97/003	10-32-44-19w5	5326.6	3.494	2.56	211.26	dol/bit
316-08	97/003	10-32-44-19w5	5326.6	3.536	2.59	212.08	dol/bit
316-08	97/003	10-32-44-19w5	5326.6	3.543	2.59	212.21	dol/bit
316-08	97/003	10-32-44-19w5	5326.6	3.564	2.60	212.62	dol/bit
316-08	97/003	10-32-44-19w5	5326.6	3.599	2.62	213.29	dol/bit
316-08	97/003	10-32-44-19w5	5326.6	3.606	2.63	213.42	dol/bit
316-08	97/003	10-32-44-19w5	5326.6	3.606	2.63	213.42	dol/bit
316-08	97/003	10-32-44-19w5	5326.6	3.620	2.64	213.69	dol/bit
316-08	97/003	10-32-44-19w5	5326.6	3.620	2.64	213.69	dol/bit
316-08	97/003	10-32-44-19w5	5326.6	3.676	2.67	214.74	dol/bit
316-08	97/003	10-32-44-19w5	5326.6	3.732	2.71	215.78	dol/bit
316-08	97/003	10-32-44-19w5	5326.6	3.739	2.71	215.91	dol/bit
316-08	97/003	10-32-44-19w5	5326.6	3.760	2.72	216.29	dol/bit
316-08	97/003	10-32-44-19w5	5326.6	3.767	2.73	216.42	dol/bit
316-08	97/003	10-32-44-19w5	5326.6	3.781	2.74	216.68	dol/bit

316-08	97/003	10-32-44-19w5	5326.6	3.788	2.74	216.81	dol/bit
316-08	97/003	10-32-44-19w5	5326.6	3.809	2.75	217.19	dol/bit
316-08	97/003	10-32-44-19w5	5326.6	3.894	2.81	218.70	dol/bit
316-08	97/003	10-32-44-19w5	5326.6	3.894	2.81	218.70	dol/bit
316-08	97/003	10-32-44-19w5	5326.6	3.971	2.85	220.06	dol/bit
316-08	97/003	10-32-44-19w5	5326.6	3.999	2.87	220.54	dol/bit
316-08	97/003	10-32-44-19w5	5326.6	4.343	3.08	226.30	dol/bit
316-08	97/003	10-32-44-19w5	5326.6	4.469	3.16	228.32	dol/bit
316-08	97/003	10-32-44-19w5	5326.6	4.763	3.34	232.83	dol/bit
316-08	97/003	10-32-44-19w5	5326.6	4.876	3.41	234.49	dol/bit
316-08	97/003	10-32-44-19w5	5326.6	5.311	3.68	240.60	dol/bit
316-08	97/003	10-32-44-19w5	5326.6	5.629	4.12	249.66	dol/bit
316-08	97/003	10-32-44-19w5	5326.6	5.889	4.20	251.18	dol/bit
317-08	NA I	2-14-50-22w5	4581.75	3.542	2.59	212.19	cc/bit/sul
317-08	NA I	2-14-50-22w5	4581.75	3.591	2.62	213.14	cc/bit/sul
317-08	NA I	2-14-50-22w5	4581.75	3.620	2.64	213.68	cc/bit/sul
317-08	NA I	2-14-50-22w5	4581.75	3.627	2.64	213.82	cc/bit/sul
317-08	NA I	2-14-50-22w5	4581.75	3.627	2.64	213.82	cc/bit/sul
317-08	NA I	2-14-50-22w5	4581.75	3.684	2.68	214.88	cc/bit/sul
317-08	NA I	2-14-50-22w5	4581.75	3.698	2.69	215.14	cc/bit/sul
317-08	NA I	2-14-50-22w5	4581.75	3.790	2.74	216.84	cc/bit/sul
317-08	NA I	2-14-50-22w5	4581.75	3.819	2.76	217.35	cc/bit/sul
317-08	NA I	2-14-50-22w5	4581.75	3.826	2.76	217.48	cc/bit/sul
317-08	NA I	2-14-50-22w5	4581.75	3.833	2.77	217.61	cc/bit/sul
317-08	NA I	2-14-50-22w5	4581.75	3.840	2.77	217.74	cc/bit/sul
317-08	NA I	2-14-50-22w5	4581.75	3.854	2.78	217.99	cc/bit/sul
317-08	NA I	2-14-50-22w5	4581.75	3.854	2.78	217.99	cc/bit/sul
317-08	NA I	2-14-50-22w5	4581.75	3.875	2.79	218.37	cc/bit/sul
317-08	NA I	2-14-50-22w5	4581.75	3.890	2.80	218.62	cc/bit/sul
317-08	NA I	2-14-50-22w5	4581.75	3.918	2.82	219.13	cc/bit/sul
317-08	NA I	2-14-50-22w5	4581.75	3.925	2.83	219.25	cc/bit/sul
317-08	NA I	2-14-50-22w5	4581.75	3.939	2.83	219.50	cc/bit/sul
317-08	NA I	2-14-50-22w5	4581.75	3.953	2.84	219.75	cc/bit/sul
317-08	NA I	2-14-50-22w5	4581.75	3.953	2.84	219.75	cc/bit/sul
317-08	NA I	2-14-50-22w5	4581.75	3.960	2.85	219.88	cc/bit/sul
317-08	NA I	2-14-50-22w5	4581.75	3.960	2.85	219.88	cc/bit/sul
317-08	NA I	2-14-50-22w5	4581.75	3.968	2.85	220.00	cc/bit/sul
317-08	NA I	2-14-50-22w5	4581.75	3.968	2.85	220.00	cc/bit/sul
317-08	NA I	2-14-50-22w5	4581.75	3.975	2.86	220.12	cc/bit/sul
317-08	NA I	2-14-50-22w5	4581.75	3.989	2.87	220.37	cc/bit/sul
317-08	NA I	2-14-50-22w5	4581.75	3.996	2.87	220.50	cc/bit/sul
317-08	NA I	2-14-50-22w5	4581.75	4.010	2.88	220.74	cc/bit/sul
317-08	NA I	2-14-50-22w5	4581.75	4.024	2.89	220.99	cc/bit/sul
317-08	NA I	2-14-50-22w5	4581.75	4.031	2.89	221.11	cc/bit/sul
317-08	NA I	2-14-50-22w5	4581.75	4.060	2.91	221.60	cc/bit/sul
317-08	NA I	2-14-50-22w5	4581.75	4.067	2.91	221.72	cc/bit/sul
317-08	NA I	2-14-50-22w5	4581.75	4.110	2.94	222.44	cc/bit/sul

317-08	NA I	2-14-50-22w5	4581.75	4.110	2.94	222.44	cc/bit/sul
317-08	NA I	2-14-50-22w5	4581.75	4.131	2.95	222.80	cc/bit/sul
317-08	NA I	2-14-50-22w5	4581.75	4.152	2.97	223.16	cc/bit/sul
317-08	NA I	2-14-50-22w5	4581.75	4.152	2.97	223.16	cc/bit/sul
317-08	NA I	2-14-50-22w5	4581.75	4.173	2.98	223.52	cc/bit/sul
317-08	NA I	2-14-50-22w5	4581.75	4.188	2.99	223.76	cc/bit/sul
317-08	NA I	2-14-50-22w5	4581.75	4.195	2.99	223.88	cc/bit/sul
317-08	NA I	2-14-50-22w5	4581.75	4.195	2.99	223.88	cc/bit/sul
317-08	NA I	2-14-50-22w5	4581.75	4.195	2.99	223.88	cc/bit/sul
317-08	NA I	2-14-50-22w5	4581.75	4.230	3.01	224.46	cc/bit/sul
317-08	NA I	2-14-50-22w5	4581.75	4.230	3.01	224.46	cc/bit/sul
317-08	NA I	2-14-50-22w5	4581.75	4.244	3.02	224.70	cc/bit/sul
317-08	NA I	2-14-50-22w5	4581.75	4.266	3.04	225.05	cc/bit/sul
317-08	NA I	2-14-50-22w5	4581.75	4.280	3.04	225.28	cc/bit/sul
317-08	NA I	2-14-50-22w5	4581.75	4.280	3.04	225.28	cc/bit/sul
317-08	NA I	2-14-50-22w5	4581.75	4.315	3.07	225.86	cc/bit/sul
317-08	NA I	2-14-50-22w5	4581.75	4.344	3.08	226.32	cc/bit/sul
317-08	NA I	2-14-50-22w5	4581.75	4.344	3.08	226.32	cc/bit/sul
317-08	NA I	2-14-50-22w5	4581.75	4.358	3.09	226.55	cc/bit/sul
317-08	NA I	2-14-50-22w5	4581.75	4.386	3.11	227.01	cc/bit/sul
317-08	NA I	2-14-50-22w5	4581.75	4.429	3.14	227.68	cc/bit/sul
317-08	NA I	2-14-50-22w5	4581.75	4.649	3.27	231.11	cc/bit/sul
317-08	NA I	2-14-50-22w5	4581.75	4.663	3.28	231.32	cc/bit/sul
317-08	NA I	2-14-50-22w5	4581.75	5.905	4.05	248.27	cc/bit/sul
317-08	NA I	2-14-50-22w5	4581.75	5.969	4.09	249.05	cc/bit/sul
317-08	NA I	2-14-50-22w5	4581.75	6.129	4.39	254.81	cc/bit/sul
317-08	NA I	2-14-50-22w5	4581.75	6.609	4.46	256.01	cc/bit/sul
318-08	NA 160	9-17-53-19W5	3696.6	2.294	1.82	183.69	dol/bit/clay seam
318-08	NA 160	9-17-53-19W5	3696.6	2.351	1.85	185.23	dol/bit/clay seam
318-08	NA 160	9-17-53-19W5	3696.6	2.387	1.88	186.19	dol/bit/clay seam
318-08	NA 160	9-17-53-19W5	3696.6	2.558	1.98	190.61	dol/bit/clay seam
318-08	NA 160	9-17-53-19W5	3696.6	2.644	2.03	192.73	dol/bit/clay seam
318-08	NA 160	9-17-53-19W5	3696.6	2.651	2.04	192.91	dol/bit/clay seam
318-08	NA 160	9-17-53-19W5	3696.6	2.701	2.07	194.12	dol/bit/clay seam
318-08	NA 160	9-17-53-19W5	3696.6	2.729	2.09	194.80	dol/bit/clay seam
318-08	NA 160	9-17-53-19W5	3696.6	2.772	2.11	195.81	dol/bit/clay seam
318-08	NA 160	9-17-53-19W5	3696.6	2.807	2.13	196.65	dol/bit/clay seam
318-08	NA 160	9-17-53-19W5	3696.6	2.843	2.16	197.48	dol/bit/clay seam
318-08	NA 160	9-17-53-19W5	3696.6	2.843	2.16	197.48	dol/bit/clay seam
318-08	NA 160	9-17-53-19W5	3696.6	2.943	2.22	199.75	dol/bit/clay seam
318-08	NA 160	9-17-53-19W5	3696.6	2.964	2.23	200.23	dol/bit/clay seam
318-08	NA 160	9-17-53-19W5	3696.6	3.000	2.25	201.02	dol/bit/clay seam
318-08	NA 160	9-17-53-19W5	3696.6	3.014	2.26	201.34	dol/bit/clay seam
318-08	NA 160	9-17-53-19W5	3696.6	3.121	2.33	203.66	dol/bit/clay seam
318-08	NA 160	9-17-53-19W5	3696.6	3.135	2.34	203.96	dol/bit/clay seam
318-08	NA 160	9-17-53-19W5	3696.6	3.192	2.37	205.17	dol/bit/clay seam
318-08	NA 160	9-17-53-19W5	3696.6	3.206	2.38	205.47	dol/bit/clay seam

318-08	NA 160	9-17-53-19W5	3696.6	3.242	2.40	206.21	dol/bit/clay seam
318-08	NA 160	9-17-53-19W5	3696.6	3.263	2.42	206.65	dol/bit/clay seam
318-08	NA 160	9-17-53-19W5	3696.6	3.285	2.43	207.09	dol/bit/clay seam
318-08	NA 160	9-17-53-19W5	3696.6	3.349	2.47	208.39	dol/bit/clay seam
318-08	NA 160	9-17-53-19W5	3696.6	3.385	2.49	209.11	dol/bit/clay seam
318-08	NA 160	9-17-53-19W5	3696.6	3.392	2.50	209.25	dol/bit/clay seam
318-08	NA 160	9-17-53-19W5	3696.6	3.399	2.50	209.39	dol/bit/clay seam
318-08	NA 160	9-17-53-19W5	3696.6	3.413	2.51	209.68	dol/bit/clay seam
318-08	NA 160	9-17-53-19W5	3696.6	3.456	2.54	210.52	dol/bit/clay seam
318-08	NA 160	9-17-53-19W5	3696.6	3.470	2.54	210.80	dol/bit/clay seam
318-08	NA 160	9-17-53-19W5	3696.6	3.499	2.56	211.36	dol/bit/clay seam
318-08	NA 160	9-17-53-19W5	3696.6	3.499	2.56	211.36	dol/bit/clay seam
318-08	NA 160	9-17-53-19W5	3696.6	3.520	2.58	211.77	dol/bit/clay seam
318-08	NA 160	9-17-53-19W5	3696.6	3.556	2.60	212.46	dol/bit/clay seam
318-08	NA 160	9-17-53-19W5	3696.6	3.655	2.66	214.35	dol/bit/clay seam
318-08	NA 160	9-17-53-19W5	3696.6	3.777	2.73	216.59	dol/bit/clay seam
318-08	NA 160	9-17-53-19W5	3696.6	3.834	2.77	217.62	dol/bit/clay seam
318-08	NA 160	9-17-53-19W5	3696.6	3.955	2.84	219.77	dol/bit/clay seam
319-08	NA 2563	13-15-60-16w5	2563	1.914	1.58	172.53	dol/bit/cc/bit/anhy
319-08	NA 2563	13-15-60-16w5	2563	1.970	1.62	174.27	dol/bit/cc/bit/anhy
319-08	NA 2563	13-15-60-16w5	2563	1.970	1.62	174.27	dol/bit/cc/bit/anhy
319-08	NA 2563	13-15-60-16w5	2563	2.012	1.64	175.54	dol/bit/cc/bit/anhy
319-08	NA 2563	13-15-60-16w5	2563	2.033	1.66	176.18	dol/bit/cc/bit/anhy
319-08	NA 2563	13-15-60-16w5	2563	2.040	1.66	176.38	dol/bit/cc/bit/anhy
319-08	NA 2563	13-15-60-16w5	2563	2.040	1.66	176.38	dol/bit/cc/bit/anhy
319-08	NA 2563	13-15-60-16w5	2563	2.054	1.67	176.80	dol/bit/cc/bit/anhy
319-08	NA 2563	13-15-60-16w5	2563	2.061	1.67	177.01	dol/bit/cc/bit/anhy
319-08	NA 2563	13-15-60-16w5	2563	2.061	1.67	177.01	dol/bit/cc/bit/anhy
319-08	NA 2563	13-15-60-16w5	2563	2.075	1.68	177.42	dol/bit/cc/bit/anhy
319-08	NA 2563	13-15-60-16w5	2563	2.082	1.69	177.63	dol/bit/cc/bit/anhy
319-08	NA 2563	13-15-60-16w5	2563	2.089	1.69	177.83	dol/bit/cc/bit/anhy
319-08	NA 2563	13-15-60-16w5	2563	2.089	1.69	177.83	dol/bit/cc/bit/anhy
319-08	NA 2563	13-15-60-16w5	2563	2.109	1.70	178.45	dol/bit/cc/bit/anhy
319-08	NA 2563	13-15-60-16w5	2563	2.109	1.70	178.45	dol/bit/cc/bit/anhy
319-08	NA 2563	13-15-60-16w5	2563	2.116	1.71	178.65	dol/bit/cc/bit/anhy
319-08	NA 2563	13-15-60-16w5	2563	2.116	1.71	178.65	dol/bit/cc/bit/anhy
319-08	NA 2563	13-15-60-16w5	2563	2.116	1.71	178.65	dol/bit/cc/bit/anhy
319-08	NA 2563	13-15-60-16w5	2563	2.116	1.71	178.65	dol/bit/cc/bit/anhy
319-08	NA 2563	13-15-60-16w5	2563	2.123	1.71	178.85	dol/bit/cc/bit/anhy
319-08	NA 2563	13-15-60-16w5	2563	2.158	1.73	179.86	dol/bit/cc/bit/anhy
319-08	NA 2563	13-15-60-16w5	2563	2.165	1.74	180.06	dol/bit/cc/bit/anhy
319-08	NA 2563	13-15-60-16w5	2563	2.179	1.75	180.46	dol/bit/cc/bit/anhy
319-08	NA 2563	13-15-60-16w5	2563	2.186	1.75	180.66	dol/bit/cc/bit/anhy
319-08	NA 2563	13-15-60-16w5	2563	2.186	1.75	180.66	dol/bit/cc/bit/anhy
319-08	NA 2563	13-15-60-16w5	2563	2.186	1.75	180.66	dol/bit/cc/bit/anhy
319-08	NA 2563	13-15-60-16w5	2563	2.207	1.76	181.25	dol/bit/cc/bit/anhy
319-08	NA 2563	13-15-60-16w5	2563	2.214	1.77	181.45	dol/bit/cc/bit/anhy

319-08	NA 2563	13-15-60-16w5	2563	2.228	1.78	181.84	dol/bit/cc/bit/anhy
319-08	NA 2563	13-15-60-16w5	2563	2.235	1.78	182.03	dol/bit/cc/bit/anhy
319-08	NA 2563	13-15-60-16w5	2563	2.242	1.79	182.23	dol/bit/cc/bit/anhy
319-08	NA 2563	13-15-60-16w5	2563	2.283	1.81	183.38	dol/bit/cc/bit/anhy
319-08	NA 2563	13-15-60-16w5	2563	2.290	1.82	183.58	dol/bit/cc/bit/anhy
319-08	NA 2563	13-15-60-16w5	2563	2.290	1.82	183.58	dol/bit/cc/bit/anhy
319-08	NA 2563	13-15-60-16w5	2563	2.290	1.82	183.58	dol/bit/cc/bit/anhy
319-08	NA 2563	13-15-60-16w5	2563	2.339	1.85	184.90	dol/bit/cc/bit/anhy
319-08	NA 2563	13-15-60-16w5	2563	2.374	1.87	185.84	dol/bit/cc/bit/anhy
319-08	NA 2563	13-15-60-16w5	2563	2.402	1.88	186.58	dol/bit/cc/bit/anhy
319-08	NA 2563	13-15-60-16w5	2563	2.416	1.89	186.94	dol/bit/cc/bit/anhy
319-08	NA 2563	13-15-60-16w5	2563	2.457	1.92	188.04	dol/bit/cc/bit/anhy
319-08	NA 2563	13-15-60-16w5	2563	2.457	1.92	188.04	dol/bit/cc/bit/anhy
319-08	NA 2563	13-15-60-16w5	2563	2.485	1.94	188.76	dol/bit/cc/bit/anhy
319-08	NA 2563	13-15-60-16w5	2563	2.520	1.96	189.65	dol/bit/cc/bit/anhy
319-08	NA 2563	13-15-60-16w5	2563	2.541	1.97	190.18	dol/bit/cc/bit/anhy
319-08	NA 2563	13-15-60-16w5	2563	2.541	1.97	190.18	dol/bit/cc/bit/anhy
319-08	NA 2563	13-15-60-16w5	2563	2.562	1.98	190.70	dol/bit/cc/bit/anhy
319-08	NA 2563	13-15-60-16w5	2563	2.638	2.03	192.61	dol/bit/cc/bit/anhy
319-08	NA 2563	13-15-60-16w5	2563	2.882	2.18	198.38	dol/bit/cc/bit/anhy
320-08	NA 208	11-29-59-16w5	2734.4	1.599	1.45	165.42	cc/bit
320-08	NA 208	11-29-59-16w5	2734.4	1.705	1.45	165.66	cc/bit
320-08	NA 208	11-29-59-16w5	2734.4	1.726	1.47	166.38	cc/bit
320-08	NA 208	11-29-59-16w5	2734.4	1.782	1.50	168.25	cc/bit
320-08	NA 208	11-29-59-16w5	2734.4	1.782	1.50	168.25	cc/bit
320-08	NA 208	11-29-59-16w5	2734.4	1.796	1.51	168.72	cc/bit
320-08	NA 208	11-29-59-16w5	2734.4	1.810	1.52	169.18	cc/bit
320-08	NA 208	11-29-59-16w5	2734.4	1.887	1.57	171.66	cc/bit
320-08	NA 208	11-29-59-16w5	2734.4	1.964	1.61	174.07	cc/bit
320-08	NA 208	11-29-59-16w5	2734.4	1.985	1.63	174.71	cc/bit
320-08	NA 208	11-29-59-16w5	2734.4	1.985	1.63	174.71	cc/bit
320-08	NA 208	11-29-59-16w5	2734.4	2.006	1.64	175.35	cc/bit
320-08	NA 208	11-29-59-16w5	2734.4	2.013	1.64	175.57	cc/bit
320-08	NA 208	11-29-59-16w5	2734.4	2.020	1.65	175.78	cc/bit
320-08	NA 208	11-29-59-16w5	2734.4	2.055	1.67	176.83	cc/bit
320-08	NA 208	11-29-59-16w5	2734.4	2.076	1.68	177.45	cc/bit
320-08	NA 208	11-29-59-16w5	2734.4	2.076	1.68	177.45	cc/bit
320-08	NA 208	11-29-59-16w5	2734.4	2.097	1.70	178.07	cc/bit
320-08	NA 208	11-29-59-16w5	2734.4	2.097	1.70	178.07	cc/bit
320-08	NA 208	11-29-59-16w5	2734.4	2.124	1.71	178.89	cc/bit
320-08	NA 208	11-29-59-16w5	2734.4	2.124	1.71	178.89	cc/bit
320-08	NA 208	11-29-59-16w5	2734.4	2.138	1.72	179.29	cc/bit
320-08	NA 208	11-29-59-16w5	2734.4	2.159	1.73	179.90	cc/bit
320-08	NA 208	11-29-59-16w5	2734.4	2.180	1.75	180.50	cc/bit
320-08	NA 208	11-29-59-16w5	2734.4	2.201	1.76	181.09	cc/bit
320-08	NA 208	11-29-59-16w5	2734.4	2.201	1.76	181.09	cc/bit
320-08	NA 208	11-29-59-16w5	2734.4	2.215	1.77	181.49	cc/bit

320-08	NA 208	11-29-59-16w5	2734.4	2.222	1.77	181.69	cc/bit
320-08	NA 208	11-29-59-16w5	2734.4	2.229	1.78	181.88	cc/bit
320-08	NA 208	11-29-59-16w5	2734.4	2.229	1.78	181.88	cc/bit
320-08	NA 208	11-29-59-16w5	2734.4	2.229	1.78	181.88	cc/bit
320-08	NA 208	11-29-59-16w5	2734.4	2.250	1.79	182.47	cc/bit
320-08	NA 208	11-29-59-16w5	2734.4	2.278	1.81	183.24	cc/bit
320-08	NA 208	11-29-59-16w5	2734.4	2.327	1.84	184.58	cc/bit
320-08	NA 208	11-29-59-16w5	2734.4	2.355	1.86	185.33	cc/bit
320-08	NA 208	11-29-59-16w5	2734.4	2.369	1.86	185.71	cc/bit
320-08	NA 208	11-29-59-16w5	2734.4	2.397	1.88	186.45	cc/bit
320-08	NA 208	11-29-59-16w5	2734.4	2.432	1.90	187.37	cc/bit
320-08	NA 208	11-29-59-16w5	2734.4	2.439	1.91	187.55	cc/bit
320-08	NA 208	11-29-59-16w5	2734.4	2.495	1.94	189.00	cc/bit
320-08	NA 208	11-29-59-16w5	2734.4	2.502	1.95	189.18	cc/bit
320-08	NA 208	11-29-59-16w5	2734.4	2.523	1.96	189.72	cc/bit
320-08	NA 208	11-29-59-16w5	2734.4	2.642	2.03	192.68	cc/bit
320-08	NA 208	11-29-59-16w5	2734.4	2.781	2.12	196.04	cc/bit
320-08	NA 208	11-29-59-16w5	2734.4	2.788	2.12	196.20	cc/bit
320-08	NA 208	11-29-59-16w5	2734.4	3.110	2.32	203.42	cc/bit
320-08	NA 208	11-29-59-16w5	2734.4	3.110	2.32	203.42	cc/bit
320-08	NA 208	11-29-59-16w5	2734.4	3.131	2.33	203.87	cc/bit
320-08	NA 208	11-29-59-16w5	2734.4	3.236	2.40	206.07	cc/bit
320-08	NA 208	11-29-59-16w5	2734.4	3.571	2.61	212.76	cc/bit
321-08	NA 3434	6-34-57-21w5	3434.4	2.799	2.13	196.44	dol/bit
321-08	NA 3434	6-34-57-21w5	3434.4	2.826	2.15	197.09	dol/bit
321-08	NA 3434	6-34-57-21w5	3434.4	2.833	2.15	197.25	dol/bit
321-08	NA 3434	6-34-57-21w5	3434.4	2.847	2.16	197.58	dol/bit
321-08	NA 3434	6-34-57-21w5	3434.4	2.847	2.16	197.58	dol/bit
321-08	NA 3434	6-34-57-21w5	3434.4	2.875	2.18	198.22	dol/bit
321-08	NA 3434	6-34-57-21w5	3434.4	2.896	2.19	198.69	dol/bit
321-08	NA 3434	6-34-57-21w5	3434.4	2.910	2.20	199.01	dol/bit
321-08	NA 3434	6-34-57-21w5	3434.4	2.938	2.22	199.64	dol/bit
321-08	NA 3434	6-34-57-21w5	3434.4	2.987	2.25	200.73	dol/bit
321-08	NA 3434	6-34-57-21w5	3434.4	2.987	2.25	200.73	dol/bit
321-08	NA 3434	6-34-57-21w5	3434.4	3.000	2.25	201.04	dol/bit
321-08	NA 3434	6-34-57-21w5	3434.4	3.000	2.25	201.04	dol/bit
321-08	NA 3434	6-34-57-21w5	3434.4	3.021	2.27	201.50	dol/bit
321-08	NA 3434	6-34-57-21w5	3434.4	3.056	2.29	202.26	dol/bit
321-08	NA 3434	6-34-57-21w5	3434.4	3.112	2.32	203.46	dol/bit
321-08	NA 3434	6-34-57-21w5	3434.4	3.147	2.34	204.20	dol/bit
321-08	NA 3434	6-34-57-21w5	3434.4	3.168	2.36	204.65	dol/bit
321-08	NA 3434	6-34-57-21w5	3434.4	3.175	2.36	204.79	dol/bit
321-08	NA 3434	6-34-57-21w5	3434.4	3.202	2.38	205.38	dol/bit
321-08	NA 3434	6-34-57-21w5	3434.4	3.209	2.38	205.53	dol/bit
321-08	NA 3434	6-34-57-21w5	3434.4	3.209	2.38	205.53	dol/bit
321-08	NA 3434	6-34-57-21w5	3434.4	3.230	2.40	205.96	dol/bit
321-08	NA 3434	6-34-57-21w5	3434.4	3.265	2.42	206.68	dol/bit

321-08	NA 3434	6-34-57-21w5	3434.4	3.265	2.42	206.68	dol/bit
321-08	NA 3434	6-34-57-21w5	3434.4	3.272	2.42	206.83	dol/bit
321-08	NA 3434	6-34-57-21w5	3434.4	3.279	2.43	206.97	dol/bit
321-08	NA 3434	6-34-57-21w5	3434.4	3.286	2.43	207.11	dol/bit
321-08	NA 3434	6-34-57-21w5	3434.4	3.293	2.43	207.25	dol/bit
321-08	NA 3434	6-34-57-21w5	3434.4	3.293	2.43	207.25	dol/bit
321-08	NA 3434	6-34-57-21w5	3434.4	3.314	2.45	207.68	dol/bit
321-08	NA 3434	6-34-57-21w5	3434.4	3.314	2.45	207.68	dol/bit
321-08	NA 3434	6-34-57-21w5	3434.4	3.356	2.47	208.53	dol/bit
321-08	NA 3434	6-34-57-21w5	3434.4	3.356	2.47	208.53	dol/bit
321-08	NA 3434	6-34-57-21w5	3434.4	3.383	2.49	209.09	dol/bit
321-08	NA 3434	6-34-57-21w5	3434.4	3.397	2.50	209.36	dol/bit
321-08	NA 3434	6-34-57-21w5	3434.4	3.404	2.50	209.50	dol/bit
321-08	NA 3434	6-34-57-21w5	3434.4	3.411	2.51	209.64	dol/bit
321-08	NA 3434	6-34-57-21w5	3434.4	3.418	2.51	209.78	dol/bit
321-08	NA 3434	6-34-57-21w5	3434.4	3.418	2.51	209.78	dol/bit
321-08	NA 3434	6-34-57-21w5	3434.4	3.502	2.56	211.42	dol/bit
321-08	NA 3434	6-34-57-21w5	3434.4	3.509	2.57	211.55	dol/bit
321-08	NA 3434	6-34-57-21w5	3434.4	3.523	2.58	211.82	dol/bit
321-08	NA 3434	6-34-57-21w5	3434.4	3.585	2.62	213.03	dol/bit
321-08	NA 3434	6-34-57-21w5	3434.4	3.683	2.68	214.86	dol/bit
321-08	NA 3434	6-34-57-21w5	3434.4	3.731	2.71	215.77	dol/bit
321-08	NA 3434	6-34-57-21w5	3434.4	3.892	2.80	218.66	dol/bit
321-08	NA 3434	6-34-57-21w5	3434.4	3.919	2.82	219.15	dol/bit
321-08	NA 3434	6-34-57-21w5	3434.4	3.989	2.87	220.37	dol/bit
321-08	NA 3434	6-34-57-21w5	3434.4	3.996	2.87	220.50	dol/bit
321-08	NA 3434	6-34-57-21w5	3434.4	4.532	3.20	229.31	dol/bit
321-08	NA 3434	6-34-57-21w5	3434.4	4.657	3.28	231.23	dol/bit
321-08	NA 3434	6-34-57-21w5	3434.4	4.998	3.49	236.26	dol/bit
321-08	NA 3434	6-34-57-21w5	3434.4	4.998	3.49	236.26	dol/bit
321-08	NA 3434	6-34-57-21w5	3434.4	5.061	3.53	237.15	dol/bit
322-08	NA 123	6-16-55-18w5	3319.3	2.025	1.65	175.94	cc/bit
322-08	NA 123	6-16-55-18w5	3319.3	2.039	1.66	176.36	cc/bit
322-08	NA 123	6-16-55-18w5	3319.3	2.074	1.68	177.39	cc/bit
322-08	NA 123	6-16-55-18w5	3319.3	2.081	1.69	177.60	cc/bit
322-08	NA 123	6-16-55-18w5	3319.3	2.115	1.71	178.62	cc/bit
322-08	NA 123	6-16-55-18w5	3319.3	2.136	1.72	179.22	cc/bit
322-08	NA 123	6-16-55-18w5	3319.3	2.136	1.72	179.22	cc/bit
322-08	NA 123	6-16-55-18w5	3319.3	2.157	1.73	179.82	cc/bit
322-08	NA 123	6-16-55-18w5	3319.3	2.157	1.73	179.82	cc/bit
322-08	NA 123	6-16-55-18w5	3319.3	2.157	1.73	179.82	cc/bit
322-08	NA 123	6-16-55-18w5	3319.3	2.164	1.74	180.02	cc/bit
322-08	NA 123	6-16-55-18w5	3319.3	2.171	1.74	180.22	cc/bit
322-08	NA 123	6-16-55-18w5	3319.3	2.171	1.74	180.22	cc/bit
322-08	NA 123	6-16-55-18w5	3319.3	2.178	1.75	180.42	cc/bit
322-08	NA 123	6-16-55-18w5	3319.3	2.192	1.75	180.81	cc/bit
322-08	NA 123	6-16-55-18w5	3319.3	2.192	1.75	180.81	cc/bit

322-08	NA 123	6-16-55-18w5	3319.3	2.198	1.76	181.01	cc/bit
322-08	NA 123	6-16-55-18w5	3319.3	2.198	1.76	181.01	cc/bit
322-08	NA 123	6-16-55-18w5	3319.3	2.205	1.76	181.21	cc/bit
322-08	NA 123	6-16-55-18w5	3319.3	2.205	1.76	181.21	cc/bit
322-08	NA 123	6-16-55-18w5	3319.3	2.240	1.78	182.18	cc/bit
322-08	NA 123	6-16-55-18w5	3319.3	2.240	1.78	182.18	cc/bit
322-08	NA 123	6-16-55-18w5	3319.3	2.247	1.79	182.38	cc/bit
322-08	NA 123	6-16-55-18w5	3319.3	2.254	1.79	182.57	cc/bit
322-08	NA 123	6-16-55-18w5	3319.3	2.268	1.80	182.95	cc/bit
322-08	NA 123	6-16-55-18w5	3319.3	2.337	1.84	184.85	cc/bit
322-08	NA 123	6-16-55-18w5	3319.3	2.344	1.85	185.04	cc/bit
322-08	NA 123	6-16-55-18w5	3319.3	2.344	1.85	185.04	cc/bit
322-08	NA 123	6-16-55-18w5	3319.3	2.351	1.85	185.22	cc/bit
322-08	NA 123	6-16-55-18w5	3319.3	2.351	1.85	185.22	cc/bit
322-08	NA 123	6-16-55-18w5	3319.3	2.351	1.85	185.22	cc/bit
322-08	NA 123	6-16-55-18w5	3319.3	2.365	1.86	185.59	cc/bit
322-08	NA 123	6-16-55-18w5	3319.3	2.372	1.87	185.78	cc/bit
322-08	NA 123	6-16-55-18w5	3319.3	2.372	1.87	185.78	cc/bit
322-08	NA 123	6-16-55-18w5	3319.3	2.379	1.87	185.97	cc/bit
322-08	NA 123	6-16-55-18w5	3319.3	2.400	1.88	186.52	cc/bit
322-08	NA 123	6-16-55-18w5	3319.3	2.420	1.90	187.07	cc/bit
322-08	NA 123	6-16-55-18w5	3319.3	2.462	1.92	188.15	cc/bit
322-08	NA 123	6-16-55-18w5	3319.3	2.476	1.93	188.51	cc/bit
322-08	NA 123	6-16-55-18w5	3319.3	2.483	1.93	188.69	cc/bit
322-08	NA 123	6-16-55-18w5	3319.3	2.483	1.93	188.69	cc/bit
322-08	NA 123	6-16-55-18w5	3319.3	2.490	1.94	188.87	cc/bit
322-08	NA 123	6-16-55-18w5	3319.3	2.497	1.94	189.05	cc/bit
322-08	NA 123	6-16-55-18w5	3319.3	2.504	1.95	189.23	cc/bit
322-08	NA 123	6-16-55-18w5	3319.3	2.552	1.98	190.46	cc/bit
322-08	NA 123	6-16-55-18w5	3319.3	2.552	1.98	190.46	cc/bit
322-08	NA 123	6-16-55-18w5	3319.3	2.559	1.98	190.63	cc/bit
322-08	NA 123	6-16-55-18w5	3319.3	2.559	1.98	190.63	cc/bit
322-08	NA 123	6-16-55-18w5	3319.3	2.615	2.02	192.02	cc/bit
322-08	NA 123	6-16-55-18w5	3319.3	3.433	2.52	210.07	cc/bit
322-08	NA 123	6-16-55-18w5	3319.3	3.447	2.53	210.34	cc/bit
322-08	NA 123	6-16-55-18w5	3319.3	3.731	2.71	215.76	cc/bit
322-08	NA 123	6-16-55-18w5	3319.3	3.752	2.72	216.14	cc/bit
322-08	NA 123	6-16-55-18w5	3319.3	3.974	2.86	220.11	cc/bit
322-08	NA 123	6-16-55-18w5	3319.3	4.057	2.91	221.55	cc/bit
322-08	NA 123	6-16-55-18w5	3319.3	4.161	2.97	223.31	cc/bit
322-08	NA 123	6-16-55-18w5	3319.3	4.300	3.06	225.61	cc/bit
323-08	NA005	9-20-59-22w5	3805.6	2.362	1.86	185.52	cc/bit
323-08	NA005	9-20-59-22w5	3805.6	2.383	1.87	186.08	cc/bit
323-08	NA005	9-20-59-22w5	3805.6	2.411	1.89	186.82	cc/bit
323-08	NA005	9-20-59-22w5	3805.6	2.425	1.90	187.19	cc/bit
323-08	NA005	9-20-59-22w5	3805.6	2.523	1.96	189.72	cc/bit
323-08	NA005	9-20-59-22w5	3805.6	2.551	1.98	190.43	cc/bit

323-08	NA005	9-20-59-22w5	3805.6	2.719	2.08	194.55	cc/bit
323-08	NA005	9-20-59-22w5	3805.6	2.739	2.09	195.05	cc/bit
323-08	NA005	9-20-59-22w5	3805.6	2.760	2.11	195.55	cc/bit
323-08	NA005	9-20-59-22w5	3805.6	2.774	2.11	195.88	cc/bit
323-08	NA005	9-20-59-22w5	3805.6	2.774	2.11	195.88	cc/bit
323-08	NA005	9-20-59-22w5	3805.6	2.795	2.13	196.37	cc/bit
323-08	NA005	9-20-59-22w5	3805.6	2.816	2.14	196.86	cc/bit
323-08	NA005	9-20-59-22w5	3805.6	2.844	2.16	197.51	cc/bit
323-08	NA005	9-20-59-22w5	3805.6	2.914	2.20	199.10	cc/bit
323-08	NA005	9-20-59-22w5	3805.6	2.977	2.24	200.52	cc/bit
323-08	NA005	9-20-59-22w5	3805.6	2.991	2.25	200.83	cc/bit
323-08	NA005	9-20-59-22w5	3805.6	3.012	2.26	201.29	cc/bit
323-08	NA005	9-20-59-22w5	3805.6	3.026	2.27	201.60	cc/bit
323-08	NA005	9-20-59-22w5	3805.6	3.033	2.27	201.75	cc/bit
323-08	NA005	9-20-59-22w5	3805.6	3.040	2.28	201.90	cc/bit
323-08	NA005	9-20-59-22w5	3805.6	3.047	2.28	202.06	cc/bit
323-08	NA005	9-20-59-22w5	3805.6	3.061	2.29	202.36	cc/bit
323-08	NA005	9-20-59-22w5	3805.6	3.075	2.30	202.66	cc/bit
323-08	NA005	9-20-59-22w5	3805.6	3.075	2.30	202.66	cc/bit
323-08	NA005	9-20-59-22w5	3805.6	3.103	2.32	203.27	cc/bit
323-08	NA005	9-20-59-22w5	3805.6	3.131	2.33	203.87	cc/bit
323-08	NA005	9-20-59-22w5	3805.6	3.131	2.33	203.87	cc/bit
323-08	NA005	9-20-59-22w5	3805.6	3.145	2.34	204.16	cc/bit
323-08	NA005	9-20-59-22w5	3805.6	3.180	2.37	204.90	cc/bit
323-08	NA005	9-20-59-22w5	3805.6	3.257	2.41	206.51	cc/bit
323-08	NA005	9-20-59-22w5	3805.6	3.264	2.42	206.65	cc/bit
323-08	NA005	9-20-59-22w5	3805.6	3.264	2.42	206.65	cc/bit
323-08	NA005	9-20-59-22w5	3805.6	3.285	2.43	207.08	cc/bit
323-08	NA005	9-20-59-22w5	3805.6	3.368	2.48	208.79	cc/bit
323-08	NA005	9-20-59-22w5	3805.6	3.375	2.49	208.93	cc/bit
323-08	NA005	9-20-59-22w5	3805.6	3.375	2.49	208.93	cc/bit
323-08	NA005	9-20-59-22w5	3805.6	3.396	2.50	209.35	cc/bit
323-08	NA005	9-20-59-22w5	3805.6	3.396	2.50	209.35	cc/bit
323-08	NA005	9-20-59-22w5	3805.6	3.403	2.50	209.48	cc/bit
323-08	NA005	9-20-59-22w5	3805.6	3.403	2.50	209.48	cc/bit
323-08	NA005	9-20-59-22w5	3805.6	3.424	2.52	209.90	cc/bit
323-08	NA005	9-20-59-22w5	3805.6	3.501	2.56	211.41	cc/bit
323-08	NA005	9-20-59-22w5	3805.6	3.515	2.57	211.68	cc/bit
323-08	NA005	9-20-59-22w5	3805.6	3.585	2.62	213.02	cc/bit
323-08	NA005	9-20-59-22w5	3805.6	3.585	2.62	213.02	cc/bit
323-08	NA005	9-20-59-22w5	3805.6	3.592	2.62	213.16	cc/bit
323-08	NA005	9-20-59-22w5	3805.6	3.907	2.81	218.93	cc/bit
323-08	NA005	9-20-59-22w5	3805.6	3.976	2.86	220.16	cc/bit
323-08	NA005	9-20-59-22w5	3805.6	4.591	3.24	230.23	cc/bit
323-08	NA005	9-20-59-22w5	3805.6	4.857	3.40	234.21	cc/bit
323-08	NA005	9-20-59-22w5	3805.6	4.864	3.41	234.32	cc/bit
323-08	NA005	9-20-59-22w5	3805.6	5.185	3.60	238.89	cc/bit

323-08	NA005	9-20-59-22w5	3805.6	5.218	3.69	240.70	cc/bit
323-08	NA005	9-20-59-22w5	3805.6	5.236	3.88	244.76	cc/bit

Abbreviations:

$\%R_0$ = bitumen reflectance values
%VRr = calculated vitrinite reflectance
Tpeak = peak temperatures (˚C)